NTNU – Trondheim
Norwegian University of
Science and Technology

Parametric Studies of Dynamic Response for a Workover Riser

Arne Vindenes

Subsea Technology
Submission date: June 2014
Supervisor: Bernt Johan Leira, IMT

Norwegian University of Science and Technology
Department of Marine Technology

NTNU
Norwegian University of Science and Technology
Department of Marine Technology

Master thesis, Spring 2014
for
Stud. Techn. Arne Vindenes

Parametric Studies of Dynamic response for a Workover Riser

Parametriske Studier av Dynamisk Respons for et Workover-stigerør

In order to compute the dynamic response of workover risers, a large number of parameters related to representation of the loading, the floating vessel and the riser systems are required as input to the analysis. The values of these parameters (and even the type of calculation model which is to be applied) are typically not precisely known, and hence they have to be estimated e.g. based on previous experience.

Verification of the applied computational models as well as the relevant design parameters is accordingly an important task. Laboratory experiments play a key role in this context, but also full-scale measurements are strongly in demand. There seems to be only a limited number of reported results in the literature which deal with measurements of workover riser response in full scale. The objective of the present work is hence to prepare for further activity within this area by performing sensitivity studies of computed riser response with respect to basic input parameters to the analysis.

The following subjects are to be examined in this thesis:

1. A description of workover riser system is to be given. Relevant types of sensors and instrumentation schemes that can be implemented are to be discussed with focus on monitoring for the purpose of estimating accumulated fatigue damage.

2. A numerical model of a specific workover riser is to be established in the Flexcom computer program based on input from Aker Solutions. A description of the connection between the physical properties of the riser and the corresponding numerical model is also to be given. Furthermore, an outline of the methodology and numerical algorithms associated with the applied computer program should be included. A corresponding numerical model of the riser is also to be implemented in the computer program Riflex.

3. The effects on the computed riser fatigue damage due to change of key analysis parameters are subsequently to be investigated to the extent that time allows. Examples are: (i)Riser tension (ii)The vessel offset (iii) The hydrodynamic coefficients (iv) The presence of current. The latter should be focused upon in particular, also comparing results obtained from both Riflex and Flexcom.

4. The implications of the findings from the parametric studies with respect to implementation of riser monitoring systems are to be discussed.

The work-scope may prove to be larger than initially anticipated. Subject to approval from the supervisor, topics may be deleted from the list above or reduced in extent.

In the thesis the candidate shall present his personal contribution to the resolution of problems within the scope of the thesis work. Theories and conclusions should be based on mathematical derivations and/or logic reasoning identifying the various steps in the deduction. The candidate should utilise the existing possibilities for obtaining relevant literature.

The thesis should be organised in a rational manner to give a clear exposition of results, assessments, and conclusions. The text should be brief and to the point, with a clear language. Telegraphic language should be avoided.

The thesis shall contain the following elements: A text defining the scope, preface, list of contents, summary, main body of thesis, conclusions with recommendations for further work, list of symbols and acronyms, references and (optional) appendices. All figures, tables and equations shall be numerated.

The supervisor may require that the candidate, at an early stage of the work, presents a written plan for the completion of the work. The plan should include a budget for the use of computer and laboratory resources which will be charged to the department. Overruns shall be reported to the supervisor.

The original contribution of the candidate and material taken from other sources shall be clearly defined. Work from other sources shall be properly referenced using an acknowledged referencing system.

The thesis shall be submitted in electronic form:

- Signed by the candidate
- The text defining the scope included
- Drawings and/or computer prints can be organised in a separate folder.

Supervisor: Professor Bernt J. Leira
Holden

Contact person at Aker Solutions: Christian Revå

Start: January 16th, 2014

Deadline: June 10th, 2014

Trondheim, 16 January 2014

Bernt J. Leira

Bernt J. Leira

Preface

This thesis has been carried out as part of the Master of Science program in Marine Subsea Engineering, at the Norwegian University of Science and Technology, Department of Marine Technology.

I would like to thank my supervisor at NTNU, Bernt Johan Leira, for his guidance and advice throughout the process for writing this thesis. Thanks are also extended to Christian Revå and Christian Øverland from Aker Solutions. A special thanks to Christian Revå, who has dedicated a significant amount of time to assist me when needed.

June 5, 2014

Arne Vindenes

Arne Vindenes

Bergen, June 2014

Abstract

A workover riser is a top tensioned riser, in essence similar to a marine riser. Workover risers differ from marine risers mainly by smaller dimensions, as well as simpler solutions at the riser ends. For instance, the lower flex joint of the marine riser is in the workover riser replaced by a tapered stress joint, and the workover riser has no telescopic joint at the upper end. The similarities between workover and marine risers make it convenient to apply the knowledge acquired for marine risers when performing analyses for workover risers. However, based on the findings in this thesis, one must be careful when assuming similarities between marine and workover risers.

The main purpose of this thesis is to investigate the feasibility of a monitoring system for workover risers. This investigation requires an understanding of a workover riser's behavior, and its response to relevant excitations. A literature review has been done, describing the various workover riser components, as well as the actual applications for a workover riser. The monitoring system suggested will utilize a set of strain sensors. Strain sensors are already mounted on the riser's stress joint and tension joint. A review of strain sensor technology is included.

A workover riser system has been modeled in two separate softwares, Flexcom and RIFLEX. A brief review of selected aspects of these softwares are provided. Two separate softwares were required in order to validate the analysis results, as the riser's dynamic behavior was different from what was expected. The unexpected results occurred as the level of current was changed. It was found that an increased current magnitude is beneficial with respect to the riser's fatigue life. By reducing the current magnitude, from the design condition with one year return period, by a factor of ten, the lifetime of certain riser components has been found to drop by a factor of approximately 16 in one of the softwares. This trend was also validated by the other software, though the factor by which the fatigue life drops remains disputable.

A monitoring system is suggested, where the fatigue damage of each component is extrapolated from the known values at the riser's stress joint. This system requires two extrapolation factors; one factor considers each component's location compared to the stress joint, while the other factor accounts for the environmental conditions. Determining the value of the factor accounting for environmental conditions has proved the biggest challenge. Particularly, the effect of current and current direction must be mapped thoroughly. Measuring the current with sufficient accuracy can prove difficult as well. Riser tension must also be studied further, as it is not only an influential parameter itself, but it also affects other parameters.

Based on the analyses done in this thesis, it is concluded that the feasibility of a riser monitoring system for estimation of fatigue damage is promising. A definite conclusion cannot be drawn, as large amounts of work remain in order to map the influence of all important parameters accurately. It is found that the development of such a monitoring system is an ambitious undertaking, though it appears possible.

Sammendrag

En «workover riser» er et vertikalt stigerør som brukes til vedlikehold av brønner. Den har mange likheter med stigerør for drilling, men skiller seg ut med sine mindre dimensjoner. Det er også vesentlige forskjeller i endene av stigerørene. Her er enklere løsninger valgt på workover riseren. For eksempel: I nedre ende, der et stigerør for drilling har et ledd, har en workover riser et konisk tverrsnitt, uten bevegelige deler. Også teleskop-funksjonen et større stigerør har i øvre ende, er fjernet. De mange likhetene mellom disse forskjellige stigerørene gjør det praktisk å benytte kunnskap fra den ene kategorien når en jobber med den andre. Dette må gjøres med forsiktighet, da det også eksisterer ulikheter som må tas hensyn til.

Formålet med denne oppgaven har vært å undersøke muligheten for et monitoreringssystem til workover risere. Dette krever forståelse av denne typen stigerørs oppførsel når den blir utsatt for forskjellige laster. En litteraturstudie har blitt gjennomført for innhenting av informasjon angående denne typen stigerør. En litteraturstudie har også blitt gjennomført for tøyningssensorer, da monitoreringssystemet vil være basert på målinger fra slike sensorer. Tøyningssensorer er allerede montert på stigerøret, en i hver ende.

Stigerør-systemet har blitt modellert i to separate programvarer, Flexcom og RIFLEX. Utvalgte, viktige aspekter av begge disse programmene har blitt gjennomgått. Grunnen til at to, uavhengige programmer er brukt, er at resultatene måtte valideres. Stigerørets dynamiske respons var forskjellig fra det som var ventet. Dette gjaldt ved forskjellige nivåer av strømning. Det viser seg at en høyere strømhastighet er fordelaktig for stigerørets levetid. Ved å redusere strømhastigheten, fra design-strømmen med et års returperiode, til en tidel av dette, dalte levetiden av enkelte komponenter med en faktor på ca 16 i den ene programmet. Denne trenden er også validert av den andre programvaren, mens styrken av effekten ennå er noe usikker.

Et monitoreringssystem er foreslått, der utmattingsskade for hver komponent er ekstrapolert fra målinger gjort av tøyningssensoren på stigerørets nedre ende. Dette systemet krever to faktorer; en faktor tar hensyn til hver enkelt komponents plassering i forhold til tøyningssensoren, mens den andre faktoren korrigerer for gjeldende betingelser, som for eksempel sjøtilstand. Den største utfordringen har vist seg å være å bestemme den andre faktoren. Spesielt må effekten av strøm og strømretning gis videre oppmerksomhet. Dette gjelder også måling av strøm. Videre må også effekten av strekkraft i stigerøret vurderes i større detalj.

Basert på de analyser som er gjort for denne oppgaven, konkluderes det med at et slikt monitoreringssystem bør kunne utvikles. Dette kan ikke sies helt sikkert, da store arbeidsmengder fortsatt gjenstår for å kartlegge effekten av alle viktige parametere. Det viser seg at utvikling av et slikt system vil være ambisiøst, men ikke uoverkommelig.

Table of Contents

Table of Figures

Table of Tables

Nomenclature

Capital Roman Letters

A	Area
BM	Bending moment
D	Diameter
$\overline{D}$	Fatigue damage
C	Riser Component lifetime
E	Young's modulus
F	Load
GF	Gage Factor
H	Wave height
I	Second moment of inertia
ID	Inner Diameter
Kc	Keulegan-Carpenter number
L	Length
LSS	Lower Strain Sensor lifetime
M	Bending moment
N	Axial force
OD	Outer Diameter
S	Spectrum
T	Period
$Temp$	Temperature
$Tens$	Tension
U	Internal virtual work
V	Volume

Small Roman Letters

$\bar{a}$	S-N curve parameter
b	Number of stress blocks
c	Hydrodynamic coefficient
d	Nodal displacement
f	Frequency in Hertz
h	Water depth (absolute value)
k	Wave number
m	S-N curve parameter
n	Number of stress cycles
t	Time
u	Velocity along x-axis
ud	Axial displacement
vd	Transverse displacement
w	Velocity along z-axis

Matrices

$\boldsymbol{B}$	Strain-displacement relationship
$\boldsymbol{D}$	Stress-strain relationship
$\boldsymbol{K}$	Global stiffness matrix
$\boldsymbol{k}$	Element stiffness matrix
$\boldsymbol{M}$	Global mass matrix

Greek Letters

α	Rayleigh damping coefficient
β	Thermal correction factor
γ	Fatigue extrapolation factor
δ	Factor
ε	Strain
ζ	Instantaneous wave elevation
ζ_a	Wave amplitude
θ	Angle
κ	Curvature
λ	Wavelength
ρ	Density
σ	Stress
τ	Wall thickness
ϕ	Rotational displacement
χ	Fatigue extrapolation correction factor
Ω	Electrical resistance
ω	Angular velocity

Abbreviations

BC	Boundary Condition
BHA	Bottom Hole Assembly
BOP	Blow-Out Preventer
CT	Coiled Tubing
DOF	Degrees Of Freedom
DP	Dynamic Positioning
EDP	Emergency Disconnect Package
FBG	Fiber Bragg Grating
LRP	Lower Riser Package
KC	Keulegan-Carpenter
LWI	Light Well Intervention
MSL	Mean Sea Level
NCS	Norwegian Continental Shelf
RAO	Response Amplitude Operator
RLWI	Riser-Less Well Intervention
SCSSV	Surface Controlled Subsurface Safety Valve
SFT	Surface Flow Tree
STD	Standard Deviation
TF	Tension Frame
TTR	Top Tensioned Riser
VIV	Vortex Induced Vibrations
WL	Wireline
WO	Workover

1. Introduction

A general trend in production of oil and gas is an increased focus on maximizing production from each well. The demand for hydrocarbons is continuously high, and the costs of drilling new wells are significant, even to the large budgets of the oil companies. These conditions increase the importance of maintaining high production rates at existing wells, which require maintenance. Performing intervention operations on a subsea well often require a riser, though a full size marine riser is unnecessarily large for most operations. The workover riser is created for these operations. A lightweight operation compared to marine risers, the workover riser enables operations from smaller, less expensive vessels. The smaller diameter of the workover riser does not allow for heavy well intervention techniques that require a drill string. However, workover risers can perform a wide range of well intervention activities, and new, innovative solutions are under continuous development. Development of workover riser systems has been rapid, helped by existing knowledge in the field of marine risers. There are however significant differences between these systems, making it important to acquire standalone knowledge of workover riser systems.

Even though a workover riser is structurally similar to a marine riser, there are certain differences that can prove influential of the riser's dynamic behavior. Its smaller diameter causes a change in the hydrodynamic excitation forces, and the lack of flex joints alters the riser's dynamic behavior. These factors can seem trivial prior to running analyses, but can prove essential for the dynamic behavior of the riser. Critical locations with respect to strength and fatigue are also altered.

Estimation of fatigue life for workover risers is another aspect that requires attention. These risers differ in dynamic behavior from marine risers. Workover risers differ from marine risers in means of attachment to the support vessel. The dynamics of this boundary condition causes a region where fatigue life is of high importance. It is desired to develop a monitoring system for a workover riser, estimating accumulation of fatigue damage for each riser segment. Such a system will cause increased efficiency of operation. It will for instance allow a real-time update of the accumulated fatigue damage of each riser joint. Joints that have been exposed to heavy wear can then be relocated to a less critical location for the next operation. By continuously estimating the state of each riser joint, inspection of the components can be scheduled based on actual usage, not constant intervals. Establishing a monitoring system that estimates riser fatigue will thus improve the overall efficiency of operation.

1.1 Development of Subsea Wells

The demand for workover risers are created by the presence of subsea well. At the present, Statoil operates approximately 500 subsea wells on the Norwegian Continental Shelf, accounting for over 50 % of the total production (Ramsnes, 2010). As seen in figure 1.1, the number of wet trees is not as high as that of dry trees, but wet trees are increasing at a higher rate.

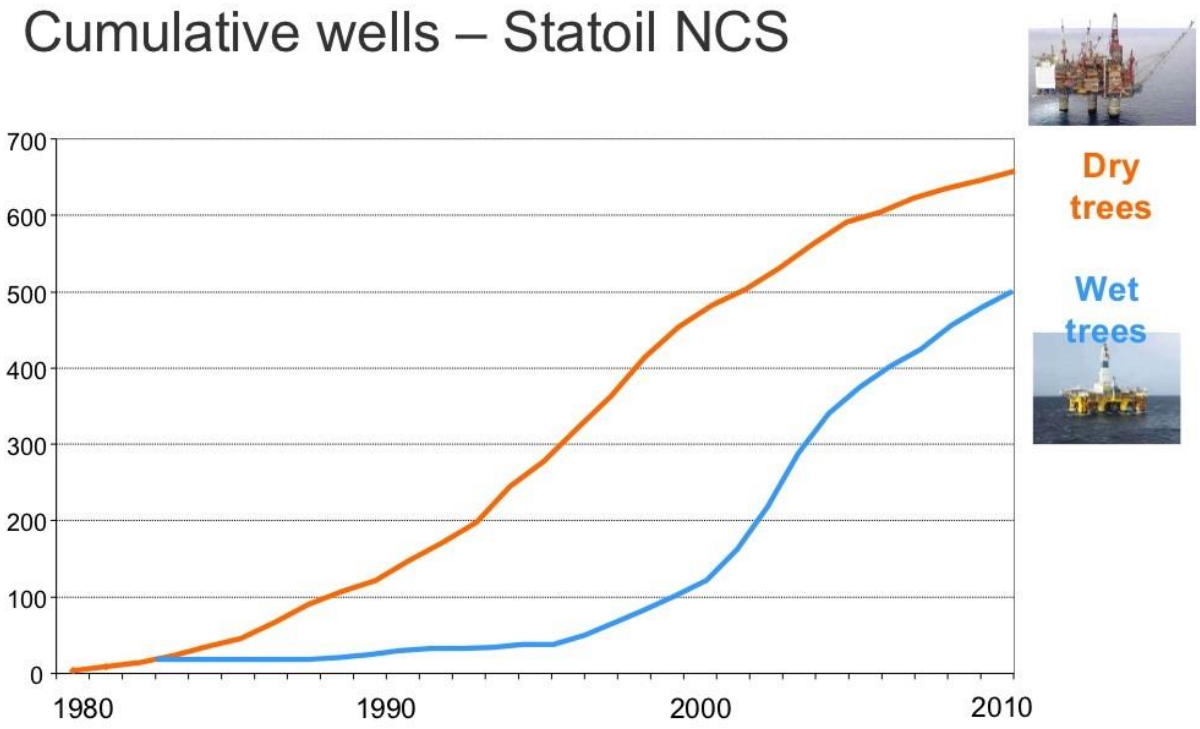

Figure 1.1: Statoil's dry and wet trees at the NCS (Ramsnes, 2010)

As illustrated by figure 1.2, intervention activities are vital for maintaining high production rates. Intervention activities are just as important for wells with wet trees as it is for other wells, though the difficulties of accessing these wells make intervention operations expensive. The workover riser is designed for performing intervention operations on such wells. It saves costs compared to marine risers, while it allows a variety of the most common intervention activities.

1.2 Fatigue Issues for Workover Risers

A workover riser is a top tensioned riser. Such risers are known to have issues with fatigue life. Unlike a marine riser, the workover riser does not have flex joints to reduce bending moments near its ends. Thus, all oscillations cause curvature of the riser's pipe sections. This causes large bending moments at critical locations, lowering fatigue life. Due to these issues, it is desired to develop a monitoring system for workover risers. The monitoring system can be used to estimate fatigue damage of critical components, whose damage cannot be measured directly. By estimating the fatigue damage of the riser's components, inspections can be scheduled according to actual usage, rather than the present day solution of fixed time steps. A monitoring system will also increase the operator's knowledge of the riser's load level. This knowledge lets the operator make better informed decisions regarding operation. For these reasons, a monitoring system will improve the efficiency of operation.

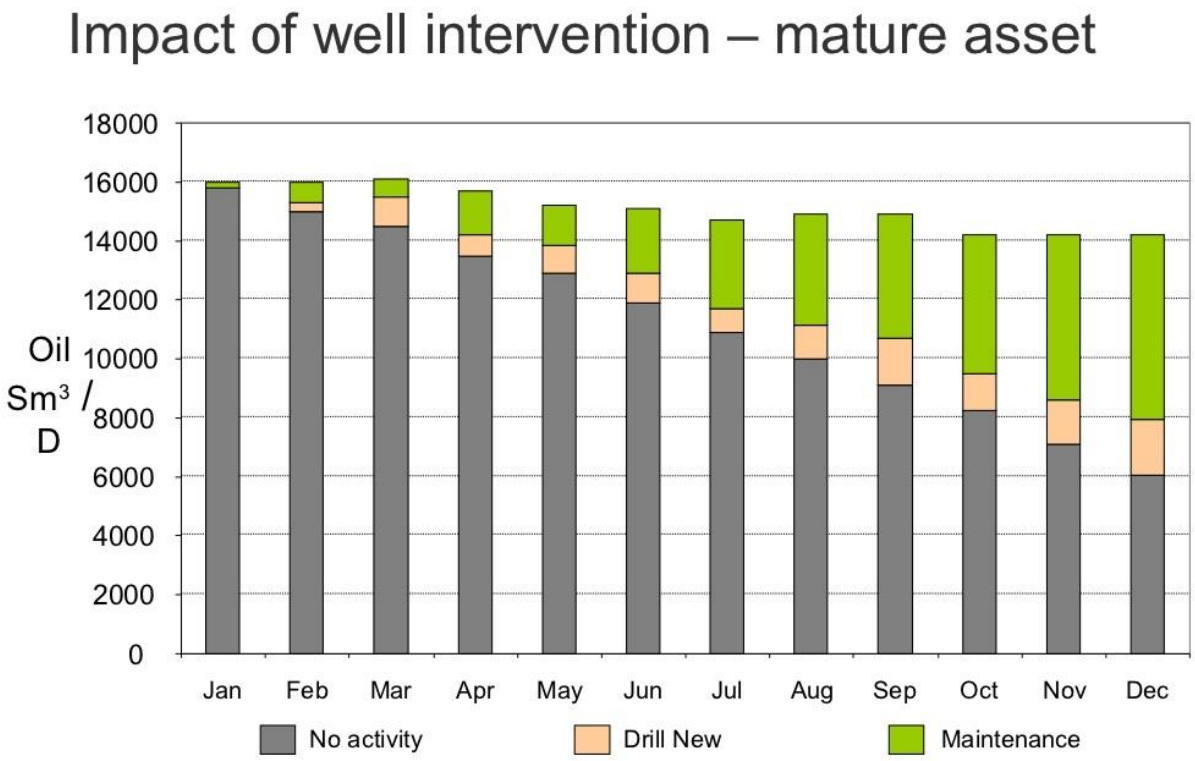

Figure 1.2: Importance of well intervention for production rates (Ramsnes, 2010)

2. The Workover Riser System

A workover riser is a top tensioned steel riser with a small diameter. It is used for establishing a connection between a floating surface vessel and a subsea well. By establishing this connection, the vessel will have the capability to perform a wide range of intervention activities. The workover riser is in essence similar to a marine riser, but it has a severely reduced size. The smaller dimensions make well intervention feasible using smaller vessels, which reduces overall costs.

Figure 2.1: The next generation workover riser system from Aker Solutions (2014)

2.1 Workover Riser Components

In order to provide a safe connection between a well and a surface vessel, the workover riser consists of several different segments. In addition to the riser joints, components such as adapters and safety equipment are needed near the subsea tree. At the vessel's end of the riser, a heave compensation system providing constant riser tension is required. At the surface, there is additional equipment, like a surface flow tree and a surface BOP. A typical workover riser system is shown in figure 2.2. The following sections will elaborate on the various components of the workover riser system.

2.1.1 Lower Riser Package

The lower riser package (LRP) is connected directly on top of the subsea tree. It is thus the lowest part of the WO riser system. The function of the LRP is to seal the riser if required. This means that the LRP must have the ability to cut any tool lowered into the well, either wireline or coiled tubing (Halvorsen & Araujo, 1993).

2.1.2 Emergency Disconnect Package

The emergency disconnect package (EDP) is used to disconnect the WO riser if an emergency should occur. As the name suggests, the EDP is used to disconnect in case of an emergency. ISO 13628-7 (2005) lists three examples for when the EDP should be used:

- Failure of the vessel's station-keeping system
- Well system emergency
- Sudden and unanticipated deterioration of weather conditions beyond allowable operational conditions.

It is noted that even though the EDP is only used in case of an emergency, the disconnection procedure is controlled. Prior to disconnection, the LRP will seal the well. This operation requires time. For the examples listed above, there is time to perform a controlled emergency disconnect. In case of more immediate problems, where there is no time to disconnect safely, the safety joint is used.

2.1.3 Stress Joint

Above the LRP and EDP, the WO riser's stress joint is mounted. The task of the stress joint is to provide a transition between the rigid components beneath, and the relatively flexible riser above. A WO riser, unlike a marine riser, does not include a flex joint/ball joint. A flex joint would reduce the bending moments in the riser, but it would also make for a more complicated structure. The stress joint is tapered, causing the bending stiffness to change along its length. The lower end will experience the largest bending moments. It also has the largest stiffness. This correlation between bending moment and bending stiffness controls the curvature of the stress joint (Zhang et al., 2010).

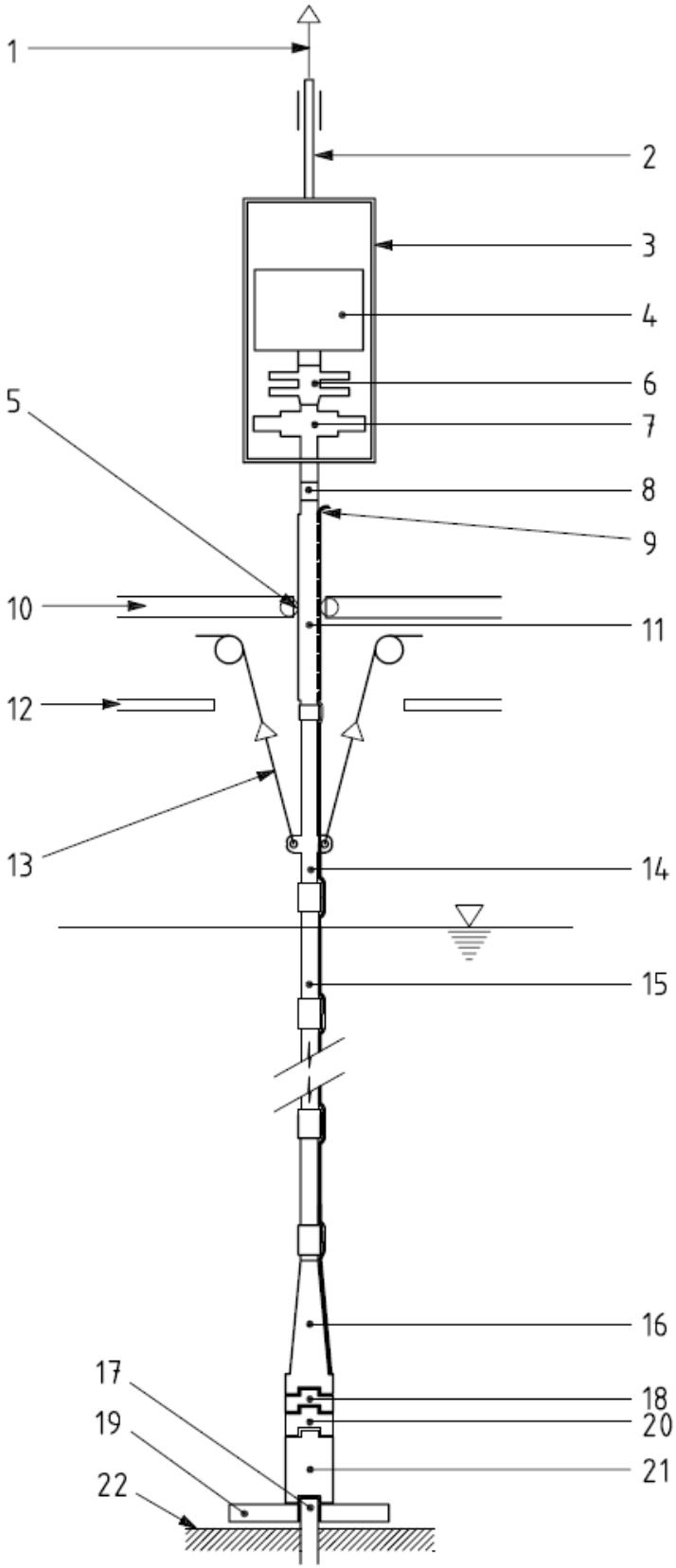

Key

1	top drive
2	drill sub
3	surface-tree tension frame
4	coiled tubing injector
5	roller bushing
6	surface BOP
7	surface tree
8	surface-tree adapter joint
9	umbilical (to hose reel)
10	drill floor
11	slick (cased wear) joint
12	moon pool area
13	riser tension wires
14	tension joint
15	standard riser joints
16	stress joint
17	wellhead
18	emergency disconnect package
19	guide base
20	lower riser package
21	subsea tree
22	seabed

Figure 2.2: Overview of a typical workover riser system (ISO, 2005)

2.1.4 Riser Joints

Most of the water depth will be traversed by regular riser joints. These joints are relatively uncomplicated structures, used for creating a jointed pipeline. The riser joints provide the physical link between the subsea tree and the surface vessel. All riser joint connectors are required to be identical. This enables repositioning of the riser joints between operations. Intelligent placement of used riser joints can increase fatigue life, as the most critical areas are generally the top and bottom parts (Kirkvik & Berge, 2011). In addition to the basic riser joints, there are pup joints. The pup joints are used to fine-tune the length of the riser.

2.1.5 Safety Joint

Certain problems, such as lock-up of the heave-compensation system, can cause immediate problems. This leaves no time to perform a controlled disconnect. If this were to occur, the riser tension could immediately be in danger of damaging the well. To avoid this, the riser also has a safety joint, located some distance above the EDP. If the riser tension exceeds a critical level, the WO riser will fail structurally in the safety joint, which thus acts as a weak link. The safety joint is dimensioned such that it is structurally incapable of carrying stresses that would damage the well or subsea tree.

2.1.6 Tension Joint

As the name suggests, the tension joint is used to provide tension to the riser. The tension joint is located near the top of the riser, below the vessel's rotary table, as seen in figure 2.2. Above the tension joint, the riser continues upwards. There is no telescope joint, meaning that the upper end of the WO riser will remain at a constant vertical elevation, regardless of vessel heave. It can thus not be attached to the vessel directly. Depending on which vessel is operating the WO riser, the design of the tension joint can vary. The connectors to the rest of the riser must be compatible, using the same connectors as the standard riser joints. The interface with the vessel's tensioner system must be designed to be compatible, which can be different for each vessel (ISO, 2005). As there is no telescopic joint, there is no strict need to apply tension below the drill floor. A possibility is to omit the tension joint, and let the top drive carry all the weight.

2.1.7 Landing Joint

As seen in figure 2.2, the WO riser passes through the drill floor. The riser is not attached to the vessel in this location, and there will be relative movement. The landing joint (slick joint) will have contact with the drill floor's rotary table. The landing joint differs from the standard riser joints due to a protective sleeve, which protects the riser from impact with the drill floor (ISO, 2005). Another possibility is to reinforce the landing joint by increasing its wall thickness. Nonetheless, the landing joint is exposed to large stresses. Based on the experience of Aker Solutions, the landing joint is more vulnerable to fatigue damage than any other component in the WO riser system (Revå, 2014). Due to the landing joint's impact issue, installation of strain sensors at critical locations are currently unfeasible. This makes it difficult to monitor the condition of the WO riser at the landing joint. Due to the criticality of the landing joint, combined with the difficulty of monitoring its condition, it is desired to estimate its state based

on extrapolation. A local analysis should be performed for the critical components, such as the landing joint (Kirkvik & Berge, 2011).

2.1.8 Tension Frame

On top of the riser, a surface flow tree and other equipment is mounted. Additional equipment can for instance be a CT injector. CT operations will be discussed in section 2.4.3. The tension frame accommodates these components. All this equipment is rigidly installed on top of the riser. The tension frame is connected to the vessel's travelling block, allowing a heave-compensated lift. It is required to be able to keep the entire riser system in tension, without assistance from the tension joint (ISO, 2005). During normal operation, the tension frame will hold the weight of all surface equipment, in addition to the riser components above the tension joint.

2.2 Overpull

The majority of the WO riser must always be in tension. Due to its slender design, its bending stiffness is almost negligible on a global scale. The riser must thus be in constant tension in order to maintain its configuration. To ensure the riser is always in tension, the mean tension must be larger than the dynamic variations of tension. It is also important that the lower end of the EDP be in tension. The tension allows the riser to release cleanly, and retract upwards at the EDP. If the riser is not in tension, the disconnect procedure might be unsuccessful. Overpull is defined as the riser tension at the lower end of the EDP.

2.3 Differences between Workover and Marine Risers

Workover risers and marine risers are very similar. There are some differences, which affect the behavior of the risers, and the required equipment and analyses. Apart from the size difference, WO risers differ from marine risers in two main areas: the lack of flex joints, and the lack of a telescopic joint. Both of these differences make the WO riser a simpler construction.

2.3.1 Flex Joints vs Stress Joints

The traditional, marine riser has two flex joints, one at each end of the riser. Flex joints limit the amount of bending moment that can be transferred between the riser and adjacent components. The rotational stiffness of flex joints are typically highly non-linear, and should be modelled as such (Bai & Bai, 2005). An illustration of a flex joint is seen in figure 2.3. Systems consisting of a marine riser and a heavy BOP are known to cause wellhead fatigue issues. It is thus logical to use flex joints in this system, limiting transferred bending moments from the riser. However, for the lightweight case of a workover riser, the simplicity of a stress joint is preferred. A requirement from ISO (2005) is that the stress joint shall be so thin that it can be lowered through the rotary table. Satisfying the same requirement with a flex joint would be difficult. As the upper end of a marine riser is firmly attached to the vessel at the drill floor, a flex joint is located there as well. A WO riser is, as mentioned in section 2.1.7, not firmly attached to the vessel. The upper end of a WO riser thus does not require a stress joint or flex joint.

2.3.2 Slip Joint vs Landing Joint

As mentioned in the previous section, the upper end of a marine riser is firmly attached to the vessel. This necessitates the riser length to be variable, due to the vessel's heave motion. Further, the riser's slip joint (telescopic joint) must necessarily be located above the riser tensioner system. A slip joint for a marine riser is illustrated in figure 2.4. The slip joint needs to allow elongation, while acting as a pressure barrier. For WO risers, a far simpler solution has been adopted. Instead of a slip joint, the riser continues straight through the drill floor, as mentioned in section 2.1.7 (ISO, 2005).

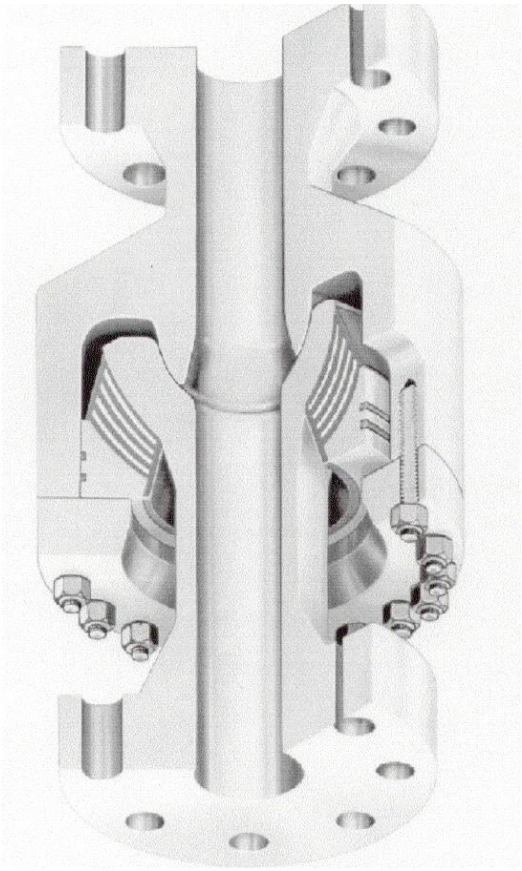

Figure 2.3: Illustration of a typical flex joint (Kumar & Hogan, 2002)

2.4 Workover Riser Operations

A workover riser is used for performing intervention operations on subsea wells. It establishes a direct, nearly vertical, connection between a floating surface vessel and the wellbore. This allows the operator to lower intervention tools down into the well. Larger equipment, like a traditional drill string, would require a marine riser. Two main types of interventions are done through a WO riser; coiled tubing and wireline. ISO (2005) states that a WO riser can be a common system with a completion riser. This enables an even wider range of activities for the riser system, but it requires replacement of certain components (ISO, 2005).

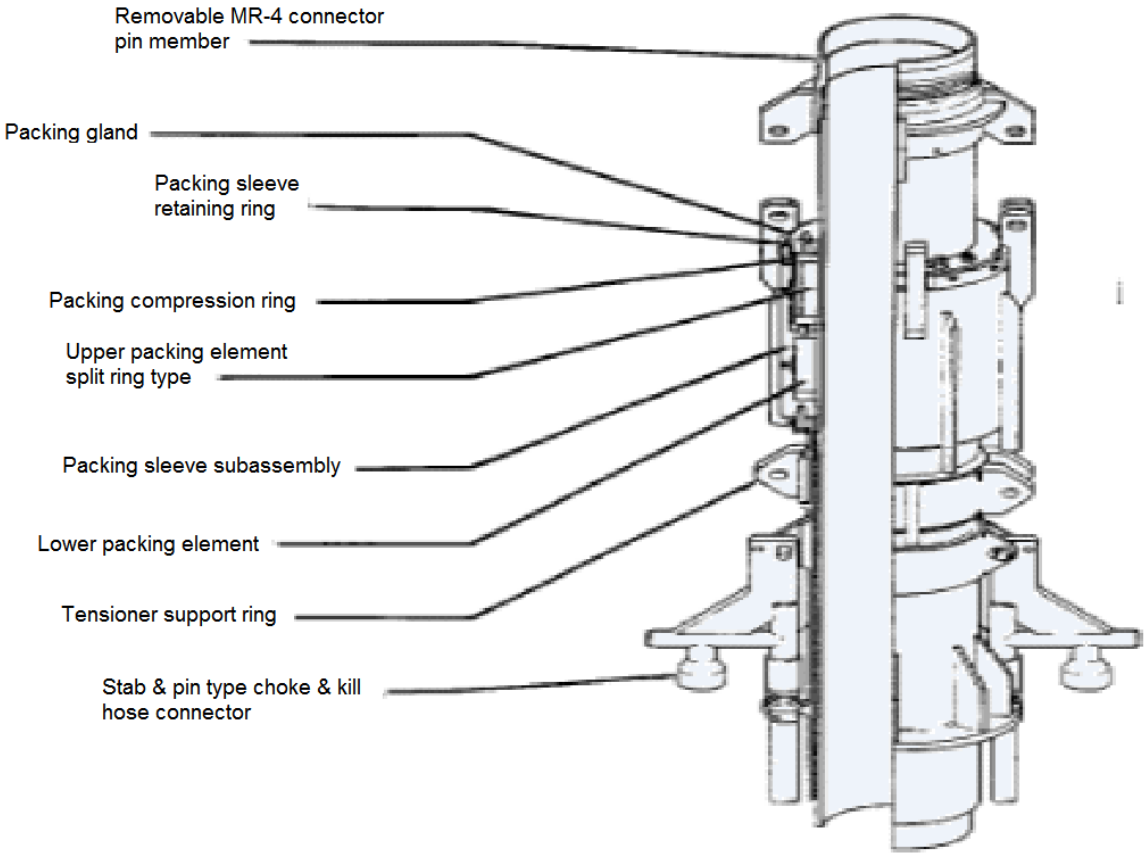

Figure 2.4: Slip joint illustration ("The marine riser,")

2.4.1 Subsea Well Intervention

Subsea well interventions are for simplicity divided into three categories, defined by the size of the equipment required. Zijderveld et al. (2012) describes the categories as follows:

Type I: Type I intervention is also called light well intervention (LWI). Interventions in this category use smaller sized vessels, typically the size of suppliers. Wireline (WL) operations are typical for this kind of intervention. This kind of intervention can often be riserless (RLWI). LWI can also be used in combination with heavier intervention tools, on other vessels.

Type II: Type II is also called medium well intervention. The operations performed in this category will in general require equipment that is more specialized. Medium well intervention will generally use coiled tubing (CT), which require more space aboard the operating vessel. In some cases, a combination of CT and WL can be applied.

Type III: Type III interventions utilizes large vessels, for performing the most heavy-duty operations. This will often require a marine riser and a full size subsea BOP. This kind of intervention will generally be done by full size drilling vessels.

In this thesis, workover risers are studied. Since type III intervention does not utilize a WO riser, these interventions will not be discussed further. Type II interventions require a WO riser. Attempts have been made to perform riserless CT intervention, but this has been unsuccessful (Drange, 2010). Type I intervention will sometimes require a WO riser, though RLWI are frequently used for WL operations. At deeper water, the difficulties of RLWI increases. By 2010, the depth limit for RLWI was approximately 760 meters (Drange, 2010). New solutions for increasing well intervention efficiency are constantly being developed. The limitations of RLWI in 2010 are not necessarily still valid. Table 2.1 lists typical tasks for interventions of type I and type II.

2.4.2 Wireline Intervention

Wireline operations are typical type I interventions. The ultimate motivation for choosing a lightweight solution is of course cost. The smaller vessel is less expensive to hire, and the operation itself should be more efficient (Al-Shawly et al., 2010). When riserless solutions are applied, the need to assemble and disassemble a riser vanishes. This saves a significant amount of time. Further, the lowering and withdrawal of a wireline is an efficient operation compared to the alternatives. Wireline tools do not allow for circulation of fluids, but electric tools can be applied. In order to access highly deviated wells, where gravity is not sufficient, a well tractor can be used. The well tractor is an electrically powered device, which provides a downhole pull. An electrical well tractor is shown in figure 2.5.

Figure 2.5: Electric well tractor (Kruger & Schwanitz, 2008)

2.4.3 Coiled Tubing Intervention

When wireline tools are not sufficient, coiled tubing operations can be performed. CT can be considered as a compromise between a wireline and a drill string; it is hollow like a drill string, but it is stored on a coil. The lack of joints on the CT makes it more convenient to lower into the well, even though the transition from coiled to straight induces plastic deformations. The CT deformations at the vessel reduces fatigue life. Particularly problems with the heave compensation system can be critical, possibly reducing the CT fatigue life to a matter of minutes (Yang et al., 1998). Conventional CT systems do not provide electricity downhole. Concepts for downhole electricity with CT systems do however exist (Turner et al., 1999). In addition to the

typical tasks for CT systems found in table 2.1, CT drilling is also possible. This is accomplished by either a positive displacement motor, or an electric downhole motor (Turner et al., 1999). CT drilling is however inconvenient to use for drilling whole wells, as it does not allow operations like setting the casing (Leising & Newman, 1993). According to Mody and O'Malley (2011), coiled tubing can be pushed into deviated wells, but there is a limit. After this limit, a well tractor must be used. The tractor used for CT operations resembles the WL tractor, except for its motor, which is hydraulic.

Table 2.1: Typical type I & II intervention tasks (Zijderveld et al., 2012)

Type I interventions	***Type II intervention***
Bore hole surveys/logging	Casing leak repairs
Fluid displacement	Fishing
Gas lift valve repair	Paraffin, asphaltenes, hydrates
Perforating/re-perforating	Plugging abandoned well
Sand washing	Remedial cementing
Setting/pulling tubing plugs	Sand control/gravel packing
Stimulation	SCSSV failure
Zonal isolation	Water shut-offs

2.5 Fatigue Issues for Top Tensioned Risers

Though top tensioned risers (TTRs) are necessary for drilling and maintaining wells, they also create difficulties. When a full size BOP is placed on top of the wellhead or subsea tree, forces and moments transferred from the riser will cause the well fatigue damage. This issue has been emphasized lately, as large values are lost if a well must be abandoned due to fatigue. However, the cost of abandoning a well however low compared to the potential disastrous consequences of a failure. In the case of the lighter equipment related to WO risers, the load on the wellhead is far lower. This is a motivating factor for using a WO riser. However, the wellhead is not the only component that accumulates fatige damage during operation. The stress joint, as described in section 2.1.3, will oscillate with significant angles. Even more vulnerable is the landing joint described in section 2.1.7. From the experience of Aker Solutions, the landing joint may have noticeable plastic deformations after use. The impacts with the drill floor cause large local forces, severely reducing fatigue life. In addition, every single riser component accumulates some fatigue damage, depending on its location.

2.5.1 Fatigue Monitoring

A certain amount of fatigue damage cannot be avoided when performing a workover operation. To avoid failure, each riser component must be inspected, and possibly repaired in good time prior to expected failure. Wherever there are uncertainties, conservative estimates must be made. Because of this, few components will ever come close to fatigue fracture. A major source of uncertainty is the estimation of riser response. Present day estimation of riser response is based on global analyses. Regardless of the quality of these analyses, there will always be

sources of uncertainty. By directly measuring the riser response, these uncertainties can be bypassed. Russo et al. (2012) attempted this for a marine riser, in order to estimate wellhead fatigue. It was found that the analysis estimates were overly conservative. Thus, by removing sources of fatigue estimate uncertainty, the operational life of the equipment can be significantly extended. Additionally, inspection intervals can be adapted to actual usage of the riser, instead of the present-day solution where regular inspections are performed, regardless of usage.

2.6 Fatigue Calculation by Rainflow Counting

When performing global riser analysis, calculation of fatigue lifetime is important. This can be done in both the frequency domain and the time domain. For linear systems, these approaches should yield approximately equal results. In order to account for non-linear effects, a time domain approach must be selected. Input for these calculations are time series of stress. For a riser, the axial force is close to constant. The mean stress level is not as important for fatigue issues, and are neglected. Bending moment is therefore the most important parameter for estimation of riser fatigue. Bending stress for the riser can be calculated according to equation (2.1) (DNV, 2005). The equation calculates stress at a specific location along the riser's circumference. DNV (2005) recommends calculating this stress for at least eight locations along the riser's circumference.

$$\sigma_M(\theta, t) = \left(M_y(t)\sin(\theta) + M_z(t)\cos(\theta)\right) * \left(\frac{D - \tau_{fat}}{2I}\right) \quad (2.1)$$

$$\tau_{fat} = \tau_{nom} - 0.5 * \tau_{corr}$$

Where:

D : Pipe diameter

I : Second moment of inertia

M_y : Bending moment around the y-axis

M_z : Bending moment around the z-axis

t : Time

θ : Angle (location within cross-section)

σ_M : Bending Stress

τ_{fat} : Fatigue pipe wall thickness

τ_{nom} : Nominal pipe wall thickness

Once the stress time series have been established for several discrete locations along the riser's circumference, this can be used as input for a rainflow counting algorithm. The stress time series are then first processed, so that only local maxima and minima remain. A rainflow counting algorithm will then count the stress cycles, as illustrated by figure 2.6.

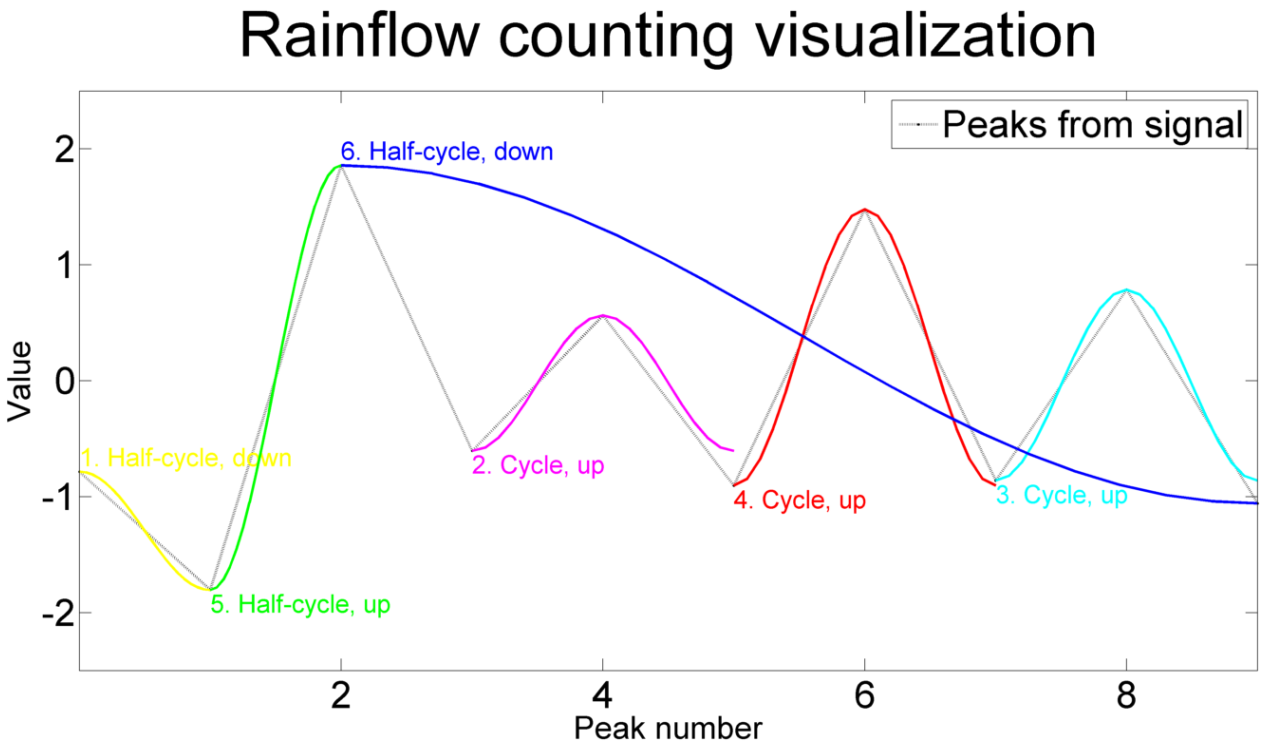

Figure 2.6: Illustration of a rainflow cycle counting algorithm (Nieslony, 2010)

The resulting data from a rainflow counting algorithm is shown in figure 2.7. This data sorts number of cycles at each stress amplitude. In the figure, the stress amplitudes are discretized into forty intervals. This is done for illustrative purposes. For an actual calculation, a significantly higher resolution is suggested. Separate rainflow counting is done for each location along the riser's circumference.

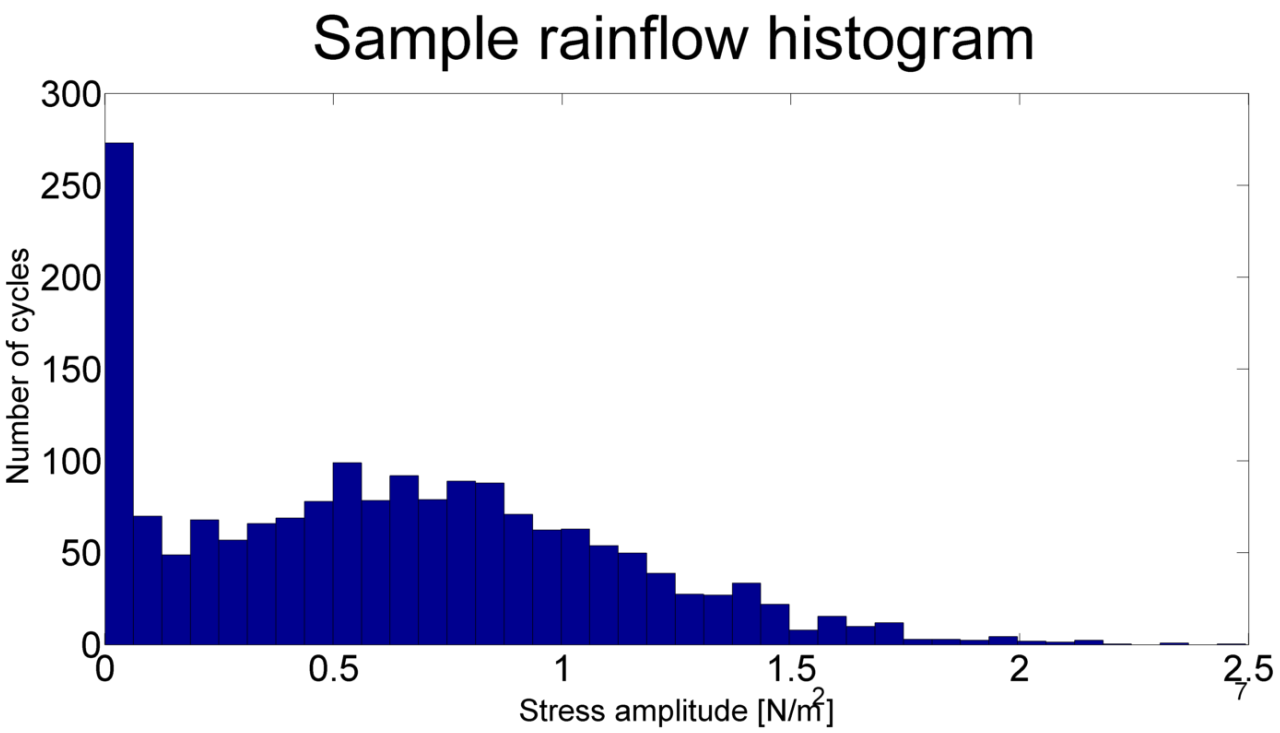

Figure 2.7: Sample rainflow histogram

2.6.1 Miner-Palmgren Summation

In order to calculate lifetime from the stress amplitudes found by rainflow counting, Miner-Palmgren summation is used. The formula for Miner-Palmgren summation is found in equation (2.2) (DNV, 2010). In this equation, two factors are needed, and these should be selected according to appropriate regulations, such as DNV (2010). Prior to running the stress amplitudes from the rainflow counting as input for Miner-Palmgren summation, they are multiplied by a stress concentration factor. This factor accounts for stress concentrations in local geometry. The value of the SCF is as well determined from DNV (2010). The result of this equation is a factor between zero and one. When this factor is zero, the component has experienced no stress cycles at all. As the component accumulates fatigue damage, the damage factor will increase linearly. When it reaches one, a fatigue fracture is expected. Due to the severe implications of a fatigue fracture, and the existence of large uncertainties, it is common to apply a safety factor of three in this summation. Thus, the damage factor will not be allowed to exceed one third.

$$\bar{D} = \frac{1}{\bar{a}} \sum_{i=1}^{b} n_i * (\Delta\sigma_i)^m \quad (2.2)$$

Where:

$\bar{a}$: Intercept of the design S-N curve with the log N axis

b : Number of stress blocks

$\overline{D}$: Fatigue damage

m : Negative inverse slope of the S-N curve

n_i : Number of stress cycles in block i

$\Delta\sigma_i$: Stress amplitude in block i

2.7 Wave Scatter Diagrams for Fatigue Calculation

For the location to be considered in this thesis, a wave scatter diagram has been created for a period of 100 years. In this diagram, the significant wave height (H_s) and peak period (T_p) has been found for each seastate. The duration of each seastate is three hours. The wave scatter diagram is found in appendix A. In a wave scatter diagram, the number of observations of each seastate is listed, described by H_s and T_p. These two parameters are not sufficient to describe a seastate completely. By assuming a wave spectrum however, they provide reasonable accuracy. Given the wave scatter diagram, the probability of occurrence for each seastate can be found. This is useful, for instance in order to perform fatigue calculations during the design stage of a project. The expected fatigue damage to be accumulated during a specific amount of time can be calculated as the weighted sum of accumulated damage for all seastates during the same time span. The formula for this is seen in equation (2.3). Given this equation, analyses simply must be run for every seastate in the wave scatter diagram, and the fatigue damage of the component in question must be calculated. However, due to the large amount of seastates in the wave scatter diagram, it is customary to lump some of the seastates. Blocks of seastates are created, and a selected seastate from the block is analyzed. This saves large amounts of computational time, at the cost of a slightly reduced accuracy.

$$\overline{D}_{tot} = \sum_{i=1}^{num} p_i * \overline{D}_i \tag{2.3}$$

Where:

$\overline{D}_i$: Accumulated fatigue damage at seastate i

$\overline{D}_{tot}$: Expected damage accumulated at representative conditions

num : Number of seastates analyzed

p_i : Probability of occurrence for seastate number i

2.8 Modes of Operation

A workover riser has two main modes of operation; connected and hung-off. When the environmental conditions allow it, the riser is connected to the wellhead, permitting access to the wellbore. However, if the environmental conditions degrade past the allowable operational envelope of the riser system, the riser will be disconnected from the wellhead (ISO, 2005). When in hang-off mode, the lower end of the riser is not exposed to the bending moments it would otherwise experience. Other components, like the landing joint, can however accumulate significant fatigue damage when hung-off (ISO, 2005). Aker Solution's workover riser will be disconnected at the EDP. This leaves the LRP connected to the wellhead, lowering the mass attached to the lower, free end of the riser. As the riser in hang-off mode in essence is a large pendulum, reducing the mass at the lower end is beneficial for the landing joint. According to Kirkvik and Berge (2011), there is no need to run analyses for the connected mode when the heave motion exceeds the acceptable range of the heave compensation system. In those conditions, only the hang-off mode is relevant. The opposite assumption cannot be made for the hang-off mode; the hang-off mode must be analyzed for all sea-states (Kirkvik & Berge, 2011). In addition to the connected and hung-off modes of operation, the riser has another configuration during running and retrieval. Running and retrieval can be considered a special case of hang off (ISO, 2005). Necessarily, the riser's length will be variable during running and retrieval, and unlike hang-off mode, the LRP is connected to the riser.

3. Strain Sensors

Many constructions, like bridges, buildings and offshore installations are exposed to dynamic loading. These load cycles cause fatigue damage, which will often limit their operational lifetime. Structural failure due to fatigue could often be disastrous. To avoid this, conservative fatigue estimates are made. The estimation of fatigue life during the design phase must necessarily be based on the expected loading, which might be inaccurate. Real-time monitoring of accumulated fatigue damage can improve the estimate of remaining fatigue life. In many cases, this can extend the operational lifetime. By attaching strain-sensors to the relevant structural components, a real-time estimate of accumulated fatigue damage can be found. Three main technologies for monitoring strain in structural components will be covered by this thesis.

3.1 Conventional Foil Gages

Conventional foil strain gages are based on Lord Kelvin's 1856 discovery, that the electric conductivity of copper and iron wires change due do tensile strain (Tuttle, 1989). By attaching a conductive wire to the structure component of interest, the wire will experience the same strains as the structural component. In tension, the wire will be elongated and reduce its diameter. This causes a measurable increase in resistance. In order to estimate strain from this phenomenon, it is necessary to run an electric current through the conducting wire. Variations in the wire's resistance must be measured extremely accurately. Tuttle (1989), lists six categories of error sources, which must be considered:

1. The strain gage must be firmly attached to the structure, so that gage and structure are exposed to the same strains. If the gage attachment were to creep, this would of course alter the measured values.
2. The strain gage's stiffness must be negligible compared to the structure's stiffness. If the gage locally reinforces the structure, the measured strains will be too low.
3. There can be no electric conductivity between the gage and structure.
4. The measured changes in electric resistance are very small. In order to achieve accurate strain measuring, the electric resistance measurements must be extremely sensitive. When the structure experiences a micro-strain, a typical 350 Ω gage will have a change in resistance of approximately 0.0007 Ω.
5. Spurious strains can be present, and measured. Most typical of these are thermal loads, which will cause the structure to expand or contract. These spurious strains must be compensated for, if they are significant.
6. The strain gage must be in working condition. An aggressive environment might over time remove the insulating material, and start oxidizing the wire.

Figure 3.1 shows an illustration of a conventional foil strain-gage. The figure shows that the conducting wire is placed so that its length in the measuring direction is as high as possible. The effect of tangential strain is generally negligible for this kind of strain sensor (Sirohi & Chopra, 2000).

3.2 Piezoelectric Strain Sensors

As the name suggests, piezoelectric strain sensors are based on the effect of piezoelectricity. Princeton University's lexical database "WordNet" (2010), defines piezoelectricity as "electricity produced by mechanical pressure on certain crystals (notably quartz or Rochelle salt); alternatively, electrostatic stress produces a change in the linear dimensions of the crystal". In other words, piezoelectric materials will become electrically charged when exposed to pressure. They will also change dimensions when exerted to electricity. This makes piezoelectric materials suited as both sensors and actuators (Sirohi & Chopra, 2000).

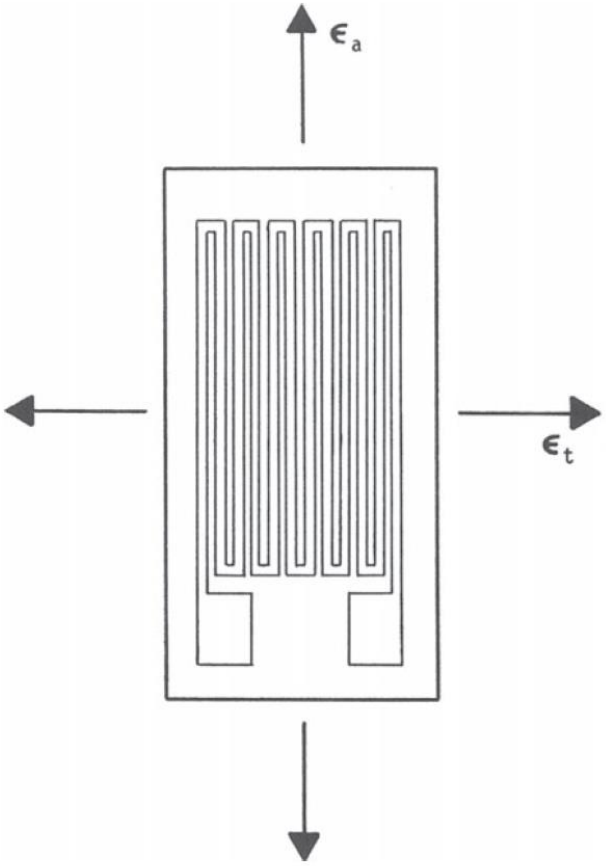

Figure 3.1: Illustration of a foil gage (Tuttle, 1989)

3.2.1 Piezoelectric Strain Measurement

Piezoelectric strain sensors detect the electrical current created by the piezoelectric material. An electrical current will however not be created by static pressure; it is created by pressure variation. As a result, piezoelectric strain sensors are incapable of measuring static strain. When estimating fatigue, the static strain of the structural component is of limited interest. The important factor is the magnitude of the stress cycles. For this use, the inability to measure absolute strain is not an issue. Sirohi and Chopra (2000), compared a piezoelectric strain sensor to a conventional strain gage by attaching the two sensors to opposing faces of a beam. The two sensors were exposed to the same strain field. The results are shown in figure 3.2. It is

emphasized that the foil gage has a much higher noise level. The noise level of the strain gage is due to imperfections in the steady electrical current. The piezoelectric sensor does not utilize an external source of electricity. This lowers the noise level significantly. It is noted that the work by Sirohi and Chopra (2000) considers frequencies in the range 5-500 Hz. For workover risers, the critical frequencies will generally be much lower. Though there are ways of adapting the system to measure lower frequencies, the sensor will lose its accuracy when the strain rate approaches quasi-static (Sirohi & Chopra, 2000).

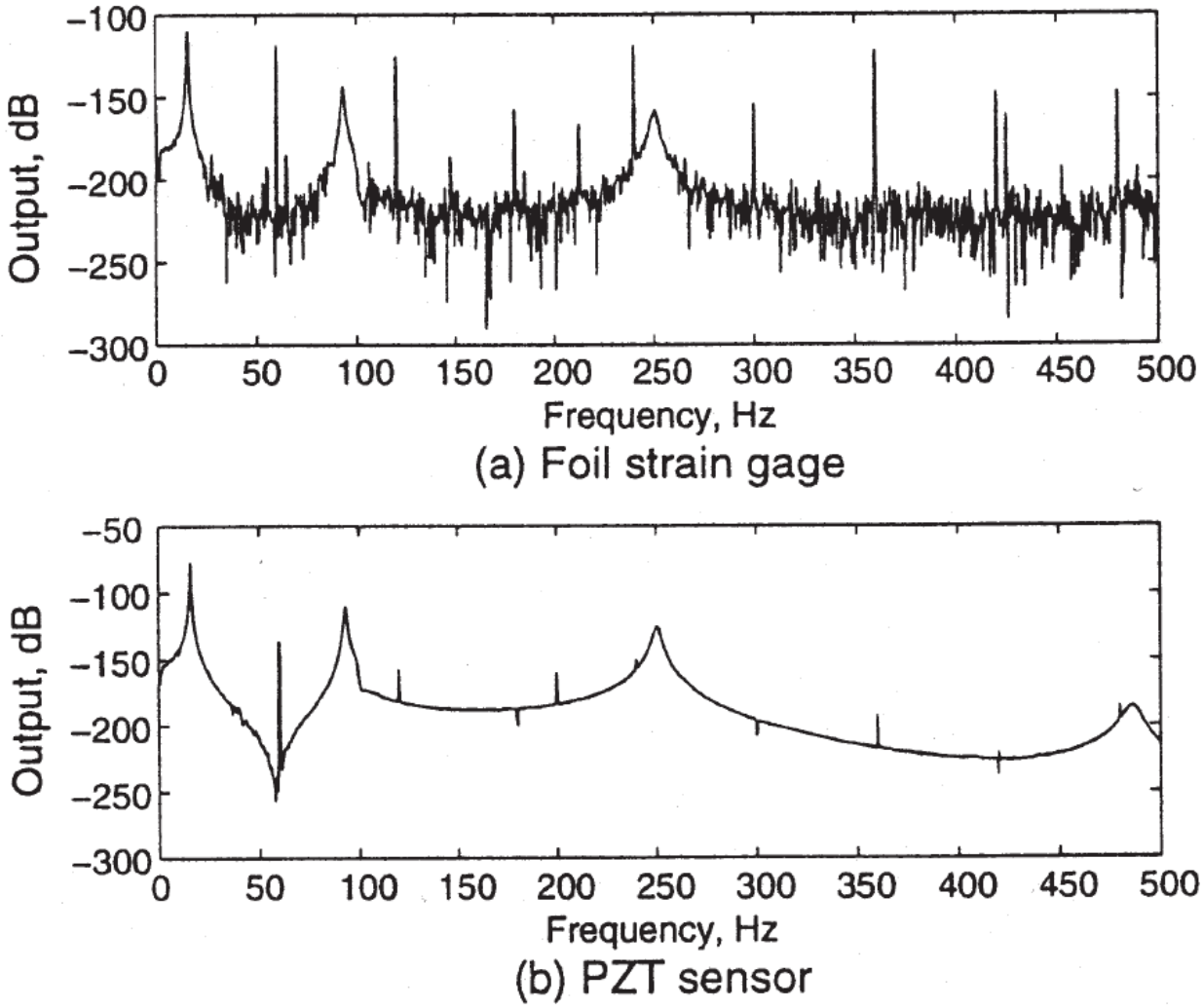

Figure 3.2: Comparison of (a) foil gage and (b) piezoelectric sensor (Sirohi & Chopra, 2000)

3.3 Fiber Optic Strain Sensors

There are several different concepts for fiber optic strain sensors. Tennyson et al. (2001) state that five different types are commercially available. In this thesis, the fiber Bragg grating (FBG) will be considered. According to Tennyson et al. (2001), the FBG is in a glass fiber core, which has been processed to make it absorb a narrow range of frequencies. The center of absorbed wavelengths is called the Bragg wavelength. When the gage is strained, the FBG responds with

a linear shift in wavelength. Equation (3.1) can be used for calculating strain as a function of wavelength shift (Tennyson et al., 2001).

$$\frac{\Delta\lambda}{\lambda_B} = GF * \varepsilon + \beta * \Delta Temp \quad (3.1)$$

Where:

$\Delta\lambda$: Wavelength shift

λ_B : Bragg wavelength

GF : FBG gage factor

β : Thermal correction factor

$\Delta Temp$: Temperature relative to the temperature at installation

An illustration of how the fiber Bragg grating affects the transmitted light is found in figure 3.3. Maaskant et al. (1997) mentions some very convenient properties of this sensor:

- The sensor can be extremely small, physically.
- The sensor is an intrinsic part of the optical fiber, making it more durable.
- Several sensors can be attached to a single optical fiber, by utilizing different Bragg wavelengths for each sensor.
- As there is no electric equipment at the sensor, it is immune to electromagnetic disturbance.

Even with all of these advantages, the FBG sensor is not ideal for all usages. An important drawback of the FBG sensor is its inability to measure dynamic strains, as reported by Robert F (2001). He reports that the strain must be constant throughout the duration of the scan, typically a few seconds. This constraint must be overcome if the FBG strain sensor is to be used for monitoring a workover riser. Modern optical sensor technology is still a relatively young field, dating back to the discovery of the laser in 1960 (Grattan & Sun, 2000). The development since the early 1970s has been enormous (Grattan & Sun, 2000), and therefore it is possible that the issues stated by Robert F (2001) have already been addressed.

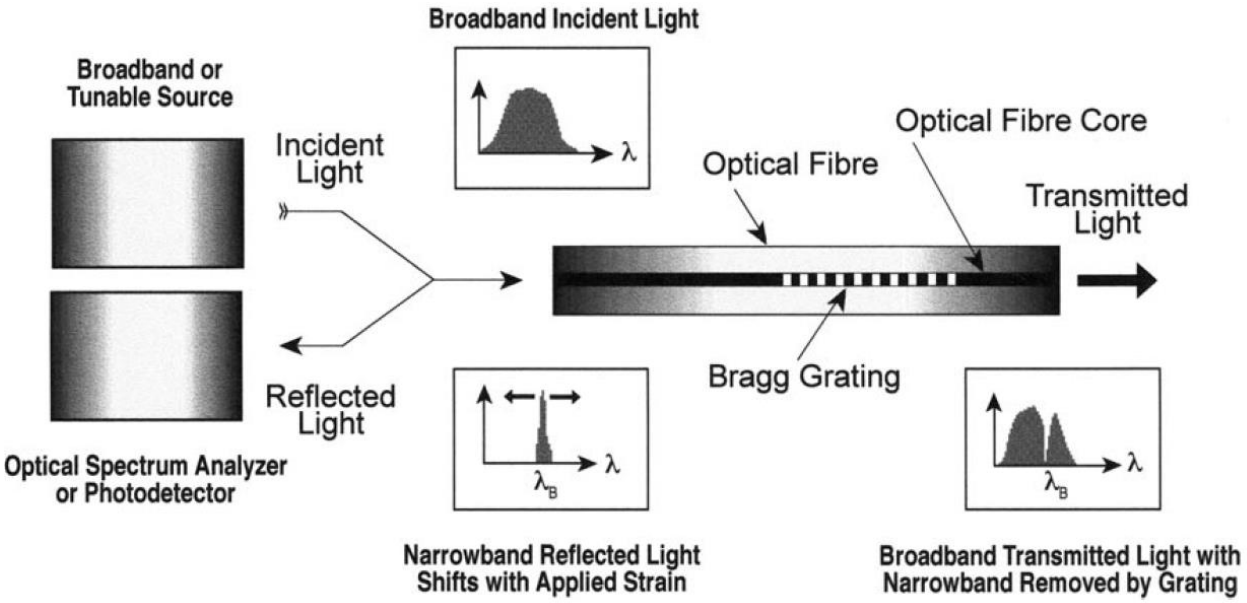

Figure 3.3: Illustration of the FBG strain measuring concept (Tennyson et al., 2001)

3.4 Strain Measuring on a Workover Riser

On the relevant workover riser, strain sensors are installed on two components: the stress joint and the tension joint. The sensors are conventional foil sensors. Though these sensors have known issues with noise and temperature sensitivity, the technology has been field-proven over long time. These small, robust sensors are the preferred solution for measuring strain in such a harsh environment. When it comes to noise, it is expected that filtering of high-frequent oscillations can remove most of the disturbances. Due to the long and slender design of a riser, its oscillations are quite slow. High-frequent oscillations do not exist, and these frequencies are thus considered noise. As for the temperature dependency, the situation is different for the lower and upper strain monitoring. At the stress joint, the environmental temperature can be considered static. There can be significant differences between operations, due to different well stream temperatures. Throughout an operation however, this temperature is expected to be close to static. Some fluctuations in well stream are expected, but these fluctuations are of small amplitude when reaching the sensor. At the tension joint, significant temperature fluctuations must be expected. It is also expected that the stress joint sensor will provide the most useful information when the riser is connected. When the riser is hung-off, the tables are turned. Then, the stress joint sensor is not expected to provide any useful information.

4. Flexcom and RIFLEX

Flexcom and RIFLEX are both analysis softwares, dedicated for the analysis of slender structures in marine environments. Flexcom is developed by MCS Kenny. This software is typically used for global analysis of slender marine structures, typically top tensioned risers, flexible risers, umbilicals and pipe laying operations. RIFLEX is developed by Marintek. It is claimed that this software is suited for all kinds of slender structures. In chapter 4, statements regarding Flexcom and RIFLEX are found from their respective user manuals. The Flexcom manuals are the introductory manual ("Flexcom - Introductory Manual," 2013), and the technical manual ("Flexcom - Technical Manual," 2013). For RIFLEX, the user manual is used ("RIFLEX User Manual," 2013), as well as the theory manual ("RIFLEX Theory Manual," 2013). In the following sections, some fundamental aspects of how Flexcom and RIFLEX perform analyses are explained.

4.1 Flexcom Finite Element Formulation

Flexcom uses a hybrid beam-column element, which was developed by McNamara et al. (1988) for analysis of flexible risers. Bar elements are also available, but these will not be discussed further, as they have not been used in this thesis. An issue for finite element analysis of slender structures is the presence of large displacements, even though the strains are small. A flexible riser has an axial stiffness several times higher than the transverse stiffness and bending stiffness. The high axial stiffness makes dynamic changes in length near negligible. Traditional formulations, like Bernoulli-Euler bending theory extended for large deformations, are not suitable for solving these problems. This is due to the extra requirement of virtually no axial elongation (McNamara et al., 1988).

4.1.1 Global and Element Coordinate Systems

In Flexcom, all elements have their own coordinate system. The local element coordinate system is placed as seen in figure 4.1, with its origin in node 1. The local x-axis extends directly through node 2, while the other axes remain fixed with respect to the twist of node 1.

4.1.2 Element Stiffness

In order to avoid an ill-conditioned set of equations, the axial force and axial strain are assumed independent. The local, internal generalized stresses for the virtual work equation are found in equation (4.1). The axial stress and axial strain are related by the Lagrangian constraint condition found in equation (4.2). Both equations are from McNamara et al. (1988). Equations (4.1) and (4.2) are combined, and second order strain is introduced. By including second order strain, the convergence rate of the solution algorithm is significantly improved (McNamara et al., 1988). The resulting expression for virtual work is seen in equation (4.3).

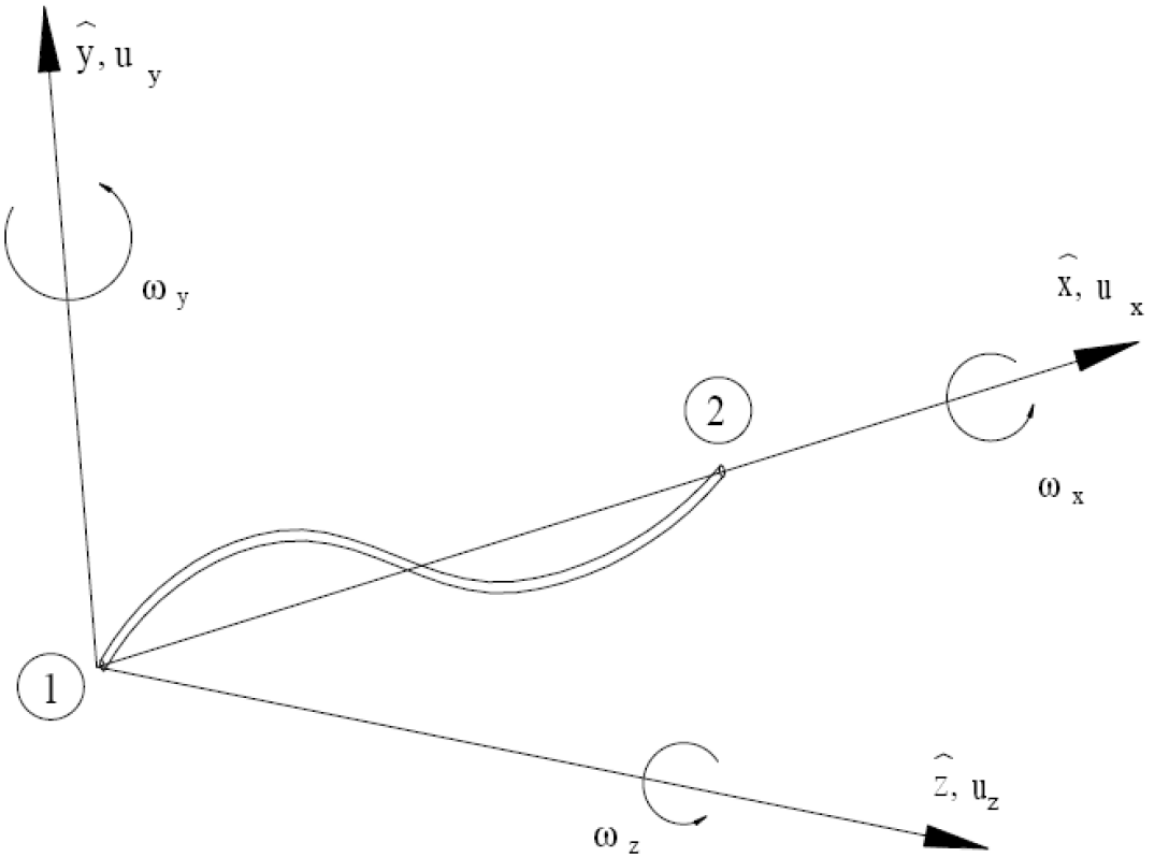

Figure 4.1: Flexcom local element coordinate system

$$\int_0^L (N\delta\varepsilon_x + BM\delta\kappa)dx \tag{4.1}$$

$$\int_0^L \left(\varepsilon_x - \frac{N}{EA}\right)\delta N dx = 0 \tag{4.2}$$

$$U = \int_0^L \left[N\delta\varepsilon_x + BM\delta\kappa + \left(\varepsilon_x - \frac{N}{EA}\right)\delta N + Tens_{eff}\frac{d(vd)}{dx}\frac{d(\delta(vd))}{dx}\right]dx_1 \tag{4.3}$$

Where:

A : Cross-sectional area

BM : Bending moment

E : Young's modulus

L : Element length

N : Axial force

$Tens_{eff}$: Effective tension

U : Internal virtual work

vd : Local transverse displacement

δ : Factor denoting a variation of the variable

ε_x : Axial strain

κ : Curvature

A 2D element of this kind will have seven degrees of freedom. The first six DOFs are corresponding to a standard beam element, which has three nodal DOFs. The seventh DOF is the axial force. The axial force is constant over the length of the element, making it proportional with the axial strain (McNamara et al., 1988). As the axial force is constant, only one DOF is needed to describe it. The corresponding 3D element used by Flexcom has 14 DOFs, where both axial force and torque are interpolated independently. The equations of (4.4) to (4.8) are defined in order to formulate the problem on matrix form (McNamara et al., 1988).

$$\overline{\varepsilon} = [\varepsilon_x \quad \kappa \quad N]^T \tag{4.4}$$

$$\overline{\sigma} = \left[N \quad BM \quad \varepsilon_x - \frac{N}{EA}\right]^T \tag{4.5}$$

$$\overline{\sigma} = \boldsymbol{D}\overline{\varepsilon} \tag{4.6}$$

$$\boldsymbol{D} = \begin{bmatrix} 0 & 0 & 1 \\ 0 & EI & 0 \\ 1 & 0 & -1/EA \end{bmatrix} \tag{4.7}$$

$$\overline{\varepsilon} = \boldsymbol{B} * [ud_1 \quad vd_1 \quad \phi_1 \quad n \quad ud_2 \quad vd_2 \quad \phi_2] \tag{4.8}$$

$$\widehat{\boldsymbol{k}} = \int_0^L \boldsymbol{B}^T \boldsymbol{D}\boldsymbol{B} dx + \boldsymbol{K}_G \tag{4.9}$$

Where:

$\boldsymbol{B}$	:	Strain-displacement relationship
$\boldsymbol{D}$	:	Stress-strain relationship
I	:	Second moment of inertia
$\widehat{\boldsymbol{k}}$	:	Element local stiffness matrix
$\boldsymbol{K}_G$	:	Initial stress stiffness matrix
ud_n	:	Local axial displacement in node n
vd_n	:	Local transverse displacement in node n
$\overline{\varepsilon}$	:	Strain vector
$\overline{\sigma}$	:	Stress vector
ϕ_n	:	Local rotational displacement in node n

Given the definitions in equations (4.4) to (4.8), the element local stiffness matrix can now be found, as seen in equation (4.9) (McNamara et al., 1988). This is defined with respect to the local element coordinate system.

4.1.3 Static and Dynamic Equilibrium

In the technical manual for Flexcom, the static and dynamic equations of equilibrium are given. These equations are seen in equations (4.10) and (4.11) respectively. When considering the equations, it is clear that they are very similar to the static and dynamic equilibrium equations normally used. Except for the part considering rigid body motions, these equations could be found in any finite element analysis textbook. The damping part of the dynamic equation is Rayleigh damping.

$$\boldsymbol{K}d = \overline{F} + \boldsymbol{K}d^{rb} \tag{4.10}$$

$$\boldsymbol{M}\ddot{d} + (\alpha_1 \boldsymbol{M} + \alpha_2 \boldsymbol{K})\dot{d} + \boldsymbol{K}d = \overline{F} + \boldsymbol{K}d^{rb} \tag{4.11}$$

Where:

$d, \dot{d}, \ddot{d}$	:	Nodal displacement, velocity, acceleration
d^{rb}	:	Rigid body nodal displacements
$\overline{F}$	:	Static and dynamic load vector
$\boldsymbol{K}$	:	Global stiffness matrix
$\boldsymbol{M}$	:	Global mass matrix
α_1	:	Mass Rayleigh damping coefficient
α_2	:	Stiffness Rayleigh damping coefficient

4.2 RIFLEX Finite Element Formulation

The finite element formulation in RIFLEX is adapted to the combination of large displacements and small strains, similar to Flexcom's formulation. Like Flexcom, RIFLEX allows both bar and beam elements, but bar elements will not be covered here. The beam elements are formulated by a co-rotated ghost reference, which has amongst others been described by Mollestad (1983). An illustration is shown in figure 4.2. By this reference mode, each element is assigned a reference configuration, which is a rigid body displacement from its initial configuration. Deformations are then described with basis in the reference configuration (Mollestad, 1983).

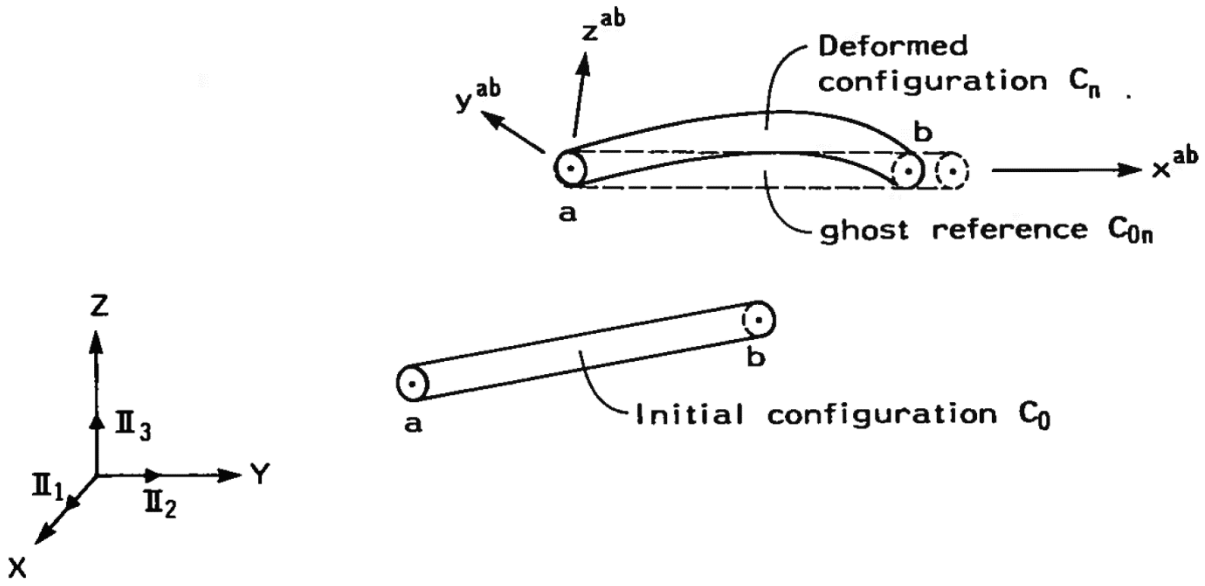

Figure 4.2: Co-rotated ghost reference illustration (Mollestad, 1983)

Beam elements in RIFLEX have 12 degrees of freedom, as is conventional for 3D beam elements with two nodes. The element degrees of freedom are illustrated in figure 4.3. Thus, RIFLEX does not de-couple axial stiffness from its equation system as Flexcom does. This makes RIFLEX potentially less suited than Flexcom for cases where the difference between axial and bending stiffness is large.

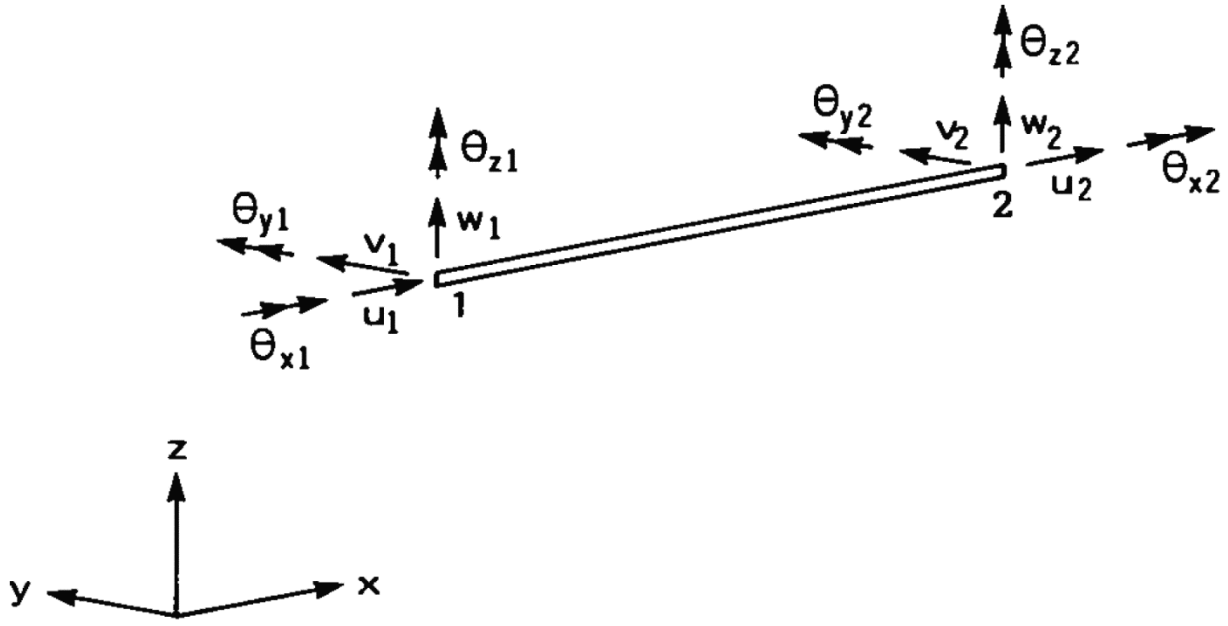

Figure 4.3: Element degrees of freedom in RIFLEX (Mollestad, 1983)

4.3 Relevant Element Types

All elements in Flexcom uses the hybrid beam-column formulation explained in section 4.1. It does however have several optional ways of defining these elements, enabling analysis of virtually any slender construction in a marine environment. RIFLEX does as mentioned allow the use of bar elements as well as beam elements, though only beam elements have been used in this thesis.

4.3.1 Conventional Riser Elements

In Flexcom, a simple riser (rigid or flexible) is simply modeled by several beam-column elements. The user can specify the riser to be rigid or flexible, though the only difference between these options are the amount of input parameters required. A rigid format will for instance calculate bending stiffness from the Young's Modulus and diameters, while a flexible format allows such parameters to be defined independently by the user. In RIFLEX, the input format is similar to the flexible format in Flexcom. All parameters, like unit weight, bending stiffness and shear stiffness are user defined.

4.3.2 Tapered Stress Joints

Flexcom and RIFLEX both have built-in options to create tapered stress joints. Defining such a joint is similar to defining a normal, rigid riser cross section in Flexcom. Each parameter require two values, one for each end. Between the two ends of the stress joint, the diameters are assumed to vary linearly. If a non-linear variation of cross-section should be desired, the user would have to specify a number of joints himself/herself. Though the definition of tapered stress joints might give the impression that the elements' parameters will vary continuously, this is not supported. The variations of the parameters are discretized into several normal elements, each with different cross section. Thus, a tapered stress joint could just as well be defined manually by the user, though this would be extremely inconvenient.

4.3.3 Heave Compensated Tensioner Systems

Flexcom does not provide a built-in method of defining a heave compensated tensioner system directly. RIFLEX allows the definition of tensioner systems, but this has not been utilized in this thesis, for the sake of consistency. Tensioner systems are thus represented by alternative elements. Based on advice from Aker Solutions, the tensioner systems were modeled by conventional elements, instead of springs. The stress-strain relationship of the beam elements has been custom defined, so that the stress is at a constant level, independent of strain. This is similar to applying a simple point load to the structure. However, where a point load would be fixed in the global or local reference frame, the described system is more adaptive with respect to direction. Springs are not used, as non-linear spring elements tend to cause issues in Flexcom.

4.4 Environmental Loads

Slender marine structures can be exposed to a variety of environmental loads. In order to analyze these structures accurately, the analysis software must be able to represent all significant loads. Flexcom and RIFLEX both have options for including several different kinds of loads. The most important of these are waves and current. Other parameters that can be considered include temperature loads, Coriolis force of internal fluids and more. For the relatively simple case of analyzing a TTR, it is expected that the significant environmental loads will be waves, current and vessel motion.

4.4.1 Hydrodynamic Loads

Flexcom and RIFLEX calculate hydrodynamic loads according to Morison's equation in three dimensions. The relative velocity and acceleration between structure and water are calculated as the sum of the contributions from each load. For instance, the velocity used for calculating drag force have can have contributions from wave action, current and structure velocity. Prior to calculating force, the velocity and acceleration are decomposed into the local coordinate system for each element. The forces are then calculated for both normal and tangential direction. Morison's equations are seen in equation (4.12) and equation (4.13).

$$F_D = \frac{1}{2}\rho_w c_d A_p u_{rel}|u_{rel}| \quad (4.12)$$

$$F_I = \rho_w c_m V_d \dot{u} \quad (4.13)$$

$$c_m = 1 + c_a \quad (4.14)$$

Where:

A_p : Projected area

c_a : Added mass coefficient

c_d : Drag coefficient

c_m : Inertia coefficient

F_D : Drag force

F_I : Inertia force

$u_{rel}, \dot{u}_{rel}$: Relative velocity, relative acceleration

V_d : Displaced volume

ρ_w : Water density

It is seen from Morison's equation that the calculation of forces are a rather simple procedure. Assuming known, time-independent values for the drag and inertia coefficients, the resulting force is only dependent of the relative velocity and acceleration. However, Sarpkaya (1981) argues that the validity of Morison's equation on its basic form should be questioned at certain conditions. In the introduction of this article, he states:

> *It is rather surprising that the preoccupation with the Morison equation tends one to forget the difficulties associated with simple flows and tempts one to attribute greater generality to Morison's equation than it deserves (at least more that its originator has intended to (…))(Sarpkaya, 1981).*

It is further stated, by Sarpkaya (1981), that Morison's equation seems best adapted to Keulegan-Carpenter outside the range 8-25. The formula for the Keulegan-Carpenter (KC) number for a cylinder is found in equation (4.15).

$$Kc = \frac{uT}{D} \tag{4.15}$$

Where:

D : Diameter

Kc : Keulegan-Carpenter number

T : Period of oscillation

u : Velocity

It is explained by Sarpkaya (1981) that Morison's equation performs poorly in this range due to the simplicity of the coefficient. These coefficients cannot account for history of motion. Neither can they account for higher frequency components due to rapid changes in the flow. There have been made attempts at improving and replacing Morison's equation, but by 1981, these had all been unsuccessful (Sarpkaya). At present day, these equations are still being used. Morison's equation is clearly far from perfect, but it is still widely used due to its simplicity and the lack of alternatives. It is also remarkably accurate in certain domains of KC- and Reynolds number (Sarpkaya, 1981). A considerable effort has been made to estimate drag and inertia coefficients as accurately as possible. Figure 4.4 shows an estimate of these coefficients as a function of KC number based on a least square method (Wolfram & Naghipour, 1999). It is seen that for low KC numbers, the drag coefficient is scattered. A large amount of uncertainty must necessarily be expected if one wishes to use Morison's equation in this domain. It is however also noted that for KC numbers above seven, the scatter diminishes.

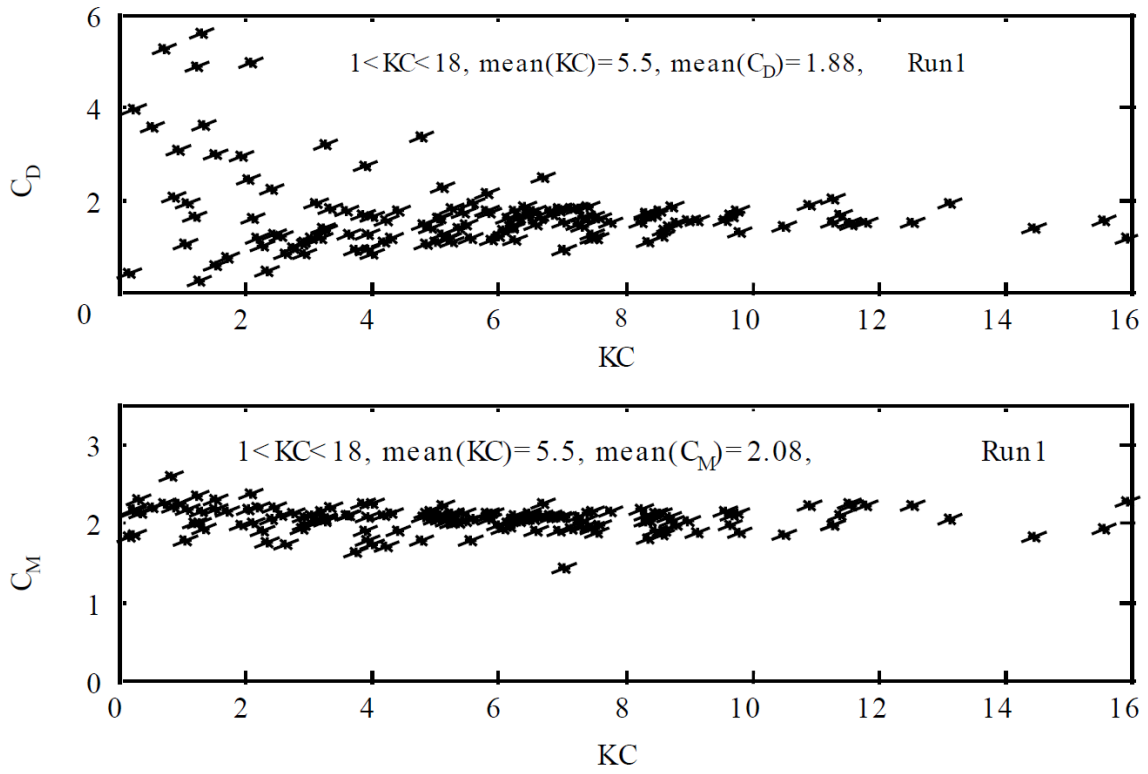

Figure 4.4: Drag and inertia coefficients estimated (Wolfram & Naghipour, 1999)

In this thesis, the majority of analyses, starting at chapter 6, are done with a significant wave height of four meters, and a peak period of nine seconds. The diameter of the riser joints are 0.241 meters. Assuming an Airy wave with these parameters, it is found that the horizontal particle velocity amplitude is approximately 1.4 m/s at the surface, and quickly diminishing with depth. The resulting KC numbers versus depth, according to equation (4.15), are seen in figure 4.5. In the figure, the grey area marks where the KC numbers are in the range 8-25. It is seen that the region is small.

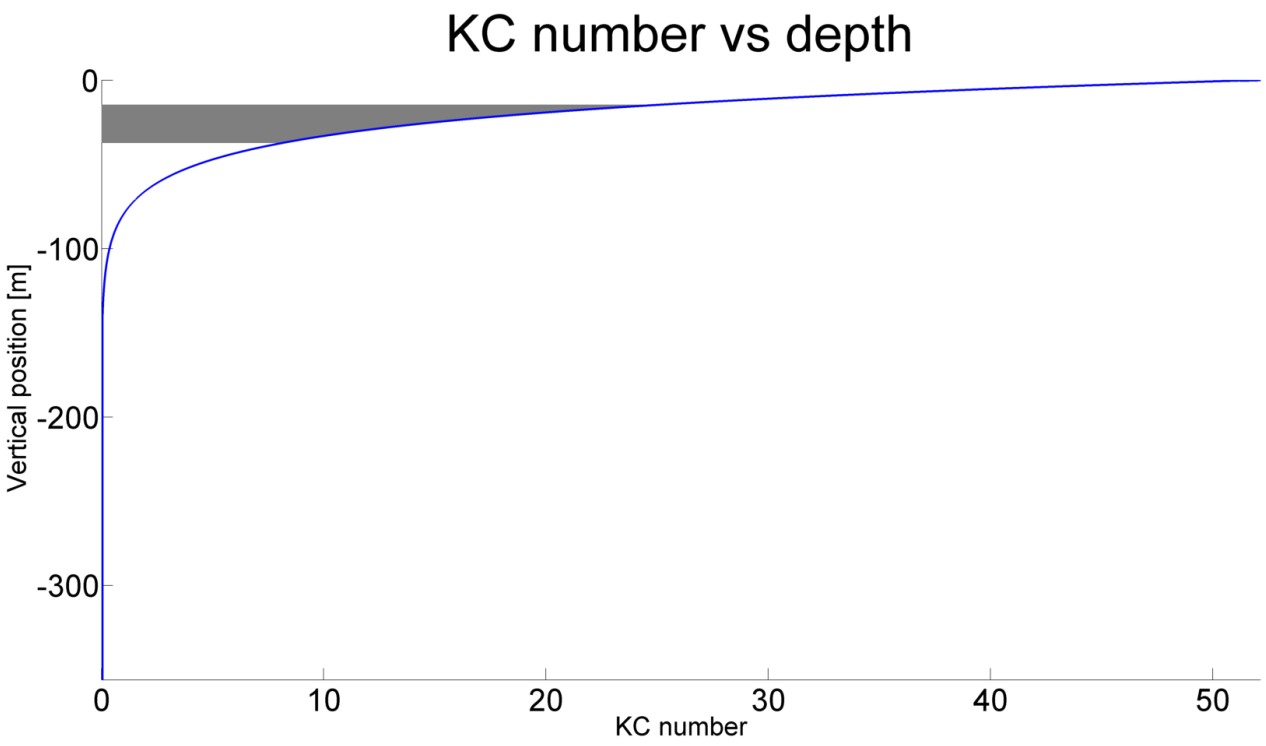

Figure 4.5: KC numbers for a workover riser at 356 m water depth

According to Söding et al. (1990), using mean force coefficients generally give good prediction of peak force for all KC numbers, particularly for fatigue calculations. For these calculations, frequently occurring loads are important. Estimation using mean force coefficients may cause too small values for extreme loads to be predicted (Söding et al., 1990). In this thesis, the primary focus is on fatigue. Thus, mean force coefficients are found satisfactory.

4.5 Definition of Wave Loads

Flexcom and RIFLEX share many possibilities for applying wave loads. Both softwares include the definitions of more than one regular wave, as well as several wave spectra. The possible wave definitions in Flexcom and RIFLEX are listed in table 4.1 and table 4.2 respectively.

Table 4.1: Available wave definitions in Flexcom

Regular Waves	***Irregular waves***
Regular Airy	Jonswap
Stokes V	Ochi-Hubble
Dean's Stream	Pierson-Moskowitz
	Torsethaugen
	User-defined

It is also possible to combine sea-states. For example, multiple regular Airy waves can be defined. In addition, regular Airy waves can be combined with one or more irregular sea-states. All wave spectra can be combined with any number of other spectra. The spectra can have a

dominant direction, or they can be omnidirectional. In the following two sections, two representative sea states will be discussed.

Table 4.2: Available wave definitions in RIFLEX

Regular Waves	***Irregular waves***
Regular Airy	Bretschneider one/two
Stokes V	Derbyshire scott
	Jonswap
	Jonswap double peaked
	Ochi
	User-defined

4.5.1 Regular Airy Wave

Regular Airy waves are a linear wave theory, assuming horizontal sea floor and infinite extent of the sea surface (Faltinsen, 1993). The formulas for instantaneous wave elevation, horizontal particle velocity and vertical particle velocity are given in equations (4.16), (4.17) and (4.18) respectively.

$$\zeta(x,t) = \zeta_a \sin(\omega t - kx) \tag{4.16}$$

$$u_p(x,t,z) = \omega\zeta_a \frac{\cosh(k(z+h))}{\sinh(kh)} \sin(\omega t - kx) \tag{4.17}$$

$$w_p(x,t,z) = \omega\zeta_a \frac{\sinh(k(z+h))}{\sinh(kh)} \cos(\omega t - kx) \tag{4.18}$$

$$k = \frac{2\pi}{\lambda}$$

Where:

h : Water depth (absolute value)

k : Wave number

t : Time

u_p : Wave particle velocity in x direction

w_p : Wave particle velocity in z direction

x : Horizontal direction of wave propagation

z : Vertical axis, zero at mean water level

ζ : Instantaneous wave elevation

ζ_a : Wave amplitude (half wave height)

λ : Wave length

ω : Wave angular velocity

4.5.2 The Pierson-Moskowitz Spectrum

The Pierson-Moskowitz spectrum is used to describe a fully developed seastate (Pierson Jr & Moskowitz, 1964). Equation (4.19) gives Flexcom's Pierson-Moskowitz formulation. Figure 4.6 shows a Pierson-Moskowitz spectrum. The Pierson-Moskowitz spectrum and its values are chosen arbitrarily in this section, for illustrative purposes. The spectra applied in the analyses for this thesis are JONSWAP spectra. JONSWAP's formulation in Flexcom is somewhat more complex, and has thus not been included in this thesis.

$$S(f) = \frac{{H_s}^2}{4\pi {T_z}^4 f^5} exp\left[\frac{-1}{\pi {T_z}^4 f^4}\right] \quad (4.19)$$

Where:

f : Wave frequency in Hertz

H_s : Significant wave height

S : Spectrum

T_z : Mean zero up-crossing period

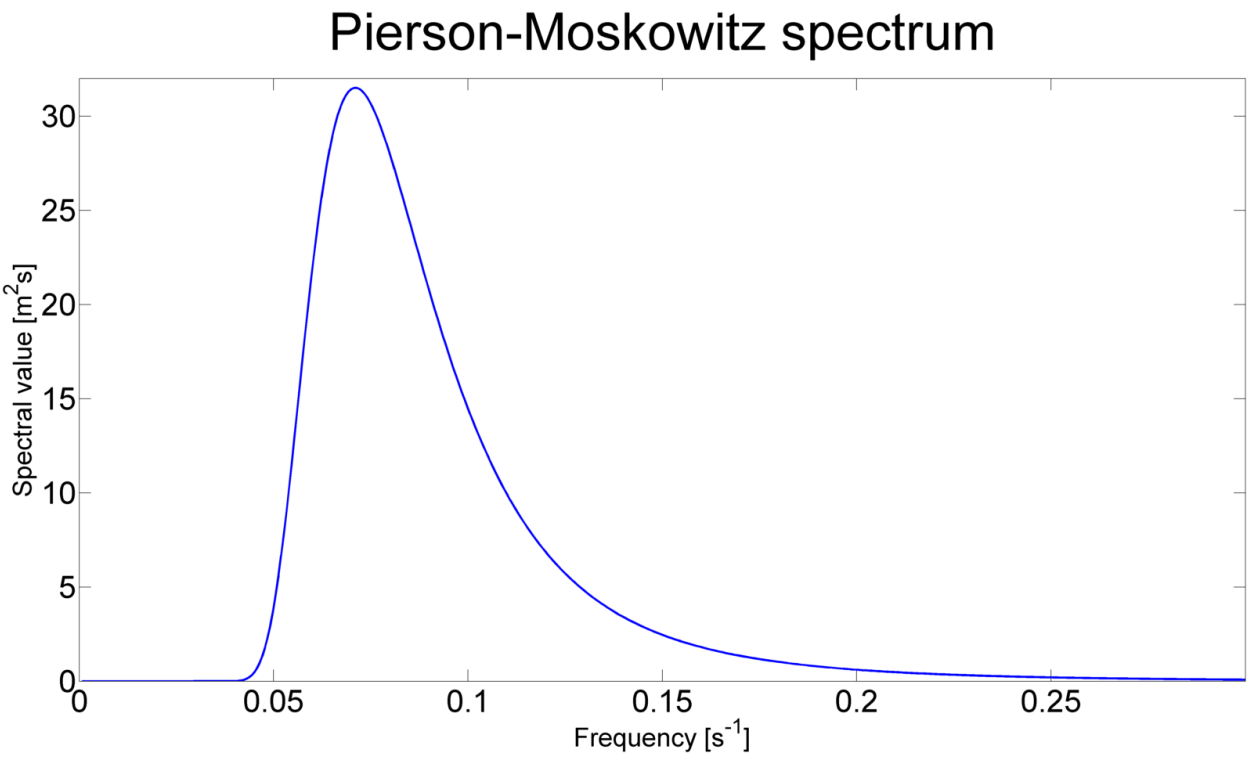

Figure 4.6: An illustrative Pierson-Moskowitz spectrum

4.6 Vessel Motion

In Flexcom, vessel position and motion can be defined in several ways. The only necessary parameter is the vessel's initial position. In addition, parameters like static offset, constant velocity and RAO's can be added. It is also possible to prescribe the vessel's motion, though this cannot be combined with RAO's. RIFLEX also have many opportunities for specification of vessel motion.

4.6.1 First and Higher Order Response

For the analysis of a top tensioned riser, wave excitation on the riser itself can be an important factor, in addition to the wave generated vessel response. It is thus important that the vessel motion is realistically dependent on the waves. This makes prescribed vessel motions unfeasible, unless the seastate realization is known in advance, and vessel motions are calculated. The preferred solution will thus be to calculate vessel motions by wave excitation and RAOs. A RAO is a first order transfer function. Vessel response is assumed proportional with wave height, an assumption that can be questioned. This means that only first order effects are represented, while higher order effects are neglected. In most cases, this will not be a problem. The magnitude of higher order effects are generally far smaller than first order effects. However, if a part of the analyzed system should have a resonant frequency corresponding to the frequency of a higher order effect, this must be considered. Flexcom has options for including both slow drift and sum frequency effects. For the analysis of a workover riser, sum frequency effects are considered irrelevant. Due to the high frequency of these effects, they will not excite any

relevant riser response. Slow drift can have a significant contribution, as this effect can be resonant with the support vessel's mooring system.

4.7 Time and Frequency Domain

Both Flexcom and RIFLEX have built-in possibilities for analysis in time domain and frequency domain. When performing analyses with irregular sea in the time domain, a random seastate realization is created, based on the selected wave spectrum. Then, forces and motions are calculated at each time step. This create time series of forces and responses, which will mimic a real operation. When analyzing in the time domain, the solution algorithms allow non-linear effects. Analyses done in the frequency domain investigates how the riser system responds to specific frequencies of excitation. The result of an analysis in the frequency domain will thus not be time series, but spectra of response and forces. After analysis, spectra can be created from time domain results, and representative time series can be generated from spectra. For an analysis of a top tensioned riser, time domain analysis will generally yield the most accurate result, while frequency domain analysis is more cost-effective (Morooka et al., 2006). According to Morooka et al. (2006), frequency domain analysis is most applicable in the early design stages, when an approximate and efficient analysis is desired. In this thesis, the analysis should be as accurate as possible. To compare analysis results with real measured data, time series are required. This can be generated from frequency domain results, but the preferred method is to generate time series by time domain analysis. Due to the desired accuracy and the necessity for time series, the preferred analysis domain will be time domain.

5. System Specifications and Environmental Data

In this thesis, a particular workover riser is analyzed. The relevant riser is the Statoil Kristin (Aker Subsea Ltd.) 10 ½" monobore workover riser operated from the semisub Scarabeo 5. This riser is designed for high pressures and temperatures. The water depth at the Kristin field varies from 356 to 372 meters. Extreme values for current, as well as wave statistics are known. Other parameters, like wind, temperature and marine growth, are not considered. A full overview of input for the riser model, as well as wave statistics are found in appendix A. The riser model created is based on the riser's design report, which was provided by Aker Solutions.

5.1 Riser Specifications

The riser model, set up for CT operation, is seen in figure 5.1. A more detailed overview of the topside components are seen in figure 5.2. The model is based on a water depth of 356 meters. The properties of the riser joints are found in table 5.1. Material properties and hydrodynamic coefficients and are listed in table 5.2. In addition to the CT case, a model for WL operation has been created. The WL model does not differ from the CT model below the SFT. Above the SFT however, the WL model has lighter equipment. The TF and two pairs of bails are replaced by a single pair of long bails.

Table 5.1: Riser Joint dimensions

Parameter	***Value***
Riser joint length	12.8 m (42 ft.)
Riser Joint Outer diameter	0.2410 m
Riser Joint Inside diameter	0.1640 m
Riser Joint hydrodynamic diameter	0.2610 m
Pup Joint Outer diameter	0.2690 m
Pup Joint Inside diameter	0.1900 m
Pup Joint hydrodynamic diameter	0.2690 m

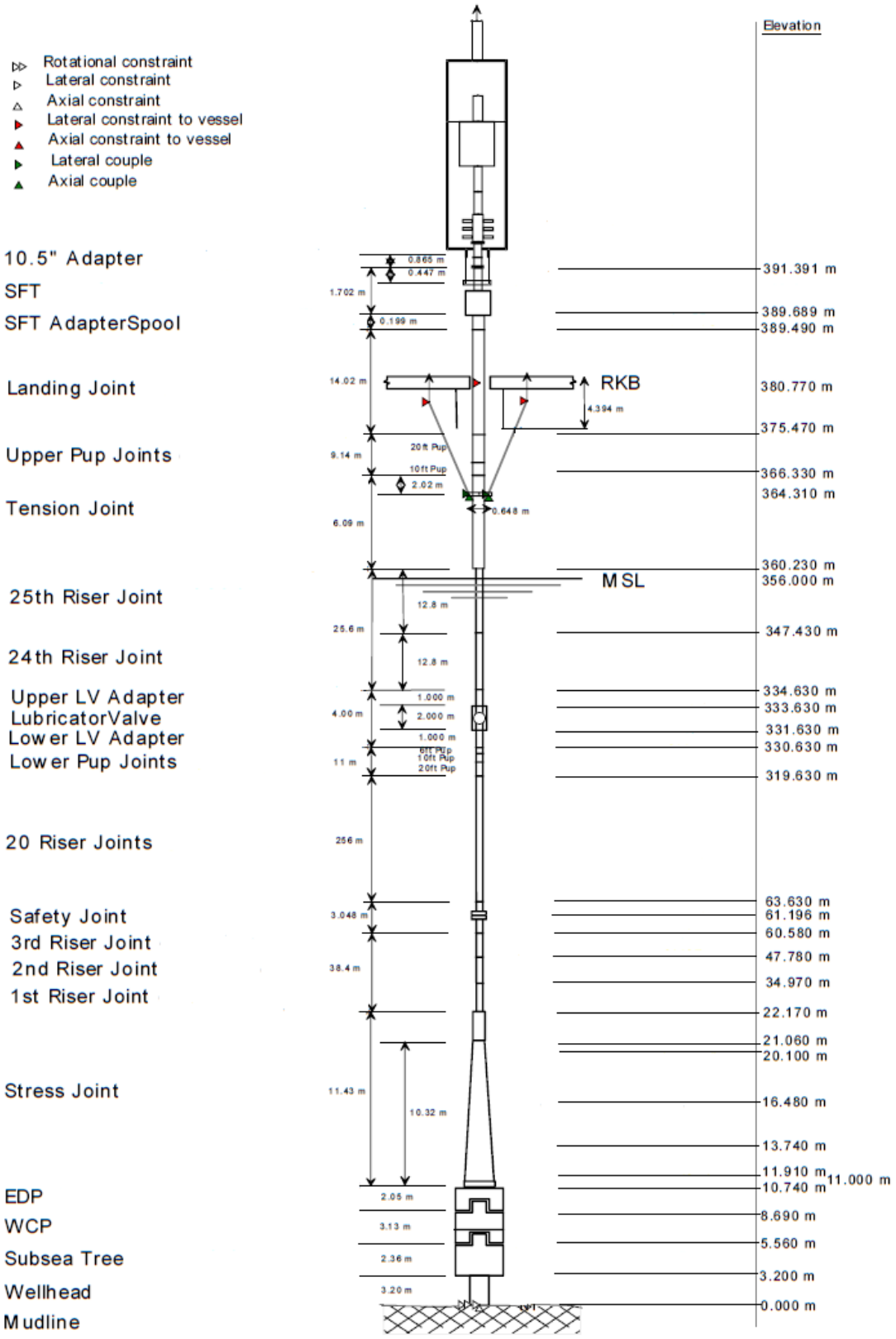

Figure 5.1: Global riser model set-up for CT

The hydrodynamic diameters in table 5.1 are used in order to achieve the correct inertia force. The same diameter will however not yield accurate drag force. In order to have both inertia and drag forces accurate, the drag coefficients are factored according to equation (5.1).

Table 5.2: Material and hydrodynamic properties

Parameter	***Value***
Yield Strength	552 MPa
Yield reduction at 145 °C	15 %
Density	7850 kg/m^3
Young's modulus	200 GPa
Max working pressure	93.79 MPa
Fluid density range	0.86-2070 kg/m^3
c_d	0.9
c_a	1.0
c_m	2.0

$$c_{df} = c_d \frac{D_d}{D_B} \tag{5.1}$$

Where:

c_d : Unfactored drag coefficient

c_{df} : Factored drag coefficient

D_B : Buoyancy diameter

D_d : Drag diameter

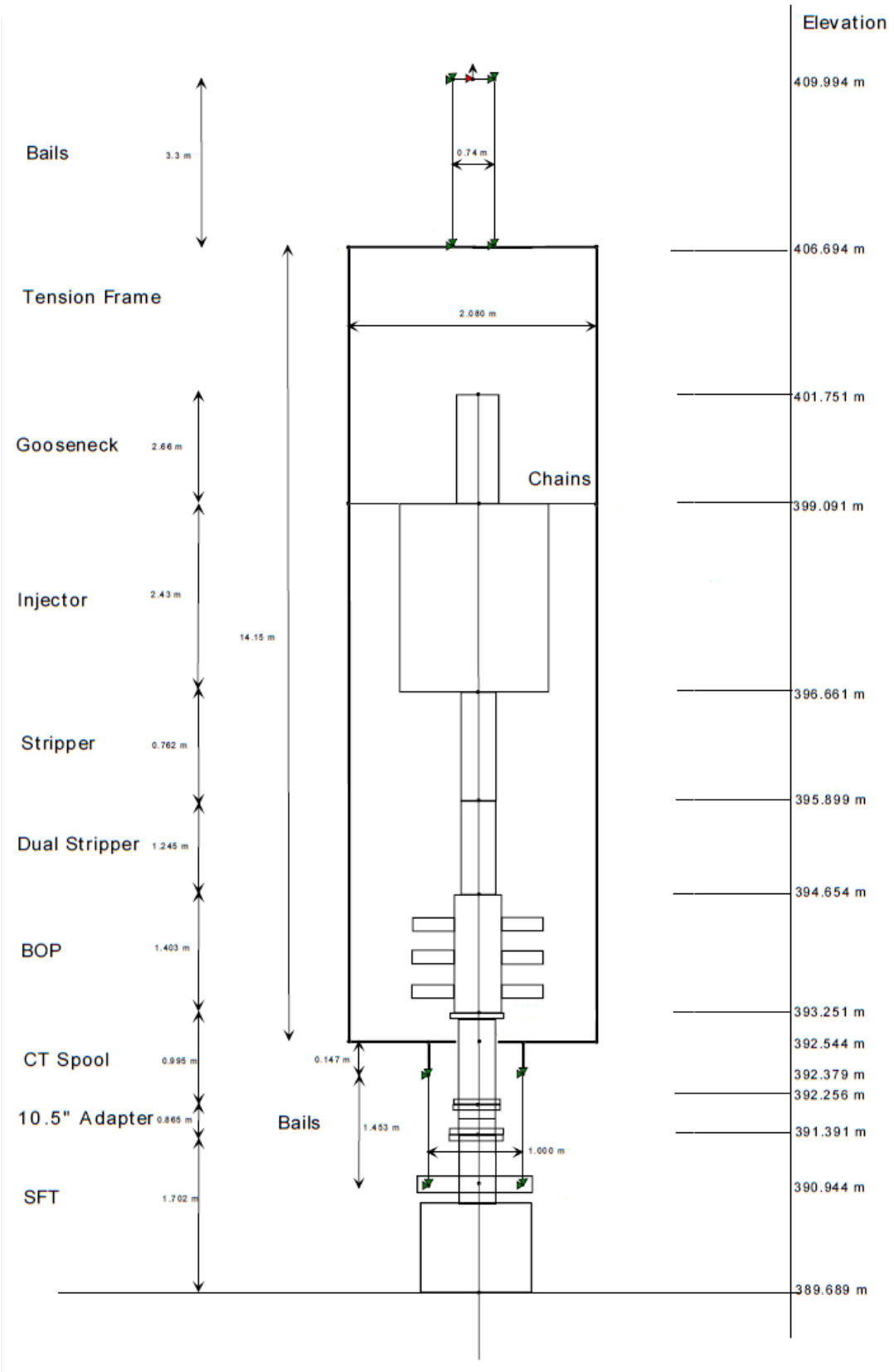

Figure 5.2: Close up of riser model tension frame

5.1.1 Stress Joint

During the design stage of the riser system, the stress joint was optimized. Its task is to provide a smooth transition of stiffness. The aim of the stress joint design is to provide a reasonably constant stress throughout its length, for any operating condition. The stress joint stiffness should also be as low as possible, to minimize the loading on the subsea connectors. The resulting stress joint dimensions are found in table 5.3. Any parameters not listed in the table are identical to the riser joint properties.

Table 5.3: Stress joint dimensions

Segment	Length (m)	Lower OD (m)	ID (m)
1	0.260	0.4272	0.1842
2	0.914	0.3085	0.1842
3	1.829	0.3029	0.1842
4	2.743	0.2934	0.1842
5	3.658	0.2834	0.1842
6	0.949	0.2713	0.1842
End	N/A	0.2686	0.1842

5.1.2 Riser Tension

Riser top tension is selected in order to provide the desired overpull. Based on the specifications of the EDP, it has been decided in the riser's design report that the desired overpull is 25 metric tons. As mentioned in section 2.1, tension can be applied to riser components through both the tension joint and the tension frame. The riser tension on the global model set up for CT operation is seen in figure 5.3. The tension applied from the wire-line tensioners through the tension joint carries the entire weight of the riser beneath. Hand calculations are used to validate the riser model, as the calculated riser tension corresponds to the values obtained from Flexcom. The data behind this is seen in appendix D.

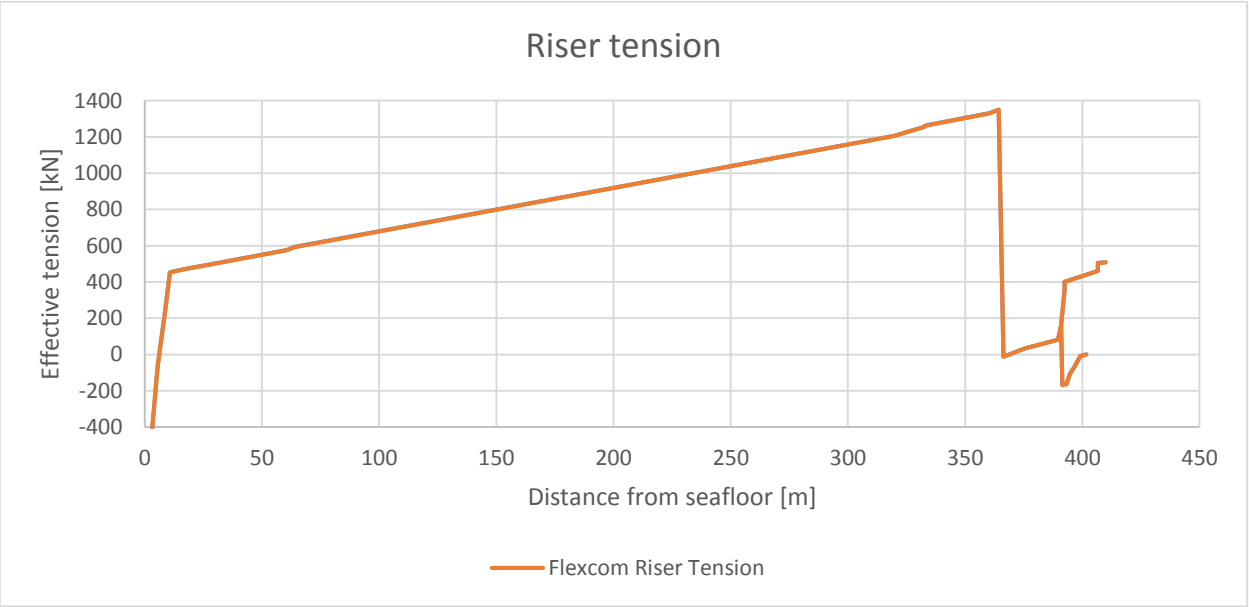

Figure 5.3: Riser Tension

5.2 Environmental Design Conditions

5.2.1 Current Extreme Values

The maximum expected current magnitudes are defined with return periods of 1, 10 and 100 years. The values are found in table 5.4. A visual representation of these values are seen in figure 5.4. These data are omnidirectional.

Table 5.4: Omnidirectional current extreme values

Depth (m)	***1 year return (m/s)***	***10 year return (m/s)***	***100 year return (m/s)***
20	0.67	0.74	0.83
50	0.61	0.68	0.75
100	0.58	0.65	0.71
200	0.52	0.59	0.65
300	0.51	0.57	0.63
Seafloor	0.43	0.47	0.51

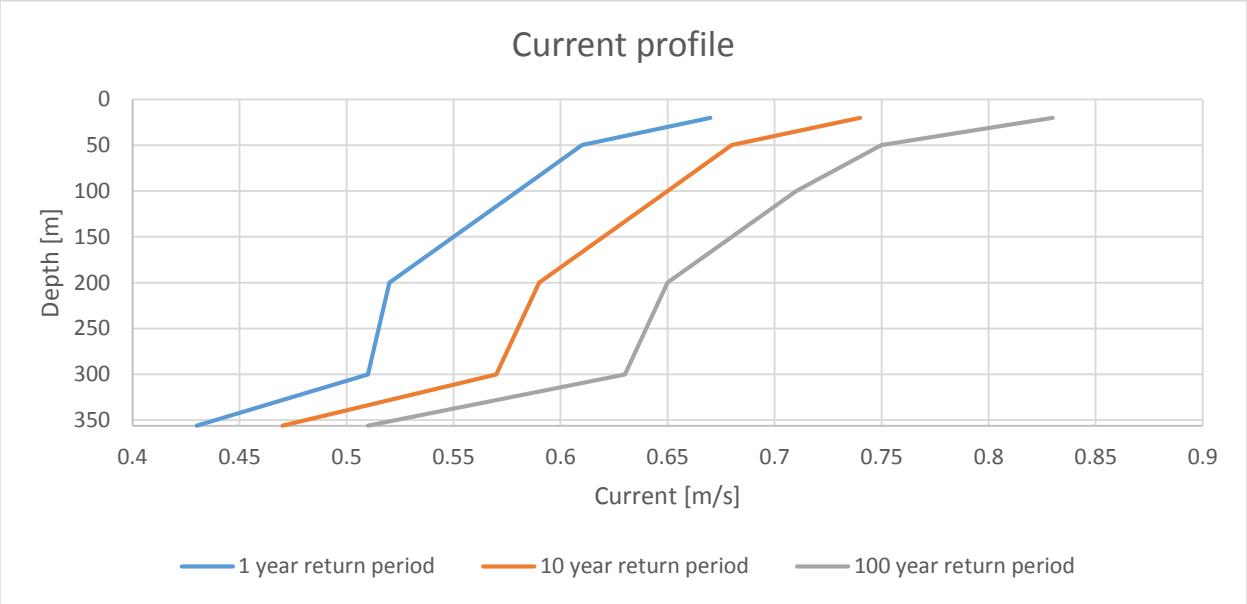

Figure 5.4: Omnidirectional current extreme values

5.2.2 Wave Statistics

The wave scatter diagram for the Kristin field is seen in table 5.5. The purpose of this data for fatigue calculations are explained in section 2.7. This data is also found in appendix A.

Table 5.5: Wave scatter diagram for the Kristin field

Hs	Peak Period									
	0-3	3-4	4-5	5-6	6-7	7-8	8-9	9-10	10-11	11-12
0-1	83	734	2300	3836	4332	3816	2857	1917	1194	707
1-2	9	319	2435	7725	13998	17408	16665	13251	9215	5813
2-3	0	5	161	1399	5181	10734	14711	14911	12083	8279
3-4	0	0	2	61	620	2660	6162	9023	9330	7386
4-5	0	0	0	1	26	301	1465	3679	5552	5624
5-6	0	0	0	0	0	13	174	910	2343	3451
6-7	0	0	0	0	0	0	8	113	589	1457
7-8	0	0	0	0	0	0	0	7	82	392
8-9	0	0	0	0	0	0	0	0	6	65
9-10	0	0	0	0	0	0	0	0	0	7
10-11	0	0	0	0	0	0	0	0	0	0
11-12	0	0	0	0	0	0	0	0	0	0
12-13	0	0	0	0	0	0	0	0	0	0
13-14	0	0	0	0	0	0	0	0	0	0
14-15	0	0	0	0	0	0	0	0	0	0
15-16	0	0	0	0	0	0	0	0	0	0
Sum	*92*	*1058*	*4898*	*13022*	*24157*	*34932*	*42042*	*43811*	*40394*	*33181*

Hs	Peak Period									Sum
	12-13	13-14	14-15	15-16	16-17	17-18	18-19	19-20	20-	
0-1	404	225	124	67	36	20	11	6	7	*22676*
1-2	3413	1901	1019	531	271	137	68	34	33	*94245*
2-3	4996	2738	1394	672	310	139	61	26	19	*77819*
3-4	4756	2609	1263	555	226	87	32	11	6	*44789*
4-5	4162	2402	1138	461	165	53	16	5	2	*25052*
5-6	3251	2137	1051	409	132	37	9	2	1	*13920*
6-7	1973	1638	911	366	112	28	6	1	0	*7202*
7-8	862	1009	702	318	101	24	4	1	0	*3502*
8-9	256	466	447	252	91	22	4	1	0	*1610*
9-10	51	155	222	168	75	21	4	1	0	*704*
10-11	7	37	83	90	53	19	4	1	0	*294*
11-12	1	7	23	37	31	14	4	1	0	*118*
12-13	0	1	5	12	14	9	3	1	0	*45*
13-14	0	0	1	3	5	4	2	1	0	*16*
14-15	0	0	0	1	2	2	1	0	0	*6*
15-16	0	0	0	0	0	1	1	0	0	*2*
Sum	*24132*	*15325*	*8383*	*3942*	*1624*	*617*	*230*	*92*	*68*	*2.92E5*

5.3 Vessel Data

The analyses in this thesis are based on operation from the platform Scarabeo 5, operating at the Kristin field. A picture of the platform is shown in figure 5.5. As can be seen in figure 5.1, the drill floor is approximately 24.8 meters above the mean sea level.

Figure 5.5: Picture of Scarabeo 5 (Fleumer, 2007)

5.3.1 Vessel RAO

Unfortunately, a complete RAO for the platform in question was not made available in time to be included in the analyses. The available RAO data are limited to head seas, represented by surge, heave and pitch. In other words, the available RAO data create realistic platform response as long is the incoming wave direction is head sea. However, waves that deviate from head sea will be decomposed into head sea and beam sea. Beam sea does not cause vessel response, which is clearly unrealistic. Thus, all analyses done in this thesis applies head sea. While the effect of different wave directions should ideally be studied, this would be far more important if the operations were performed from a ship. Due to the lack of a complete RAO, the effect of wave direction and wave spreading is unknown. Figure 5.6 shows the known RAO magnitudes.

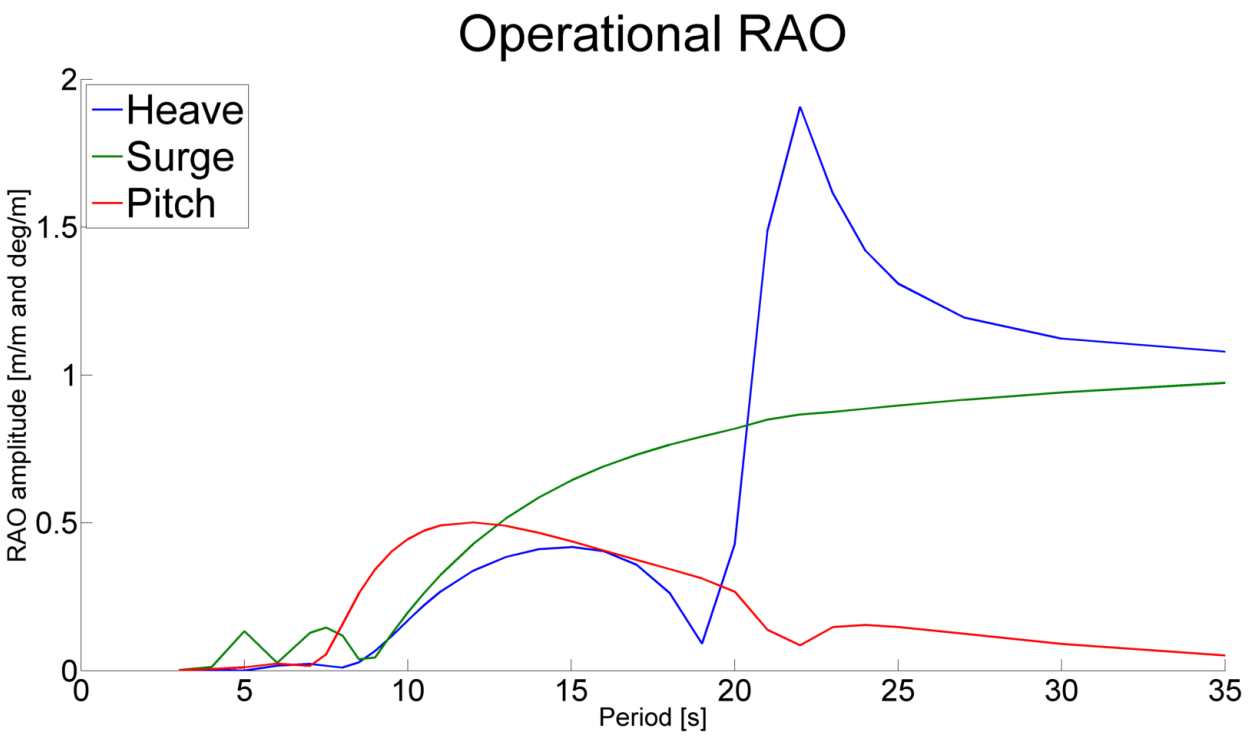

Figure 5.6: RAO data for Scarabeo 5

5.3.2 Topside Boundary Conditions

The link between riser and vessel must be modeled properly in order to achieve accurate forces and moments in the upper end of the riser. This connection is rather complicated, as is consists of two separate tensioner systems and a contact area at the drill floor. The riser tensioner systems apply tension as described in section 0. The topside boundary conditions are applied as illustrated by figure 5.7. It is seen that the riser is constrained in two locations, the drill floor and the crown block. At the drill floor, the riser passes through a hole. The hole is too large to give the riser an angular constraint, but it effectively locks the riser in surge and sway. At the crown block, a force is applied vertically. The structure is hinged, so only tensile loads are applied. This is represented by a beam element that is locked against any rotations, connected to the structure by a hinge. These BCs contain a significant simplification; the drill floor contact is locked at a specific node. In reality, the drill floor contact would move, as the vessel moves in heave. This effect could be represented by modeling the drill floor contact as a short pipe-in-pipe section. Such a solution would allow the drill floor to act like an actual contact surface, adaptive to vessel motions. In this thesis, the main area of interest is the lower end of the riser. Thus, the simplified solution has been found sufficient. The simplified solution is conservative, as there is a bending moment peak near the contact area. The fatigue damage would be lower if these peaks were distributed along a length of the landing joint.

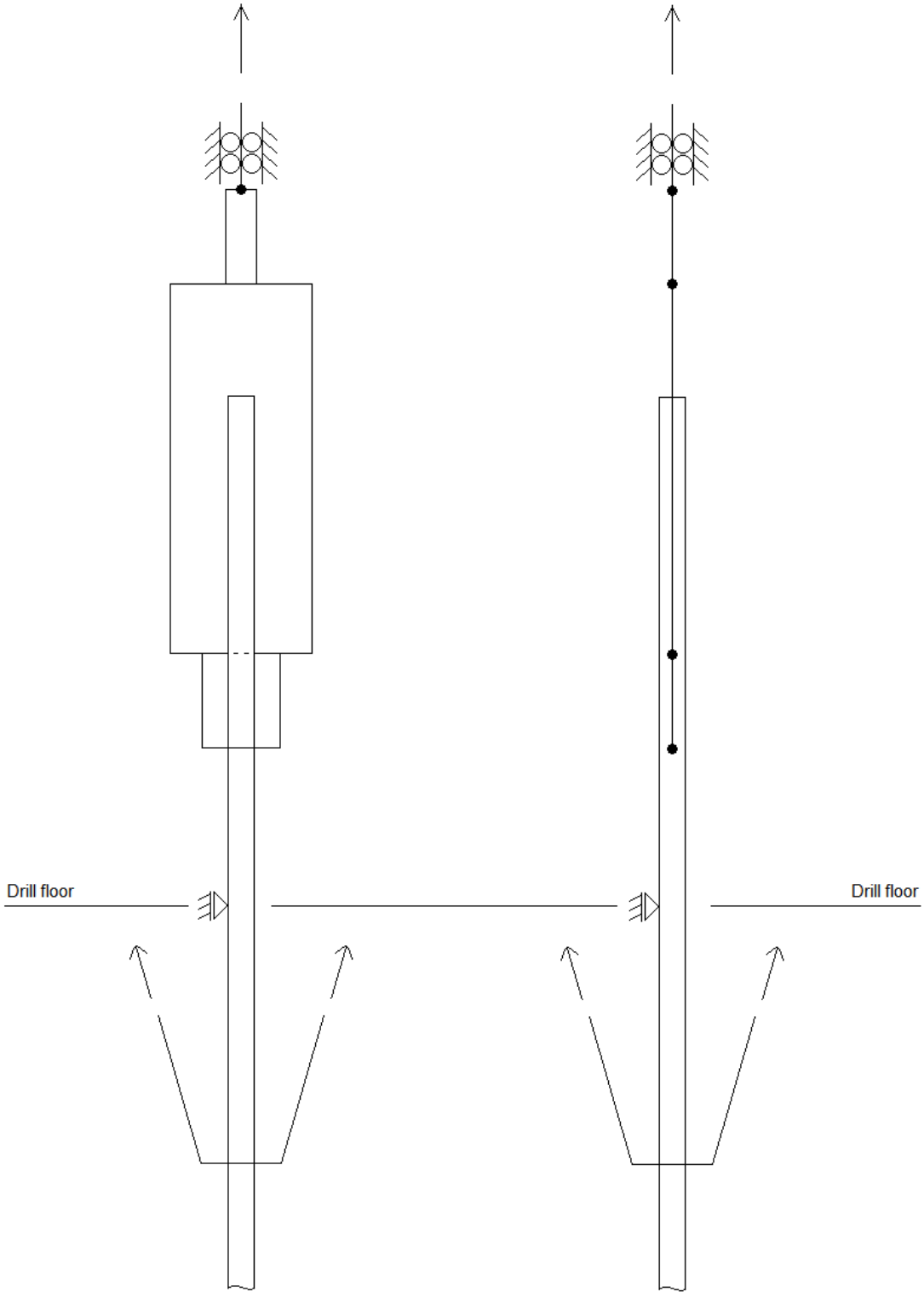

Figure 5.7: Sketch of topside BCs. Figure is not to scale

There is information that suggests the hinges of the tension frame are locked during operation. The hinges are thus only used to ease the process of assembly and disassembly. Unfortunately,

this information is not validated, and it was acquired too late to make changes in the analyses. Thus, the topside dynamics might be invalid for this riser model. However, it is in section 6.11 found that there is minimal differences in fatigue life for the CT and wireline model. When the riser is set up for wireline operation, the tension frame is not present. It is assumed that any error in then tension frame model causes a negligible effect for the riser's fatigue life.

6. Results

In order to estimate the loads on the various riser components, the influence of all significant parameters must be mapped. It is desired to estimate the load level on several riser components, based on the load level at the stress joint, as measured by the lower strain sensor. The relation between load level at the stress joint and the load level at other points along the riser cannot be assumed linear. Thus, several sensitivity studies are run. In all studies, timetraces of axial force and bending moment is extracted at select locations along the riser. These locations are listed in table 6.1. All analyses are solved in the time domain, with a duration of three hours and a hundred seconds. In order to avoid any transient effects, the output databases neglect the first hundred seconds of the analyses. Thus, the output duration of the databases are exactly three hours. As the results are extensive, it is important to post-process the data in a way that makes them useful for a riser monitoring system. In this case, fatigue life is of particular interest. This means that the amplitude of stress oscillations are important, while mean stress levels are of less importance. Most of the results presented in this chapter are normalized with respect to the fatigue life at the lower strain sensor. These are the primary values of interest for extrapolation of fatigue damage, based on measurements made at the stress joint. If the magnitudes of fatigue lives are desired, these are found in appendix E. The raw data of bending moment time series are included digitally, as described in appendix F.

Table 6.1: Selected locations along the riser

Location	Abbreviation	Distance from seafloor [m]
Wellhead	WHD	3.2
Lower Strain Sensor	LSS	11.1
Location 1	50	50
Location 2	100	100
Location 3	200	200
Location 4	300	300
Below Lubricator Valve	LV	325
Landing Joint	LJ	380.8

6.1 Base Case

In order to compare sensitivity for the various parameters, a base case was first created. The analysis results from this case are intended to provide a reference, to which all sensitivity studies will be compared. The parameters for this analysis are seen in table 6.2. Other parameters, such as wellhead angle, offset and increased riser tension are not included in the base case analysis.

Table 6.2: Parameters for the base case analysis

Parameter	Value
Wave spectrum	JONSWAP
Significant wave height	4 meters
Peak period	9 seconds
Wave heading	Head sea
Wave spreading	No wave spreading
Current	One year current (see table 5.4)
Current direction	Same as wave direction

6.2 Calculation of Riser Fatigue

The fatigue lives of the various riser components have been calculated using Matlab functions. In addition to functions created by the author of this thesis, two additional software packages were used. WAFO functions, created by WAFO-group (2000), and a rainflow counting algorithm created by Nieslony (2010) were used. The Matlab functions created by the author of this thesis are found in appendix B. As mentioned in section 2.6, the mean level of stress is not important for calculation of fatigue life. The axial force contribution is not negligible for considerations of stress magnitudes, but the oscillations of this stress are negligible. Shear stress is also very low throughout most of the riser's length, and has thus been neglected. Near the ends of the riser, particularly near the wellhead, the assumption of neglecting shear stress can be questioned. The effect of shear stress in these regions should thus be further investigated. Also neglected are stress contributions from other factors such as VIV, higher order vessel motions, and others. There are several additional load factors which can influence fatigue life, though their importance will be case-specific (DNV, 2005). For this case, the only load included is bending moment, caused by a combination of waves, current and first order platform motion.

6.2.1 Fatigue Calculation Parameters

The riser's stress time series have been calculated according to equation (2.1). This has been done for twenty points, evenly spaced along the riser's circumference, comfortably higher than the minimum of eight points recommended by DNV (2005). Thus, twenty stress time series are established for each of the eight locations listed in table 6.1. Then, the time series are used as input for a rainflow counting algorithm. The result of the rainflow counting is similar to what was seen in figure 2.7. However, where the illustration shows forty blocks, the actual calculations use four thousand blocks. This increased resolution improves the accuracy of calculation. Based on the result from the rainflow counting algorithm, Miner-Palmgren summation is performed, according to equation (2.2). As mentioned in section 2.6.1, the parameters required for this summation should be found from relevant regulations. The parameters used in these calculations are found in DNV-RP-C203 (DNV, 2010). The B1 S-N curve for free corrosion has been selected. It can be argued that the S-N curve valid for cathodic protected materials would be more accurate, as the riser is protected from corrosion by a layer of paint. In order to have a conservative estimate, however, the free corrosion curve was chosen. The aim of this fatigue

assessment is to estimate relative levels of damage accumulation along the riser, rather than detailed calculations for structural components. Due to this, the B1 S-N curve was chosen, and stress concentration factors of 1.5 was selected at all locations. These calculations result in accumulated damages over a three-hour interval. In order to consider a more intuitive value, they have been converted to expected lifetime in years.

6.3 Seastate Realization

In order to build confidence in the analysis results, the seastate realization is validated. To achieve this, the base case analysis has been run three additional times, changing nothing but the seastate seed. These four analyses should ideally provide identical results in terms of fatigue life, though small differences must be expected. In table 6.3, the estimated fatigue lives are listed. It is seen that the calculated lifetimes are very high. The absolute values of lifetimes are however not of interest in this thesis, as the important parameters for a fatigue monitoring system are relative lifetimes along the riser. The high lifetimes are explained by the fact that the fatigue lives are calculated for uniform cross sections of steel. In reality, the limiting components will be the small components, such as bolts and welds. Such components will experience both higher stresses, and their SCFs will be higher. Additionally, no safety factors are included in the lifetimes seen in the table. Due to the uncertainty of fatigue calculations, best practice would be to divide the fatigue life by a factor of three. For components that cannot be inspected, a safety factor of ten is used. However, safety factors have not been considered in this thesis, as the magnitude of fatigue life is not of interest. The important parameter in this thesis is relative fatigue life, a parameter that is not affected by safety factors or SCFs.

Table 6.3: Riser fatigue life in years for various seastate realizations

	WHD	***LSS***	***50***	***100***	***200***	***300***	***LV***	***LJ***
Base Case	4389	647	107257	155665	470277	273261	28021	44.9
Seed 1	4445	655	106279	157546	474183	273716	28404	47.5
Seed 2	4393	648	106945	156199	468541	276608	28480	45.4
Seed 3	4361	643	105770	157140	464796	273899	28135	45.3

It is seen from the table that only small deviations of fatigue life occur for different seastate realizations. It is also seen that the fatigue life varies greatly along the riser. The highest fatigue life of all the measured locations occurs at 200 meters above the seafloor. It is over 700 times higher than the fatigue life at the lower strain sensor. This implies that fatigue issues in this region will be of little interest, assuming this trend remains regardless of environmental conditions. At the landing joint however, the fatigue life is low. At this location, fatigue issues are essential, and a real-time estimate of accumulated fatigue damage would be very helpful during operation.

6.4 Peak Period

The wave peak period is expected to be an influential parameter for the riser's fatigue life. Changes in wave period will affect vessel response, as well as influence the riser directly. Four additional analyses have been made in order to investigate the effect of variations in peak period. The results of these analyses are seen in table 6.4.

Table 6.4: Fatigue life variation due to peak period

	WHD	LSS	50	100	200	300	LV	LJ
Tp 08 s	6.73	1.00	153.38	224.47	744.90	404.04	44.80	0.26
Tp 09 s	6.78	1.00	165.81	240.64	726.99	422.43	43.32	0.07
Tp 10 s	6.87	1.00	214.50	290.17	920.31	606.64	61.92	0.05
Tp 11 s	6.97	1.00	329.88	388.90	1315.86	1057.78	101.74	0.05
Tp 12 s	7.04	1.00	511.63	521.50	1824.50	2024.74	187.57	0.05

It is clearly seen from the table that variations in peak period will cause great variations in fatigue life. A graphical representation of these data is found in figure 6.1. As it is seen, the largest differences in fatigue life occurs in the upper middle section of the riser. The fatigue life in these locations are, as mentioned in the previous section, very high. Due to the high lifetime in these sections, the importance of accurate fatigue life estimation is reduced – even if large safety factors are included, the calculated fatigue life is abundantly high. At the ends of the riser however, particularly at the landing joint, accurate estimation of fatigue is highly beneficial.

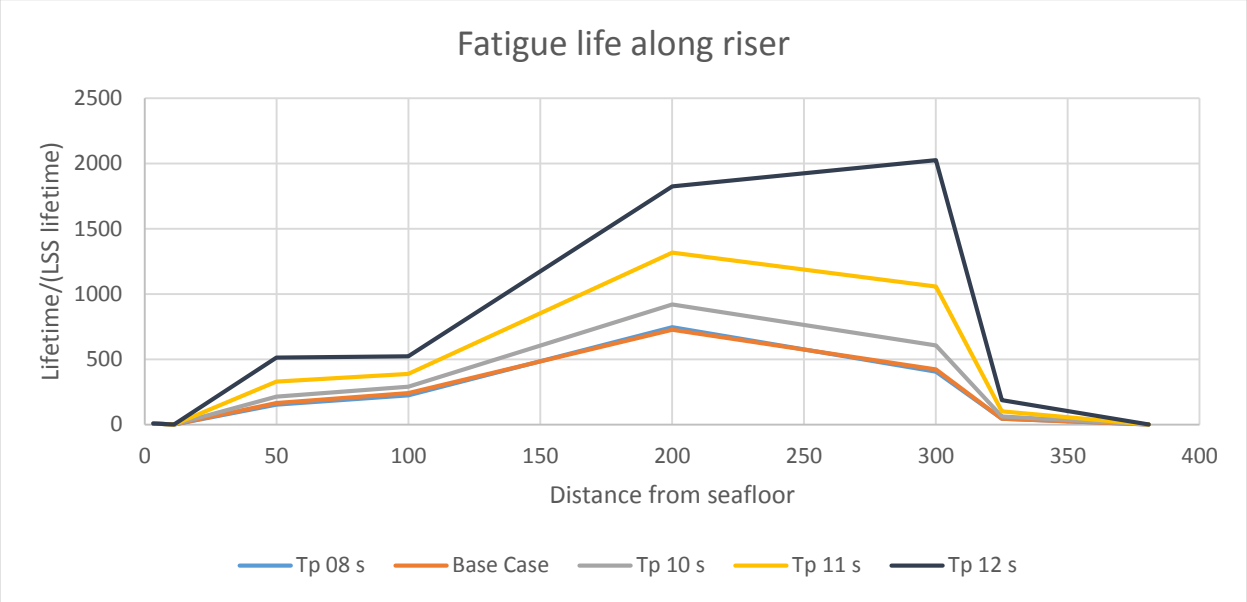

Figure 6.1: Fatigue life variation due to peak period

6.5 Current Magnitude

The influence of current on the workover riser system is complex. Along the length of the riser, great variations in current velocity and direction are expected. The complexity in current loading makes simplifications necessary. Initially, the influence of current velocity is studied in a simplified form, where the established current profile from the base case analysis is scaled linearly. In addition to the base case analysis, three lower levels of current are applied. These load cases apply current as 75, 50 and 10 % of the base case current, scaled linearly. Initially, it was assumed that this sensitivity study with respect to current velocity would be sufficient. After reviewing the results, however, it was clear that the influence of current should be investigated further. The initial assumption was that the current would provide a static load contribution, barely influencing the dynamics of the riser system. However, the results imply that the current is an essential factor for the dynamic behavior of the riser. A lower current magnitude increases the rate of fatigue damage accumulation. Table 6.5 shows the fatigue lives at the different locations along the riser, each value divided by the same component's base case lifetime. In figure 6.2, a part of the bending moment time series created by the analyses at the lower strain sensor are shown. The dramatic difference in moment amplitudes explains the difference in fatigue life.

Table 6.5: Fatigue life percentage for each location, base case as reference

	WHD	***LSS***	***50***	***100***	***200***	***300***	***LV***	***LJ***
10 % Current	6.2 %	6.1 %	6.0 %	6.3 %	14.4 %	20.7 %	53.1 %	107 %
50 % Current	16.9 %	16.9 %	16.0 %	21.0 %	38.1 %	52.2 %	91.5 %	115 %
75 % Current	43.8 %	43.9 %	43.1 %	49.9 %	70.4 %	83.0 %	106 %	109 %
100 % Current	100 %	100 %	100 %	100 %	100 %	100 %	100 %	100 %

From the table, it is clear that the difference in fatigue life is most critical near the lower end of the riser, while the surface equipment does not seem to be affected as much. This will however make extrapolation more difficult, as the change in fatigue life at the lower strain sensor seems uncoupled from the trend at the landing joint. Prior to using these data as basis for a monitoring system, the data should be validated. The extreme influence of current were unexpected by all parties involved in this thesis. Additionally, Professor Karl Martin Larsen at NTNU were consulted. He found the extreme importance of current to be unexpected as well. Due to the surprising results, additional analyses have been run in order to verify them. This verification is found in chapter 7.

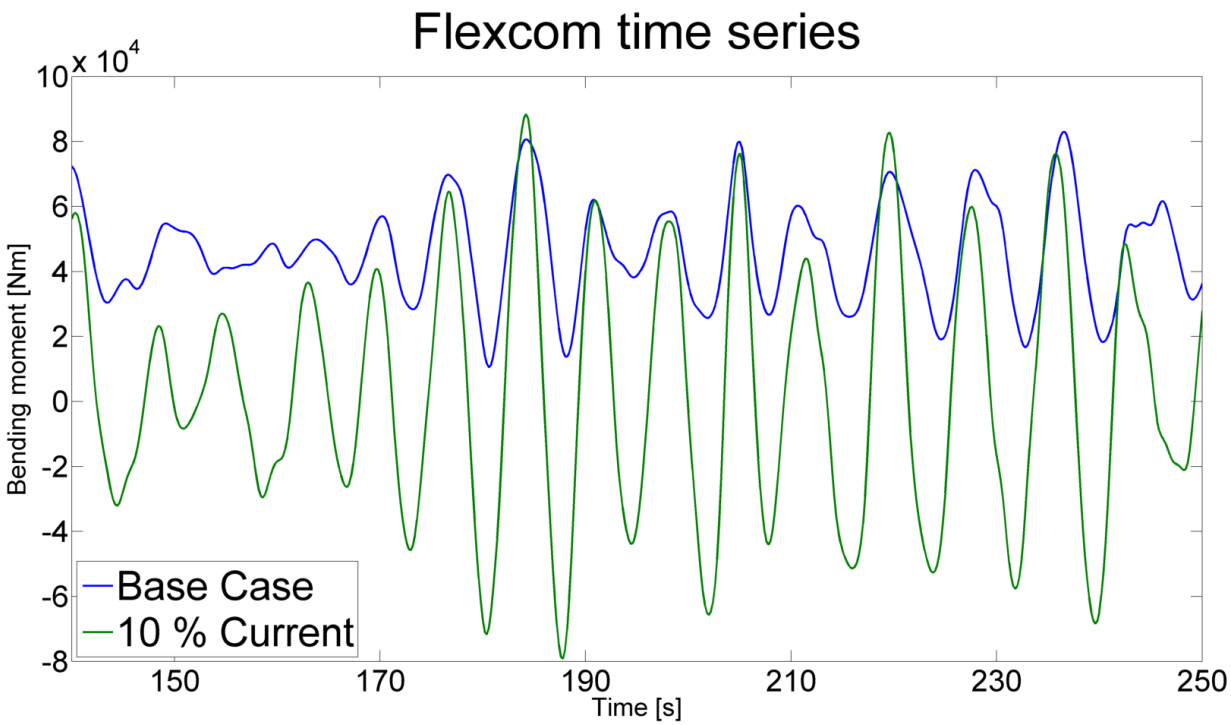

Figure 6.2: Time series of bending moment at LSS, demonstrating current sensitivity

6.6 Current Direction

In addition to knowing the influence of current magnitude, the importance of current direction must be mapped. Like the analyses with respect to current magnitude, also this is simplified. A real, observed current might vary in direction throughout the water depth. In the analyses run, the current direction does not change with water depth. Instead, the current profile used in the base case analysis is applied unchanged in several different directions. Five analyses are run to investigate the effect of current direction, including the base case. These five analyses are sufficient to cover directions from 0 to 180 degrees, with 45 degree steps. Due to the riser's symmetric design, current directions above 180 degrees are not required. The results of these analyses are found in table 6.6. The wave direction remains unchanged at head sea (0°).

Table 6.6: Fatigue life variation due to current direction

Current dir	WHD	LSS	50	100	200	300	LV	LJ
0°	100 %	100 %	100 %	100 %	100 %	100 %	100 %	100 %
45°	37.4 %	37.2 %	40.1 %	44.6 %	73.2 %	82.3 %	107 %	108 %
90°	21.8 %	21.6 %	25.2 %	26.5 %	51.6 %	65.7 %	112 %	116 %
135°	37.8 %	37.5 %	41.7 %	45.3 %	77.3 %	86.2 %	111 %	112 %
180°	104 %	103 %	107 %	104 %	109 %	108 %	105 %	105 %

It is seen in from the table that current direction, like current magnitude, is an important parameter for fatigue life at the lower end of the riser. Further, it is seen that the expected

lifetimes are similar in pairs; the results are similar whether the current direction is 0 or 180 degrees. 45 and 135 degrees also form a pair, while a current from 90 degrees does not match the results of any other current direction. It appears that the current can be decomposed into two components – along and transverse with respect to the wave direction. As the component of current along the wave direction diminishes, the fatigue life at the lower end of the riser is severely reduced. This trend is similar to the effect of reduced current magnitude in the previous section. An explanation of this effect is included in section 7.1.3.

6.7 Vessel Offset

During real operations, it is rarely the case that the vessel is located exactly above the wellhead. The operator has the ability to adjust the length of the mooring lines in order to avoid drift-off due to steady state forces such as current and wind. Still, some offsets must be expected. Sensitivity studies have been run for offsets of ten, twenty and forty meters. The offsets are all in the same direction as the waves and current. With the water depth of 356 meters, these offsets represent approximately 3.8 %, 5.6 % and 11.2 % offset respectively. These values are comfortably outside of what is expected during normal operation. The results of these analyses are seen in table 6.7. In this table, the values of each row are normalized with respect to the fatigue life at the lower strain sensor at the same row.

Table 6.7: Fatigue life along riser for various offsets

	WHD	***LSS***	***50***	***100***	***200***	***300***	***LV***	***LJ***
0 m offset	6.78	1.00	165.81	240.64	726.99	422.43	43.32	0.07
10 m offset	6.79	1.00	165.86	239.10	723.99	422.71	43.75	0.07
20 m offset	6.79	1.00	167.44	238.16	727.55	425.60	44.86	0.07
40 m offset	6.78	1.00	176.16	239.10	753.35	433.99	48.86	0.07

By considering the values in the table, it appears that vessel offset is of little interest for extrapolation of fatigue damage. Even when the offset is forty meters, which is considered an extreme case, the changes in fatigue life throughout the riser are minor. It is noted that these values are normalized with respect to the values at the lower strain sensor. This is convenient for extrapolation of damage based on what is measured at this location, though a global change in fatigue life throughout the riser would not be possible to read from these values. Figure 6.3 confirms the trend read from the table. Deviations in fatigue life remain low throughout the length of the riser.

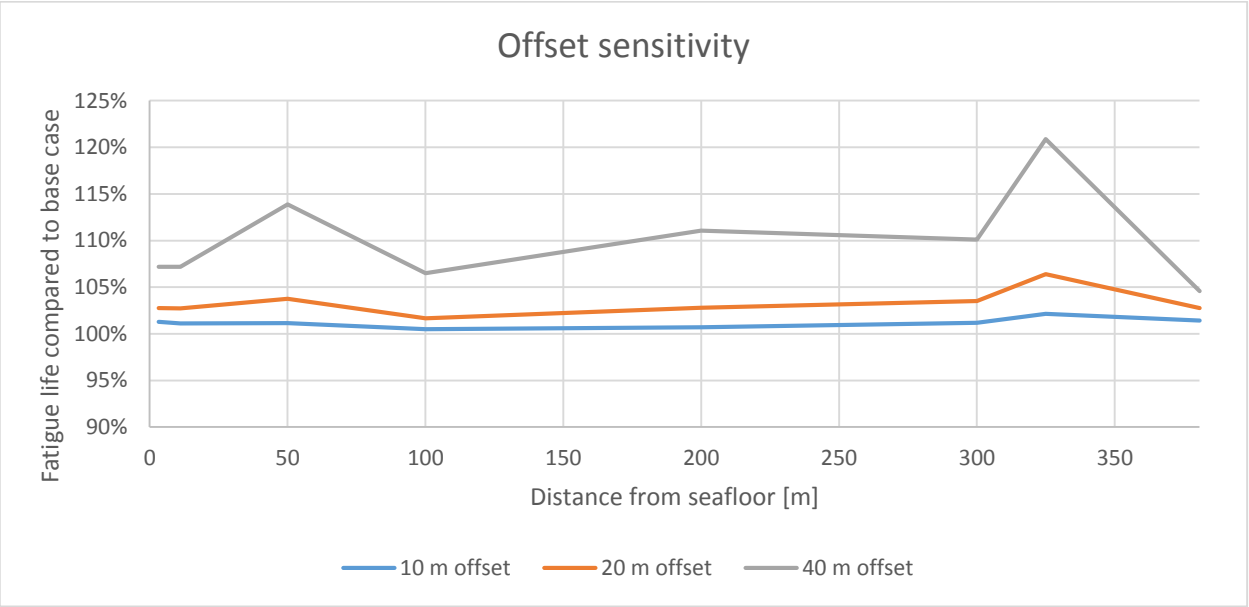

Figure 6.3: Deviations in fatigue life along the riser due to vessel offset

While offset seems to be of little interest for fatigue life, an offset will clearly give the riser a static moment. Figure 6.4 shows a part of the time series created, comparing the case of zero offset to the highest offset of forty meters. While the bending moment amplitudes in this figure appears to be close to equal, the offset clearly changes the mean level. Such a parameter will be of high interest for other aspects of a monitoring system, such as estimation of extreme values. For estimation of fatigue however, this static contribution does not contribute significantly.

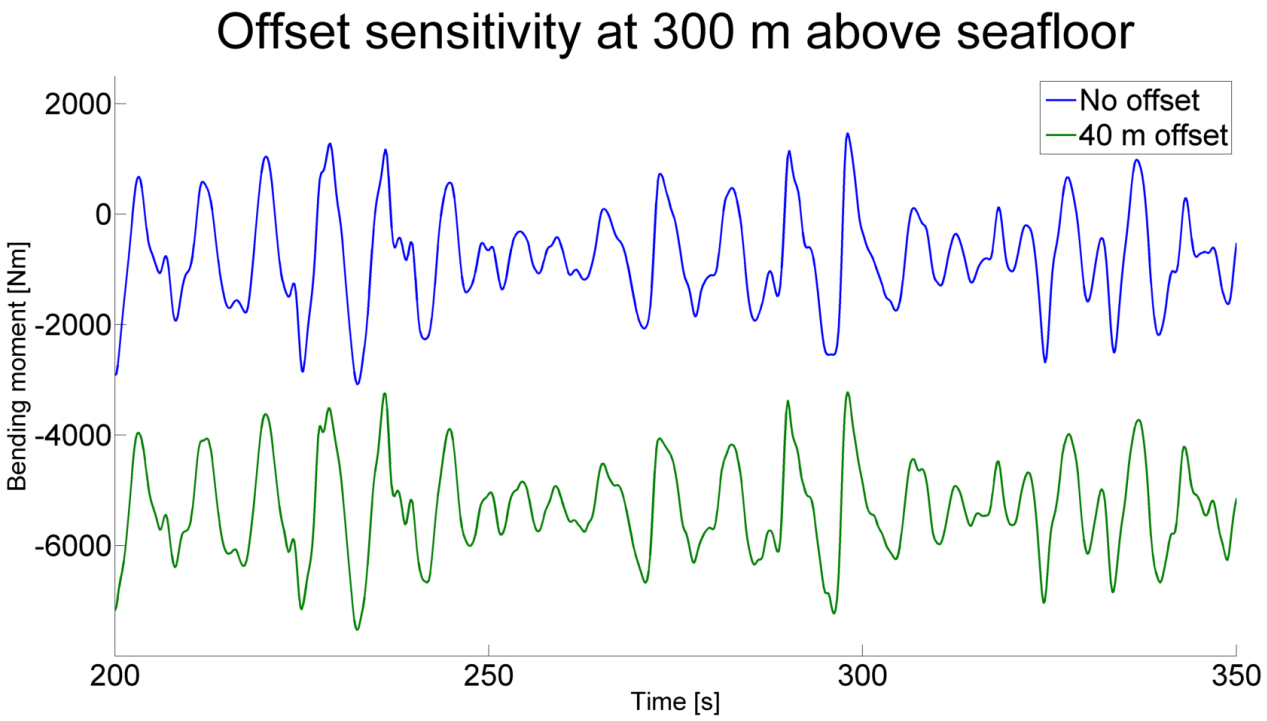

Figure 6.4: Bending moment time series at 300 meters above seafloor, demonstrating offset sensitivity

6.8 Vessel and Wellhead Tilt

In the base case analysis, both the wellhead and the static orientation of the vessel are perfectly level. In real life however, this is rarely the case. A wellhead will generally not be vertical, though strict regulations apply for the highest allowed deviation. The support vessel is also unlikely to be perfectly level – small static pitch and trim angles are expected. Static pitch and trim angles of the vessel are also assumed low, as the operator would surely abort the operation otherwise. Due to this, the sensitivities for vessel and wellhead tilt are run with small angles. The vessel tilt angle is set to one degree, while the wellhead tilt angle is 1.5 degrees. The results are seen in table 6.8. By considering these results, it appears that small tilt angles for the vessel and wellhead is almost irrelevant for the fatigue life of the system. The deviations of fatigue life along the riser is seen in figure 6.5. The change in fatigue life stays within one per cent for both cases, at all locations along the riser.

Table 6.8: Fatigue life along riser for vessel and wellhead tilt

	WHD	***LSS***	***50***	***100***	***200***	***300***	***LV***	***LJ***
No tilt	6.78	1.00	165.81	240.64	726.99	422.43	43.32	0.07
Vessel tilt	6.78	1.00	165.23	240.52	723.29	419.51	43.00	0.07
Wellhead tilt	6.79	1.00	165.46	240.14	725.26	421.83	43.25	0.07

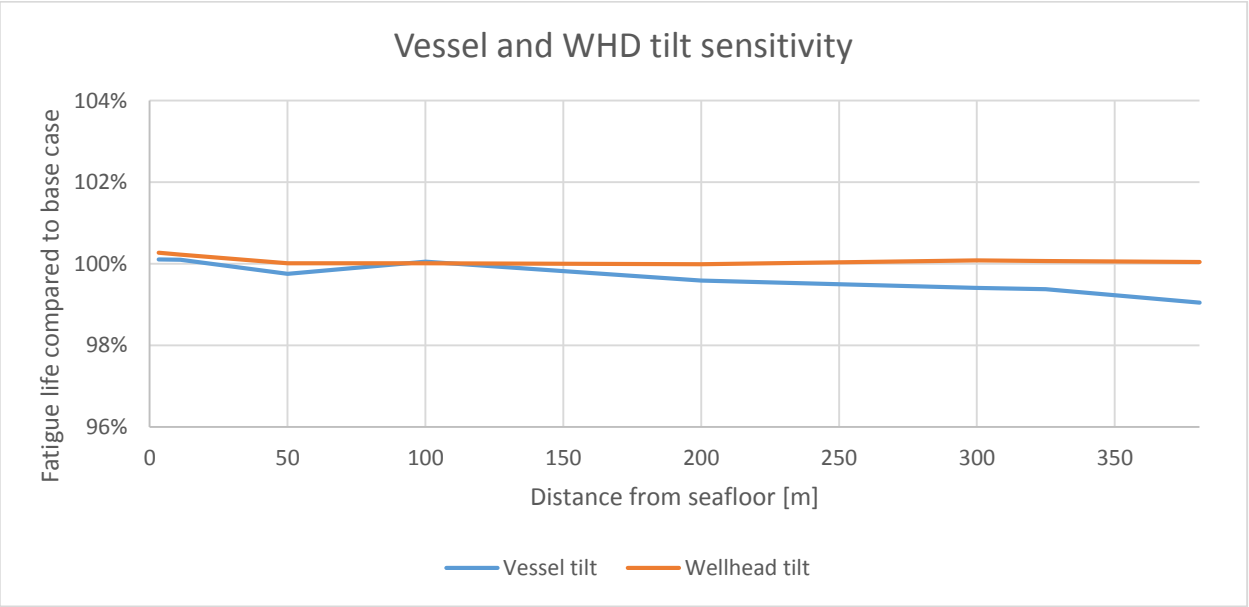

Figure 6.5: Deviations in fatigue life along the riser due to vessel and wellhead tilt

6.9 Riser Tension

Based on conversations with Aker Solutions, it is understood that the effect of riser tension can be complex. Whether an increased riser tension will improve or reduce the fatigue life is dependent on other parameters, such as water depth. The static overpull in the base case analysis was 25 metric tons, as mentioned in section 0. Significant reduction in riser tension would not be allowed, as the EDP requires a certain overpull to ensure its ability to disconnect. Two sensitivities have been run, where the overpull have been increased to 35 and 50 metric tons. The results of this sensitivity study is seen in table 6.9.

Table 6.9: Fatigue life along riser for dependent on riser tension

	WHD	***LSS***	***50***	***100***	***200***	***300***	***LV***	***LJ***
25 mt overpull	6.78	1.00	165.81	240.64	726.99	422.43	43.32	0.07
35 mt overpull	6.15	1.00	267.75	328.59	1132.2	553.46	52.35	0.07
50 mt overpull	5.40	1.00	518.80	510.06	1930.7	866.94	69.93	0.07

From the table, it is seen that riser tension is an influential parameter for extrapolation of fatigue damage. It is seen that a higher riser tension increases the lifetime of most riser components, relative to the LSS lifetime. It is also seen that a change in riser tension affects the relative lifetimes of LSS and WHD. For other sensitivity studies, the relative lifetimes of the LSS and WHD has been approximately constant. Due to the high stiffness of the lower end of the riser, this section will not move significantly. It can thus be considered quasi-static. A change in riser tension however, alters the stiffness of the system. The lower end of the riser still behaves quasi-static, but the altered stiffness affects the relative lifetime of LSS and WHD. In figure 6.6, the lifetime of the riser compared to the base case lifetimes are plotted. It is confirmed that an

increased riser tension improves the lifetimes throughout most of the water depth. However, the end components are less affected. The lifetime at the LSS is almost constant, while the WHD lifetime is reduced. The lifetime at the landing joint is also close to constant.

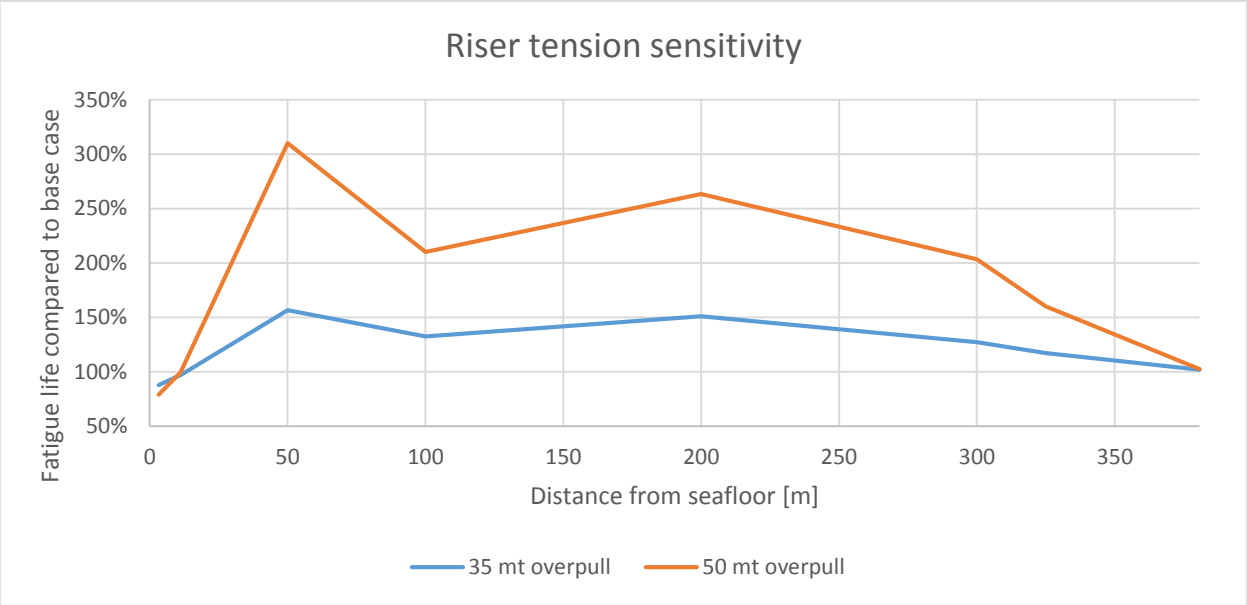

Figure 6.6: Deviations in fatigue life along the riser due to overpull variation

6.10 Hydrodynamic Coefficients

As discussed in section 4.4.1, the simplicity of Morison's equations makes them susceptible to error. They are dependent on correct drag- and inertia coefficients in order to provide an accurate estimate of force. As the coefficients are linear factors in their respective equations, the error in force is proportional with the coefficient's error. Even though it is expected that the values of these coefficients are accurate, some uncertainty must always be assumed. Thus, sensitivity studies are run where the drag- and inertia coefficients are scaled. The drag coefficient is scaled $^{+}/_{-}$ 20 %, and the inertia coefficient is scaled $^{+}/_{-}$ 10 %. In figure 6.7 and figure 6.8, time series of bending moment at the LSS are shown for drag- and inertia coefficient sensitivity.

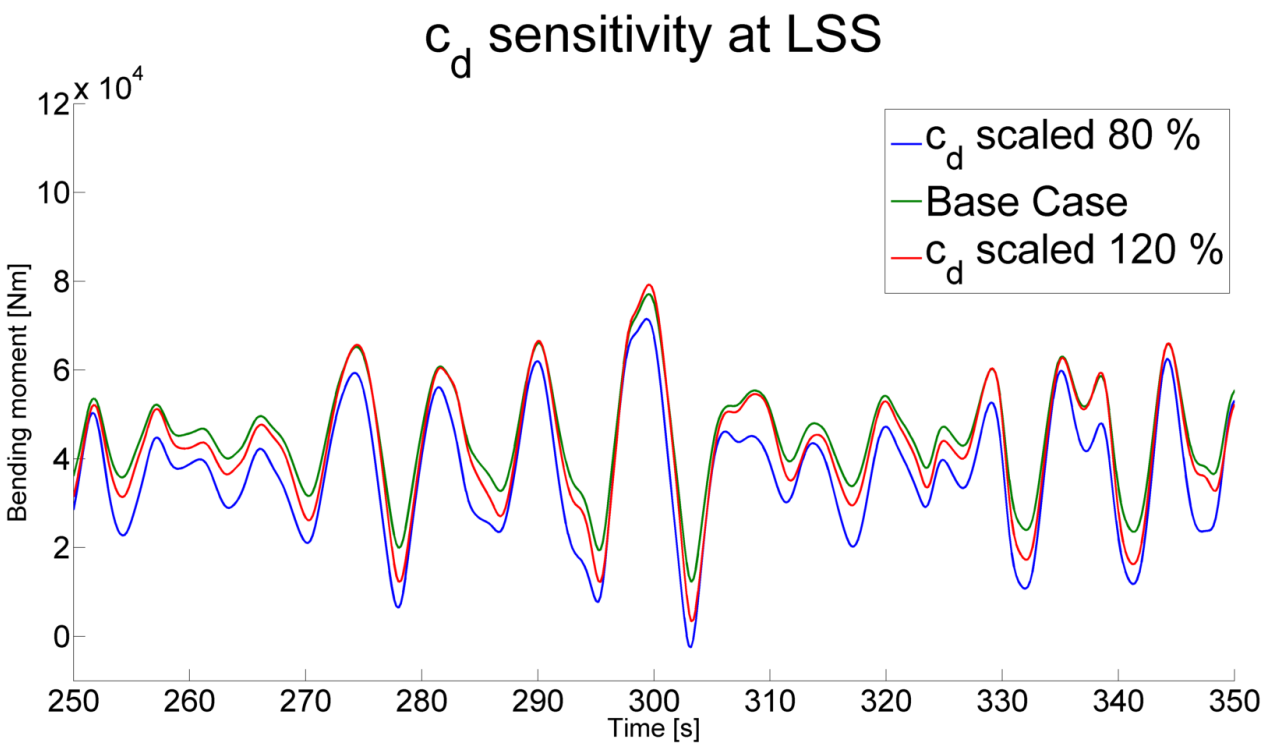

Figure 6.7: Time series demonstrating drag coefficient sensitivity at LSS

It is clearly seen that a change in drag coefficient changes the result. However, the majority of the difference appears to be an offset of the mean level. This can be explained quite easily; the mean level of bending moment is determined by the steady current, which affects the riser through drag force. It is however clear that a change in drag coefficient also affects the riser's fatigue life. Figure 6.9 shows the change in fatigue life due to scaled drag coefficients. Surprisingly, both a reduction and increase in drag coefficient reduces the fatigue life at the lower end of the riser.

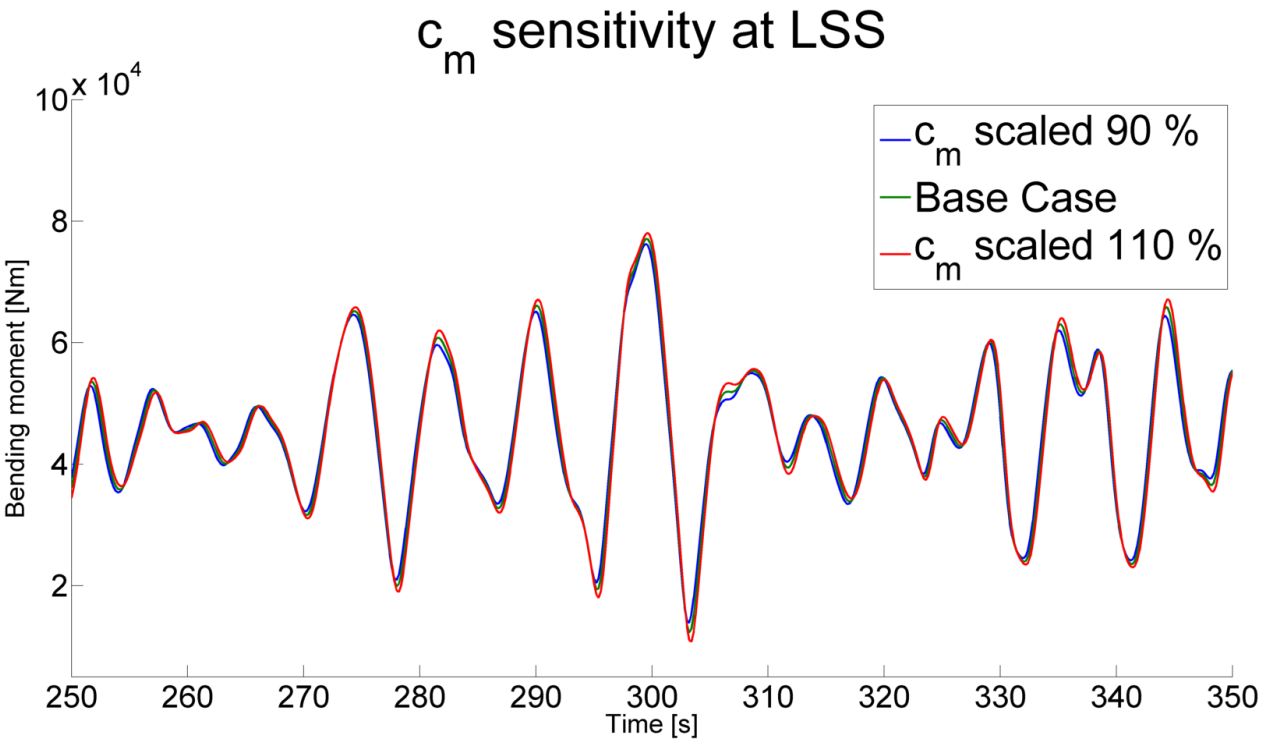

Figure 6.8: Time series demonstrating inertia coefficient sensitivity at LSS

By considering figure 6.8, it is seen that a change in inertia coefficient appears less influential than what was seen by changing the drag coefficient. There are two factors, which contribute to this. Firstly, the inertia force does not contribute to the mean level on the plots, unlike the drag force. Thus, a change of inertia coefficient does not cause a shift of mean bending moment. Secondly, the riser system is drag-dominated, as will be discussed in section 7.1.2. However, when considering the variations of fatigue life along the riser, as illustrated in figure 6.10, it is clear that the inertia coefficient is an important parameter as well.

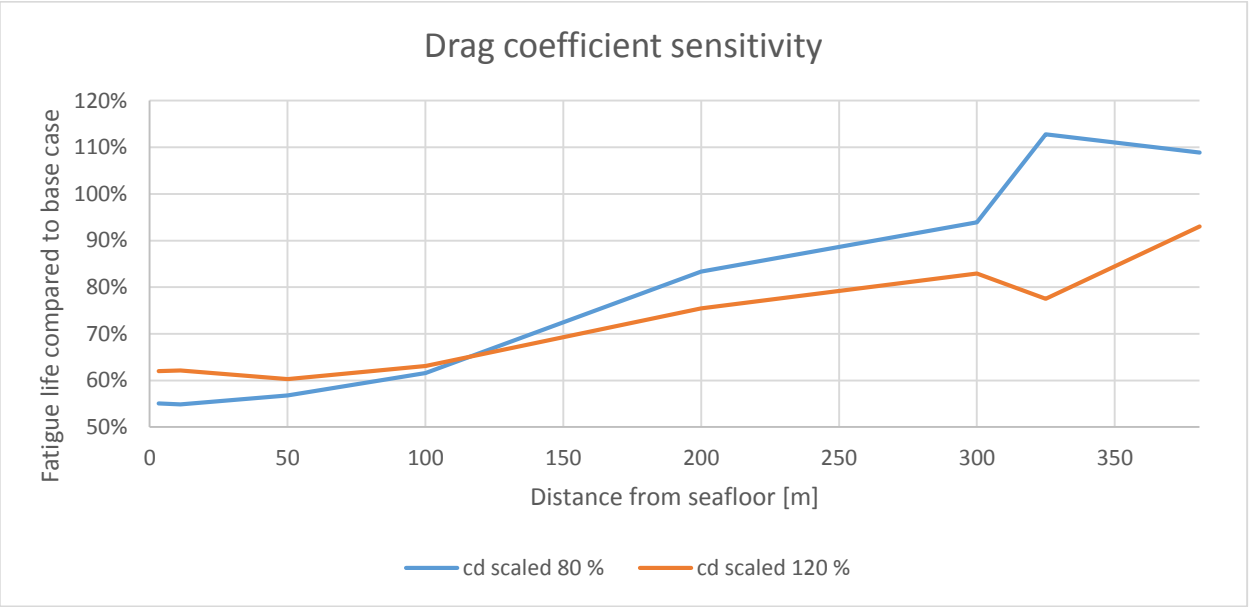

Figure 6.9: Deviations in fatigue life along the riser due to variation in drag coefficient

Table 6.10 lists the required data for extrapolation of fatigue damage based on measured values at the LSS. It is seen that there is significant scattering for both drag- and inertia coefficients.

Table 6.10: Fatigue life along riser dependent on hydrodynamic coefficients

	WHD	***LSS***	***50***	***100***	***200***	***300***	***LV***	***LJ***
Base Case	6.78	1.00	165.81	240.64	726.99	422.43	43.32	0.07
c_d *80 %*	6.81	1.00	171.62	270.15	1104.62	723.48	89.09	0.14
c_d *120 %*	6.77	1.00	160.93	244.57	882.75	564.17	54.04	0.10
c_m *90 %*	6.80	1.00	173.59	246.64	748.84	415.79	41.40	0.06
c_m *110 %*	6.77	1.00	159.29	235.08	703.49	431.59	45.34	0.08

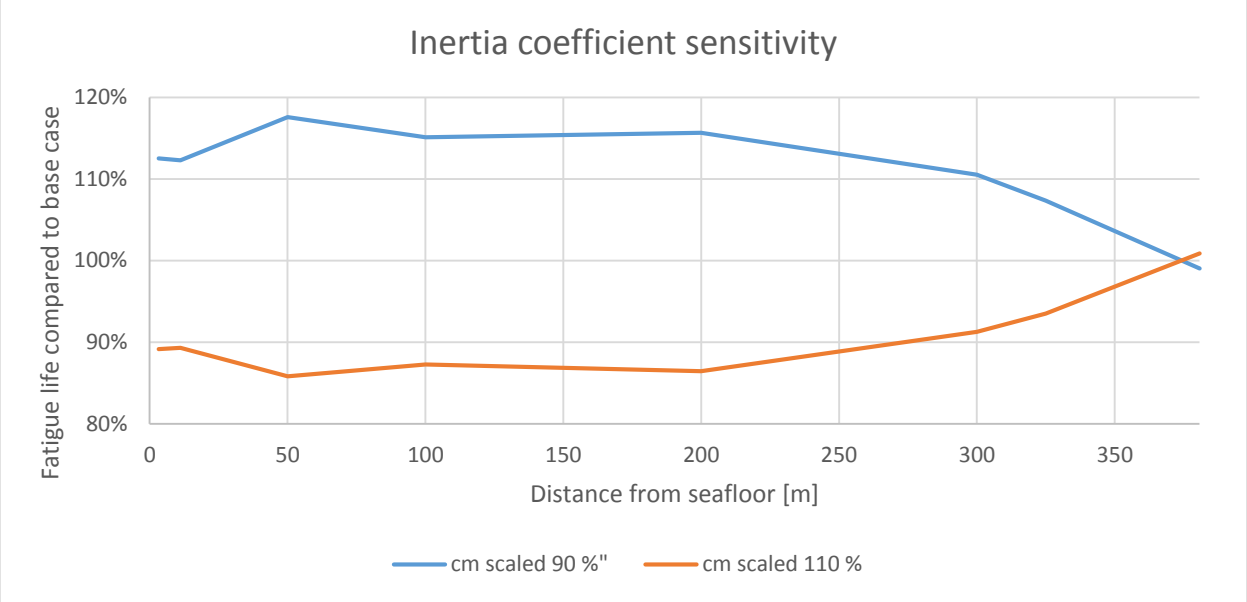

Figure 6.10: Deviations in fatigue life along the riser due to variations in inertia coefficient

6.11 Additional Sensitivities

In addition to the previously studied sensitivities, three more parameter variations are run. These parameters are:

1. The effect of content density. In all analyses run so far, the riser has been filled with a fluid of density 2070 kg/m^3. This corresponds to the highest expected content density for this riser. For a monitoring system however, it must be expected that the internal fluid density will vary for different operations. As the internal fluid affects the weight of the entire riser system, the riser tension must be adjusted to keep the overpull constant. This causes a change in riser tension throughout the water depth. A sensitivity analysis has been run, with an internal fluid of density 1025 kg/m^3.
2. The orientation of the tension frame. All analyses run so far use the setup for coiled tubing operations, which is illustrated in figure 5.1 and figure 5.2. This setup includes a tension frame, which provides the riser with tension through hinges, allowing riser rotations. The tension frame is however only hinged in one direction. In the case of beam sea, an increase in topside bending moments must be expected. Thus, a sensitivity analysis has been run where the tension frame is rotated 90 degrees.
3. Topside equipment for wireline operations. As mentioned, all previous analyses have been run with a model setup for coiled tubing operations. In the case of wireline operation, much of the topside equipment is removed, including the entire tension frame. This lighter setup is expected to alter the topside dynamics. A separate model has been created, where the topside equipment is adapted to wireline operations.

The results of these sensitivities are seen in table 6.11. It is seen that the effects of a wireline setup or a rotated tension frame cause negligible variations. Even at the landing joint, where

significant changes in the riser dynamics were expected, the fatigue life is not altered significantly. Internal fluid density is however important for the riser's fatigue life. Altering the internal fluid density requires a new riser tension. The riser tension will thus remain constant at the EDP, while the tension applied at the vessel is lower. A change in riser tension affects the riser's fatigue life, as was seen in section 6.9.

Table 6.11: Fatigue life along riser dependent on other parameter variations

	WHD	LSS	50	100	200	300	LV	LJ
Base Case	6.78	1.00	165.81	240.64	726.99	422.43	43.32	0.07
Light Content	6.82	1.00	177.12	224.09	631.47	322.88	31.20	0.05
TF orientation	6.78	1.00	165.81	239.69	725.88	420.79	43.23	0.08
Wireline	6.79	1.00	163.85	241.18	721.14	422.25	43.70	0.07

The same trend is seen in figure 6.11. The effect of a rotated tension frame and a wireline setup does little to change the fatigue life along the riser, though a minor improvement is seen at the landing joint for both these sensitivities. The internal fluid sensitivity has a significantly higher fatigue life at the lower end of the riser, though this improvement diminishes with height.

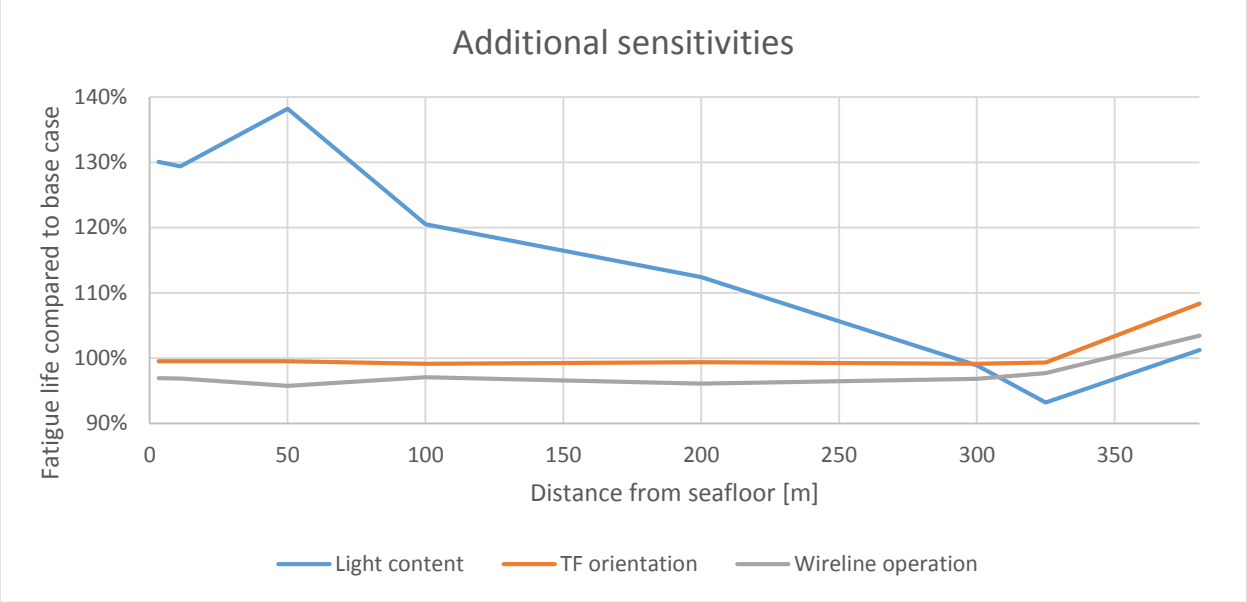

Figure 6.11: Deviations in fatigue life along the riser due to other parameter variations

7. Current Sensitivity Verification

Due to the unexpected results of the current sensitivity analysis found in section 6.5, verification of the results is necessary. First, an explanation as to why the observed trend is reasonable will be offered. Then, analysis results from RIFLEX will be provided, as well as the results of a simplified, one DOF Morison model created in Matlab.

7.1 Current Influence on Damping

As mentioned in section 4.4.1, Flexcom uses Morison's equation to determine external load on the riser. The inertia force, whose equation number is (4.13), is proportional with the relative acceleration between the riser and surrounding water particles. It is thus not changed by the presence of a steady state water velocity. The drag force however (equation (4.12)), is quadratic with respect to the relative velocity between riser and surrounding water. It is thus highly affected by a steady state current. Figure 7.1 shows the effect of a current on the drag force throughout a period. In this figure, the static contribution from the current has been subtracted. Thus, only the dynamic force components remain. It is clearly seen that the current increases the magnitude of the drag force, due to the quadratic relationship between relative velocity and force.

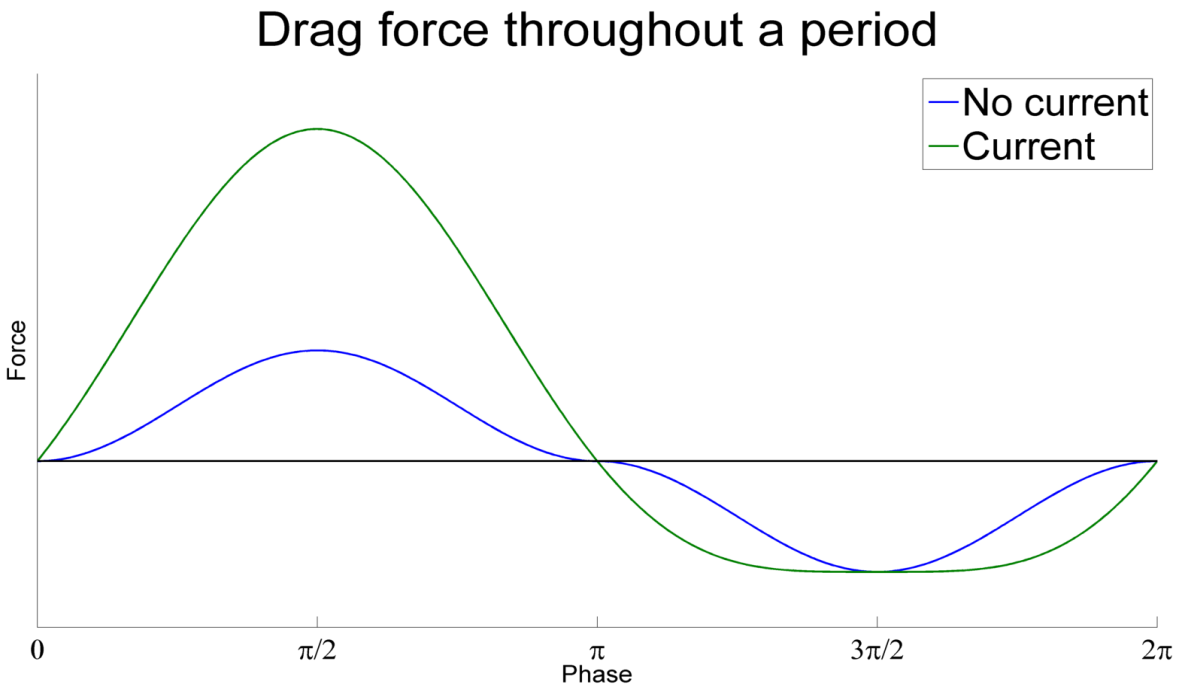

Figure 7.1: Drag force thoughout a period with and without the presence of a current

7.1.1 Drag Forces Along Riser

The horizontal particle velocity along the water depth for a given wave can be calculated according to equation (4.17). In figure 7.2 the velocity amplitude profile is plotted, using a regular wave with height four meters, and period nine seconds – the peak values from the

analyses. It is clearly seen that the velocity amplitude quickly diminishes with depth. Below a depth of 150 meters, the particle motion due to waves appears negligible. Thus, below this point, only two sources of drag forces remain. There are a static drag force due to current, and there are dynamic drag forces due to riser motion.

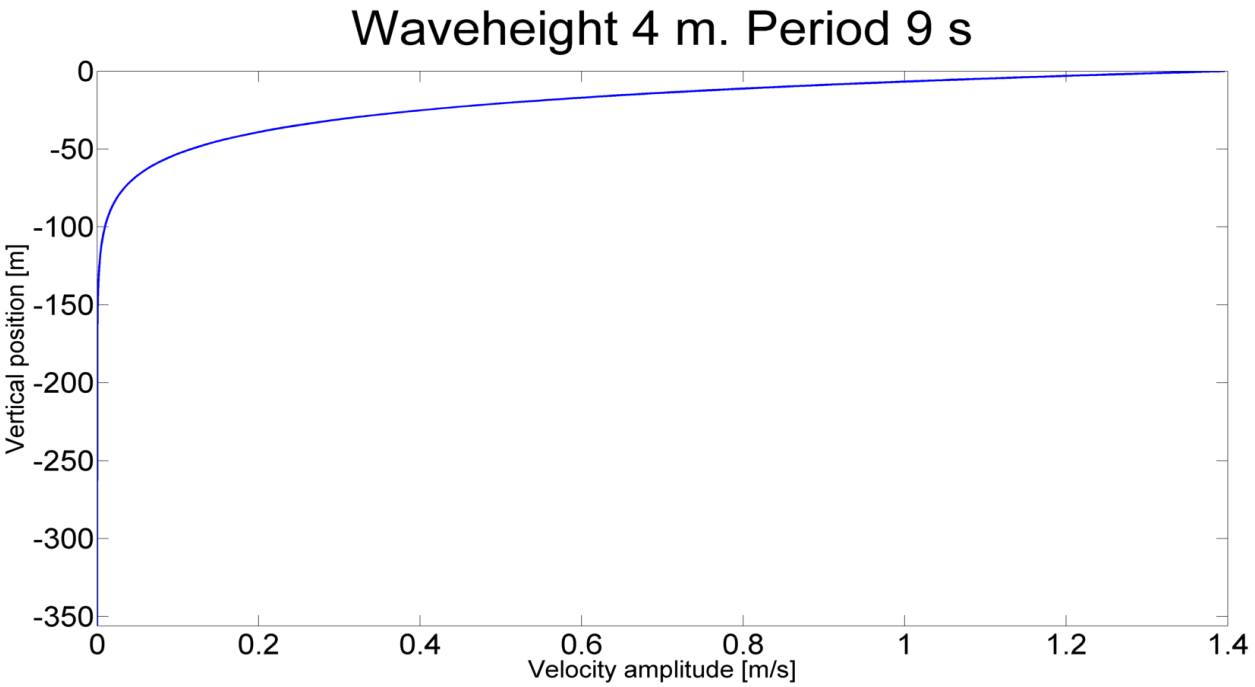

Figure 7.2: Horizontal particle velocity amplitude versus depth for a given regular wave

While drag forces are normally thought of as excitation, a drag force can also serve to provide a system with damping. Drag forces are speed dependent, like any damping force. In a case where there is no wave excitation and no current, all dynamic behavior is caused by riser motion. In this case, the drag force resultant will at any time be directed opposite of the riser motion, and thus serve to dampen the response. As was seen in figure 7.1, the presence of a current does not only provide a static force. It also increases the magnitude of the dynamic force component. Thus, below the influence of wave excitation, a more powerful current will serve to increase the damping power of the drag forces.

7.1.2 Importance of Drag Forces for the Workover Riser

The field of workover risers are largely based on the acquired knowledge from marine risers. Their similarities have made the development of workover risers easier, as marine risers have been field-tested over decades, and significant knowledge exists. It is thus logical to expect their behavior to be similar. However, the smaller diameter of workover risers influence the magnitude of the Morison forces. The drag forces, which are dependent on the projected area of the riser, diminish linearly with a decrease in riser diameter. Inertia forces are dependent on the displaced volume of the riser. A decrease in riser diameter will thus cause the inertia forces a quadratic reduction. Due to this extra reduction of inertia forces, a workover riser will be far more drag-dominated than a larger, marine riser. Figure 7.3 categorizes regimes where the effect of drag forces and inertia forces are important. It is seen that when the wave height

divided by the riser's diameter is close to eleven, the drag forces and inertia forces are approximately equal. A larger wave height increases the domination of drag forces. The figure is based on the work of Faltinsen (1993). It has been modified to represent the actual hydrodynamic coefficients of the workover riser in this thesis.

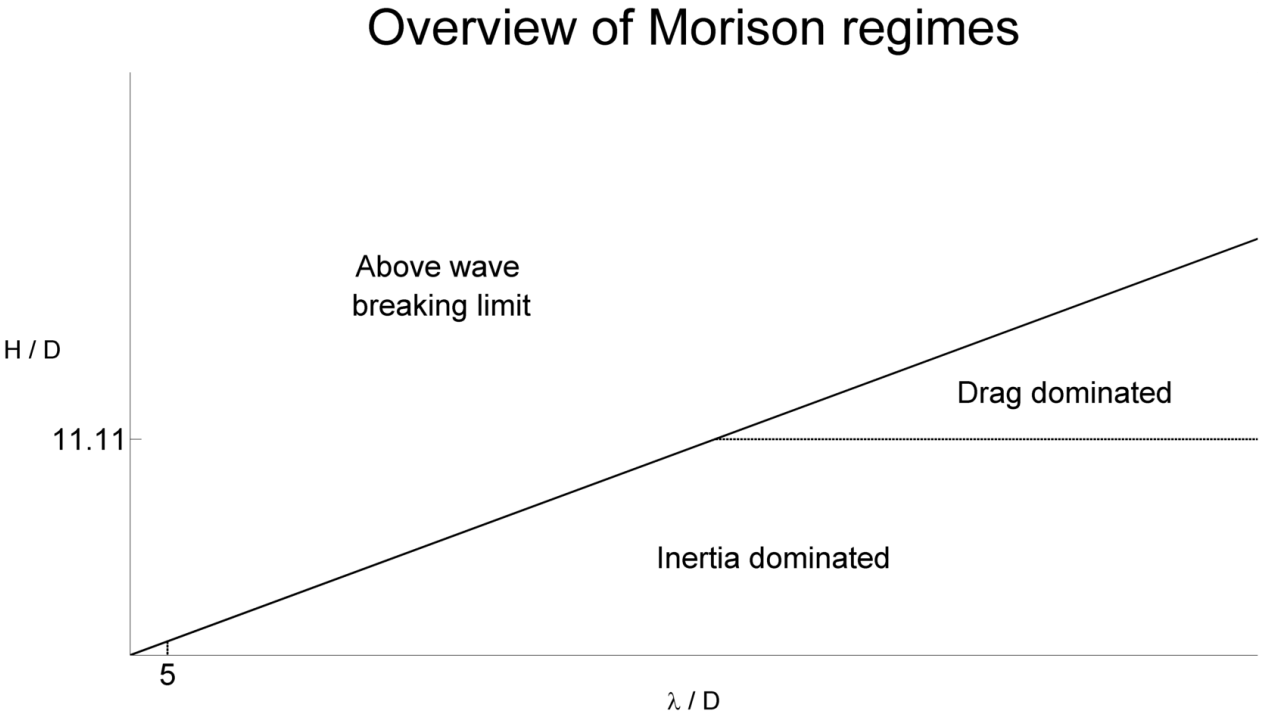

Figure 7.3: Regimes of drag and inertia domination (Faltinsen, 1993)

Equations (7.1) and (2.3) shows the relation between wave height and riser diameter for the workover riser in question, as well as a typical marine riser. The wave height chosen is four meters – identical to all analyses. It is seen that the workover riser is clearly drag dominated, whereas a typical marine riser is in the region dominated by inertia forces.

$$\frac{H}{D_{workover}} = \frac{4\,m}{0.261\,m} = 15.3 \tag{7.1}$$

$$\frac{H}{D_{marine}} = \frac{4\,m}{0.5\,m} = 8 \tag{7.2}$$

Where:

D_{marine} : A typical diameter of a marine riser – 0.5 m

$D_{workover}$: The workover riser's diameter

H : Wave height

7.1.3 Effect of Current Direction

Similar to the current magnitude sensitivity observed in section 6.5, current direction was in section 6.6 found to be important for the fatigue life at the lower end of the riser. The observed trend is that a current transverse with respect to the wave direction provides less damping. This can as well be explained by the drag force's quadratic velocity dependence. A current transverse to the riser's oscillations will still increase the magnitude of the relative velocity. It will however be far less efficient at doing so than a current in-line with the riser's oscillations. The effect of a current transverse to the wave excitation will thus have a similar effect as a longitudinal current of lower magnitude, when it comes to damping the riser's response.

7.2 Control Analyses in RIFLEX

While the previous sections explain why more current can improve fatigue life, the extreme differences in fatigue life require further study. In these cases, where a software provide results that might appear erroneous, a sensible course of action is to validate the results using another, independent software. This eliminates the chance of a software bug causing an issue. For this analysis, the software RIFLEX is chosen. RIFLEX is developed by Marintek, and it is available for NTNU's students on demand. Like Flexcom, RIFLEX is a software for analyzing slender structures in a marine environment.

7.2.1 RIFLEX Model

Initially, the RIFLEX model were created to be an exact copy of the Flexcom model. This would serve to highlight any differences in the solution algorithm. The upper part of the created RIFLEX model is seen in figure 7.4.

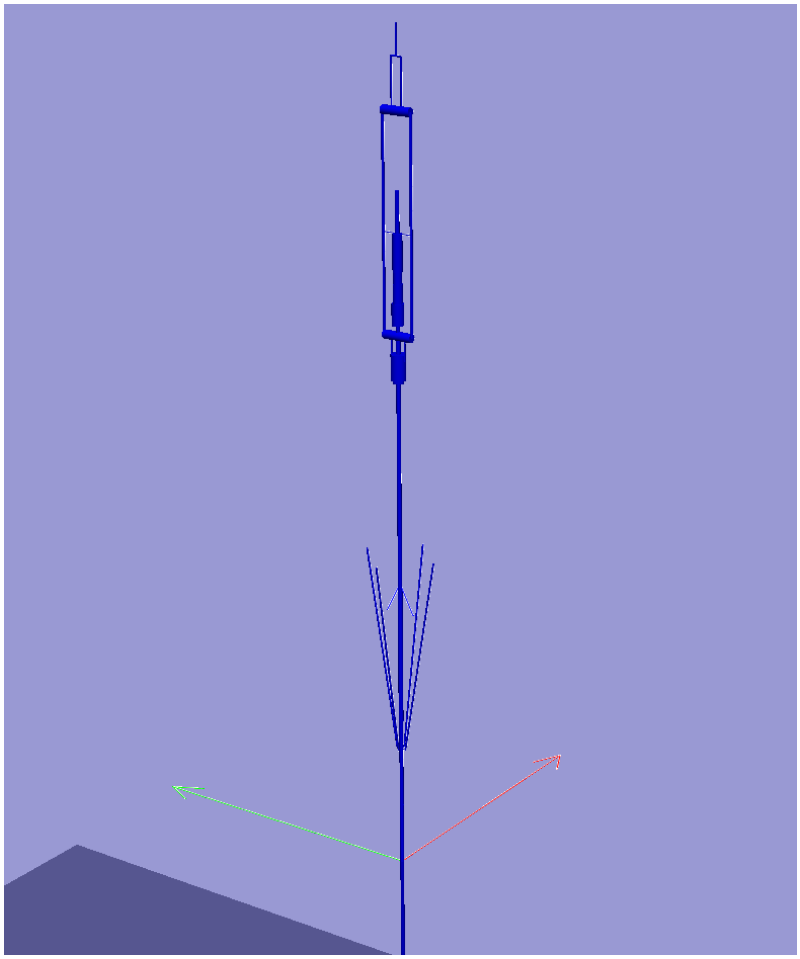

Figure 7.4: Upper part of initial RIFLEX model

Unfortunately, RIFLEX clearly does not handle large differences in stiffness as well as Flexcom. The hinged structure, whose model is based on figure 5.2, appears to cause spurious vibrations. It was thus found necessary to simplify the RIFLEX model. All components above the SFT have been removed, and replaced by a simple, vertical force. This is an extreme simplification with respect to the dynamics of the topside structure, but it is not expected to be significant for the dynamic behavior of the lower part of the structure. Except for the topside simplifications, the Flexcom and RIFLEX models are designed to be identical.

7.2.2 Results from RIFLEX Model

Just like in Flexcom, the RIFLEX analyses are set up to create three-hour time series. Figure 7.5 shows a part of the time series, corresponding to the Flexcom time series shown in figure 6.2. By comparing the two figures, the same trend is clearly present – the bending moment amplitudes are larger when the current magnitude is lower. The difference does however appear smaller than what was reported by Flexcom. This is confirmed by table 7.1. The same trend is clearly present, though the differences in fatigue life are not as extreme as suggested by Flexcom.

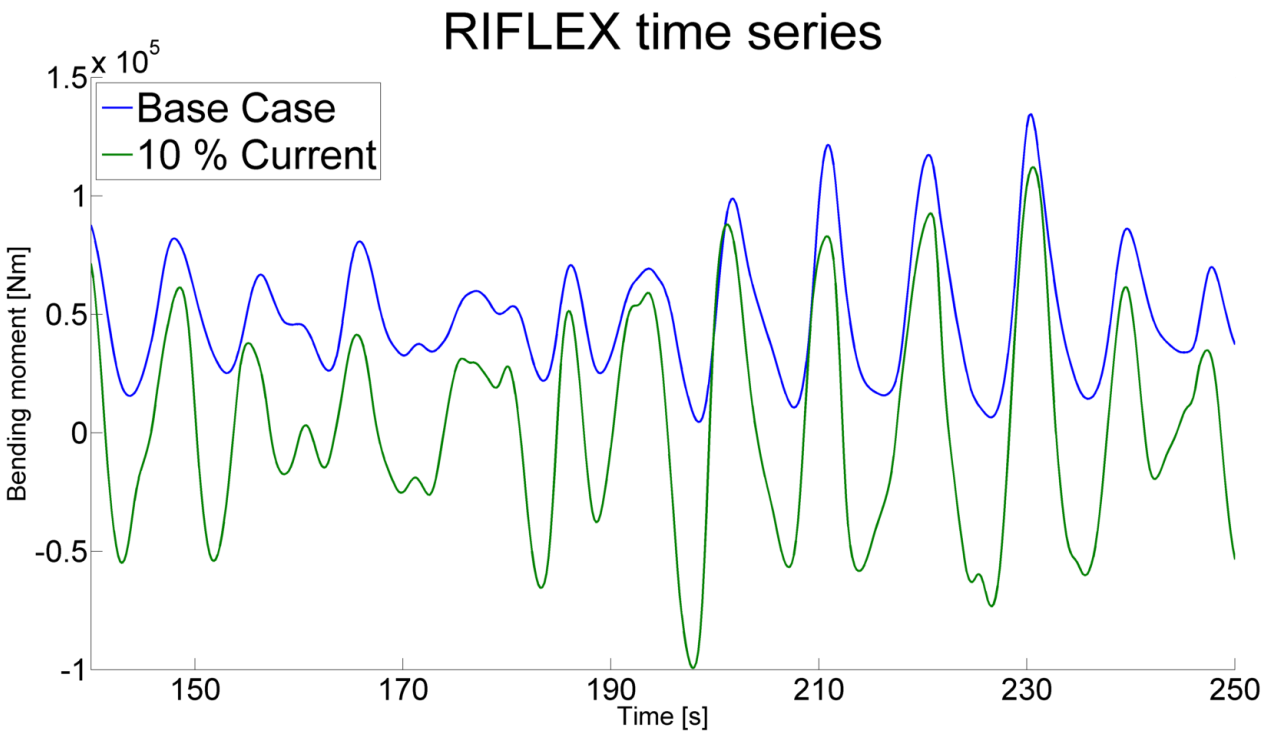

Figure 7.5: Time series from RIFLEX. Corresponding to the Flexcom time series in figure 6.2

While the differences in fatigue life according to RIFLEX are not as extreme as what was indicated by Flexcom, there is no doubt that the difference is still dramatic. By removing 90 % of the current, the fatigue life in the lower end of the riser is reduced by approximately 75 %. Clearly, current is essential for fatigue life calculations. It is noted that the overall stress level in the RIFLEX results are higher than the values provided by Flexcom. This results in a severely reduced fatigue life estimation. Though the absolute fatigue life according to RIFLEX is lower, the trends along the riser appears consistent.

Table 7.1: Current sensitivity along riser, according to RIFLEX

	WHD	***LSS***	***50***	***100***	***200***	***300***	***LV***	***LJ***
10 % Current	25.1 %	25.1 %	26.6 %	21.3 %	31.3 %	59.8 %	83.4 %	97.4 %
50 % Current	29.5 %	29.5 %	33.4 %	27.8 %	43.3 %	68.2 %	88.2 %	99.9 %
75 % Current	55.4 %	55.4 %	55.5 %	55.9 %	75.3 %	88.8 %	102 %	97.3 %
Base Case	100 %	100 %	100 %	100 %	100 %	100 %	100 %	100 %

7.2.3 Alternate RIFLEX Model

As mentioned in section 7.1.1, drag forces provide the riser system with damping, where the dynamic contribution is due to riser motion. It is thus reasonable to assume that the riser's dynamic motion is important for the drag forces' damping effect. In order to evaluate the importance of this effect, an alternate RIFLEX model has been created. In this model, the riser is kept fixed at both ends, with no topside motion. The riser is also given an extreme bending stiffness, which causes any riser motion throughout the water depth to be negligible. With this

high stiff model, the dynamic effects of the riser's response is not included. The result of this analysis is seen in figure 7.6. Here, it is seen that a current mainly produces a static contribution to bending moment. A higher current magnitude also appears to increase moment amplitudes. This result indicates, as assumed, that the riser's response motion is essential for its current sensitivity.

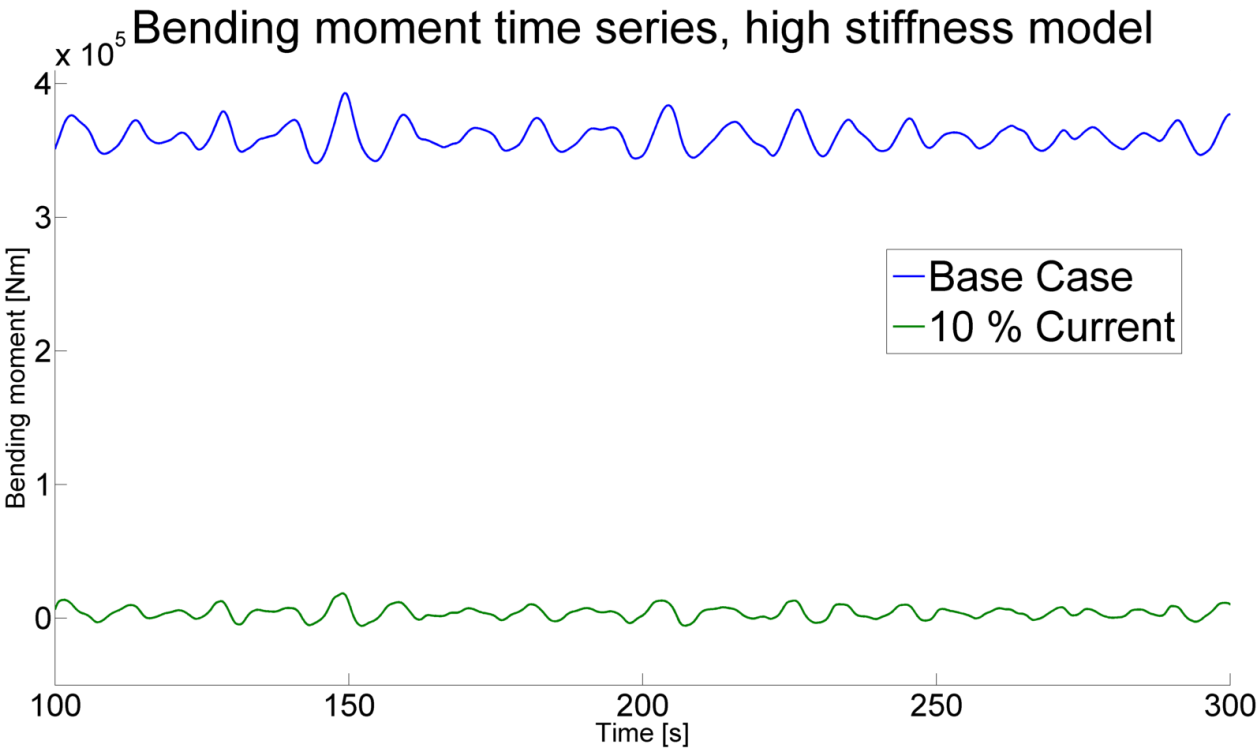

Figure 7.6: Bending moment time series near LSS, high stiffness model

7.3 Additional Current Profiles in RIFLEX

So far, all current profiles have been based on the one-year current profile seem in figure 5.4. Due to the extreme importance of current, it is desired to investigate the effect of different current profiles. Particularly, the influence of current at different depths is desired. In order to investigate this, the existing current profile is customized. At five different depths, the current profile is cut off, so that only current above or below remains. These depths are 25, 50, 100, 150 and 200 meters below MSL. The cut off depths are chosen based on figure 7.2 – in this region, the wave induced particle motion changes from highly significant to negligible. As mentioned in section 7.1.1, it is expected that the main current induced damping is present below this region. The results of this is seen in figure 7.7. It is seen from the figure that removing the current from the uppermost 25 or 50 meters causes little effect for the fatigue life at the LSS. In these cases, only a very small part of the current profile were changed. Any other reduction in current, regardless of depth, causes a reduction in fatigue life. This indicates that the dominant effect of current is to provide damping for the structure, regardless of depth.

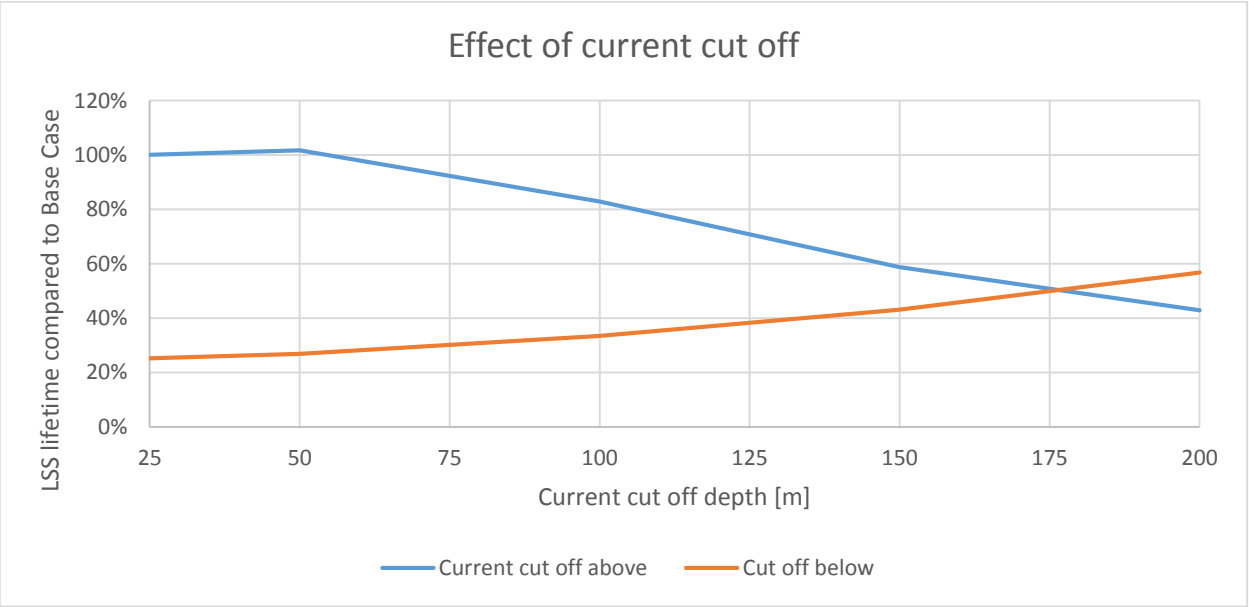

Figure 7.7: Current cut off effect on LSS lifetime

7.4 One DOF Morison Model

In order to provide additional verification of the acquired current sensitivity, simple calculations have been carried out using a one DOF Morison model in Matlab. This model calculates motion of a riser segment of finite length. As there is only one degree of freedom, rotations are neglected. Further, only one riser segment can be calculated at each time. The riser segments are thus analyzed discretely. Two analyses are run, with different levels of current. The seastate is identical for both cases – a regular wave with a wave height of four meters, and a period of nine seconds.

7.4.1 Description of Matlab Code

All scripts used in this section are coded by the author of this thesis, and are found in appendix B. The core Matlab code used to analyze the riser is a time domain solver, which iterates to obtain correct relative velocity and acceleration. It calculates environmental loads using Morison's equations, and calculates response using an Euler-Gauss time integration algorithm. Relative velocity, which is input for calculation of drag forces, is calculated as the result of current, waves and riser velocity. Relative acceleration is calculated as the result of waves and riser acceleration. In addition to the Morison forces, an external load is added, which is intended to simulate the effect of surrounding geometry. Finally, a small stiffness is added to the model. This needs to be small, as it cannot be explained by a physical phenomenon. It is present in the model, as it is required to prevent drift-off. By running this code for a sufficiently long time, the response amplitude of one riser segment is found. This code is run for each riser segment individually. With this approach, the response values cannot be trusted, as boundary conditions are not represented in a satisfactory manner. When comparing the response of two analyses however, it is expected that the trends in response amplitude will be present.

7.4.2 Definition of Excitation Forces

Drag forces and inertia forces are calculated according to Morison's equations, and corrected as the solver iterates for relative velocity and acceleration. In addition to the Morison forces, each riser segment is loaded with a harmonic load. This load corresponds to the net shear force over the riser segment. To obtain this load, an analysis with identical environmental conditions is run in RIFLEX. The load to apply is found as the change in shear force over each segment.

7.4.3 Result

As previously mentioned, the two load cases run are identical when it comes to seastate. The load cases differ only at the level of current applied. As in the original sensitivity study, the current is scaled linearly from the current profile defined as one-year current. The result is seen in figure 7.8. Near the lower end of the riser, the response amplitude is clearly higher when the current is lower. Thus, the trend observed from Flexcom and RIFLEX are confirmed by these calculations. However, this calculation does not properly describe the relative response along the length of the riser. For a large riser segment, it is seen that a lower current gives a lower response amplitude – opposite of what is seen in the analysis results from both Flexcom and RIFLEX. What causes this effect is unknown, though it is theorized that it is due to the artificial stiffness applied. In the riser's mid-section, both wave excitation forces and shear forces are low. It is possible that the magnitude of stiffness, which were found necessary to obtain consistent oscillations, is influential in this region. This artificial stiffness reduces the riser's response.

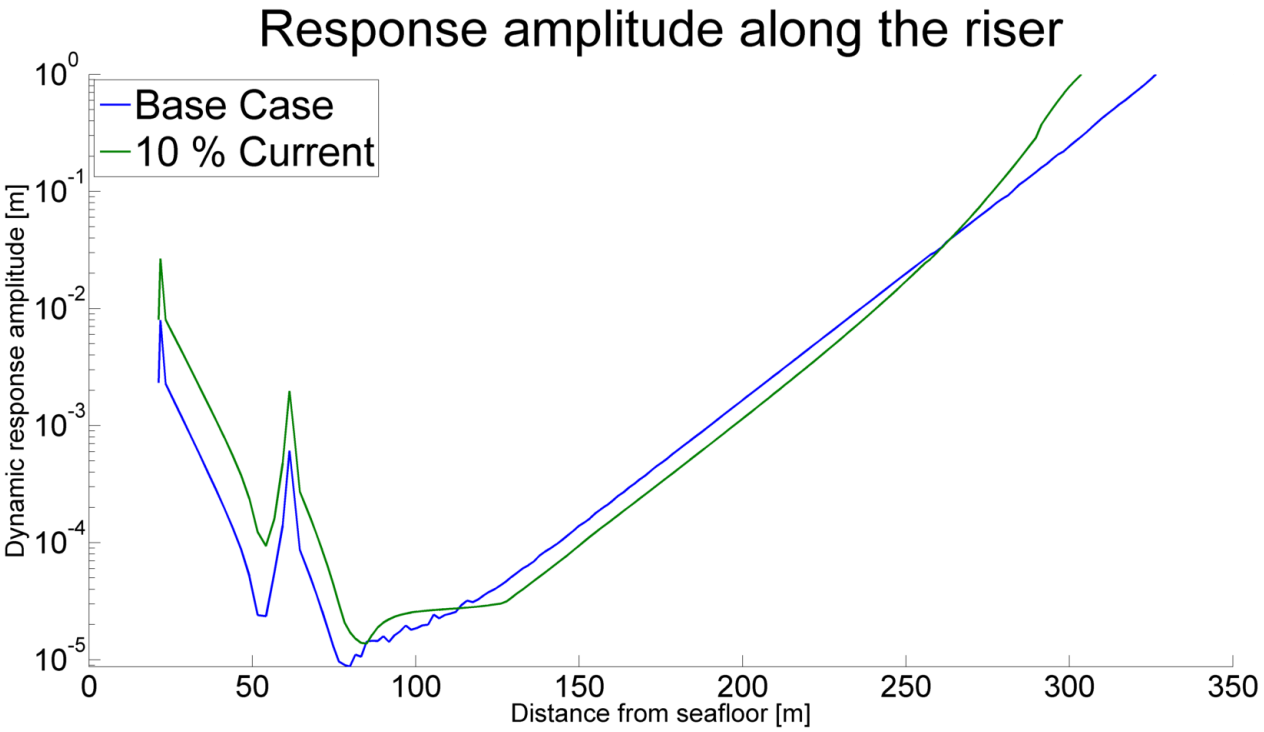

Figure 7.8: Response amplitude along riser. Calculated by user created Matlab functions

8. Proposal of Monitoring System and Discussion

The overall aim of the proposed monitoring system is provide the best possible estimate of fatigue damage along the riser, based on a few parameters. The more parameters used as input, the more accurate the fatigue estimate would be. It is however not feasible to accurately measure all of the previously mentioned parameters real-time. Thus, assumptions must be made. It is again stressed that the magnitude of fatigue life is of little concern for the development of a monitoring system. The important parameter is rather each component's fatigue life, relative to that of the lower strain sensor. At this location, the fatigue damage can be calculated real-time. Thus, a sensitivity that changes the fatigue life by an equal factor along the entire riser will not require further study. Other sensitivities, which affects the various riser components unequally, are far more important to map. In the following sections, a monitoring system is suggested by the author of this thesis.

8.1 Calculation of Extrapolation Factors

It is desired to estimate each component's lifetime according to equation (8.1). This is based on the real-time accumulation rate of fatigue damage at the lower strain sensor, as well as two factors. γ is the reference extrapolation factor, as seen in equation (8.2). This gives the relation between fatigue life at the LSS and component in question, at a reference environmental condition. χ is the extrapolation correction factor, as seen in equation (8.3). This factor accounts for variations in extrapolation factors due to environmental conditions.

$$C_{estimate} = LSS_{real} * \gamma * \chi \tag{8.1}$$

$$\gamma = \frac{C_{ref}}{LSS_{ref}} \tag{8.2}$$

$$\chi = \prod_{i=1}^{num} \frac{C_i}{LSS_i * \gamma} \tag{8.3}$$

Where:

$C_{estimate}$: Estimated riser component lifetime
C_{ref} : Riser component lifetime, reference value
C_i : Riser component lifetime, sensitivity analysis number i
LSS_i : LSS lifetime, sensitivity analysis number i
LSS_{ref} : LSS lifetime, reference value
LSS_{real} : LSS lifetime, actual condition
num : Number of different sensitivities
γ : Base case extrapolation factor
χ : Extrapolation correction factor

The real-time accumulation of fatigue damage at the lower strain sensor is easy to find during operation. An operational monitoring system should utilize the strain sensor signals for live calculation of accumulated fatigue damage. Thus, the current rate of fatigue damage accumulation will be easily available.

8.1.1 Estimation of γ

γ, which is found in equation (8.2), is used for calculating a reference fatigue life at a specific location along the riser. Throughout an operation, each riser joint will have a designated value of γ. This factor accounts for the component's location along the riser, and nothing else. It will thus be constant throughout an operation. In order to estimate this factor, a reference environmental condition must be selected. In this thesis, the chosen reference environmental condition corresponds to the base case analysis, as described in section 0. Whether or not this is the best choice of reference condition should be further investigated during the development of this monitoring system. As the sensitivity study of seastate realization include three additional analyses, all with the same environmental condition, these analyses have been used to improve the accuracy of γ. The resulting γ values are seen in table 8.1. Here, γ values are calculated for seven locations along the riser, in addition to the LSS. These locations are listed in table 6.1. For a fully developed monitoring system, a significantly higher resolution is suggested. The calculation time for estimating γ at an additional location along the riser have been found marginal. Compared to the calculation required for performing a three-hour time domain analysis in Flexcom, this extra calculation requirement is negligible. It is thus feasible to calculate a γ value for each riser joint of the entire riser. This enables the ability to log each riser joint's accumulated fatigue damage more accurately, which will improve the prediction of fatigue damage of each joint.

Table 8.1: γ estimate

	WHD	LSS	50	100	200	300	LV	LJ
Base Case γ	6.784	1.00	165.81	240.64	726.99	422.43	43.32	0.0694
Seed 1 γ	6.781	1.00	162.14	240.36	723.42	417.59	43.33	0.0725
Seed 2 γ	6.779	1.00	165.03	241.03	723.02	426.84	43.95	0.0701
Seed 3 γ	6.780	1.00	164.45	244.31	722.64	425.84	43.74	0.0705
Mean γ	6.781	1.00	164.36	241.59	724.02	423.18	43.59	0.0706
St.dev. γ	2.2E-3	0.00	1.58	1.84	2.01	4.18	0.31	1.3E-3

8.1.2 Estimation of χ

χ is calculated according to equation (8.3). The purpose of χ is to account for the environmental conditions that deviate from the reference condition. It is seen in chapter 6 that several parameter variations alter the extrapolation factors along the riser. These variations will be considered by χ, correcting the extrapolation factors. Thus, a parameter variation that affects the riser's fatigue life along the entire riser evenly will not alter the value of χ. However, a parameter variation that affects different riser segments by uneven factors must be corrected by the value of χ. Like γ, χ must be calculated for each monitored location along the riser. By considering the implications of equation (8.3), it is understood that all sensitivities are assumed uncoupled. This assumption is reasonably accurate for most of the parameter variations. For some of the more influential parameters however, like current magnitude, current direction and riser tension, the assumption of uncoupled sensitivities are unlikely to be valid. For these cases, the more complex relationships must be mapped, and implemented in the monitoring system. In figure 8.1, the influence of peak period on χ is mapped. A complete overview of all sensitivities' influence on χ is seen in appendix C.

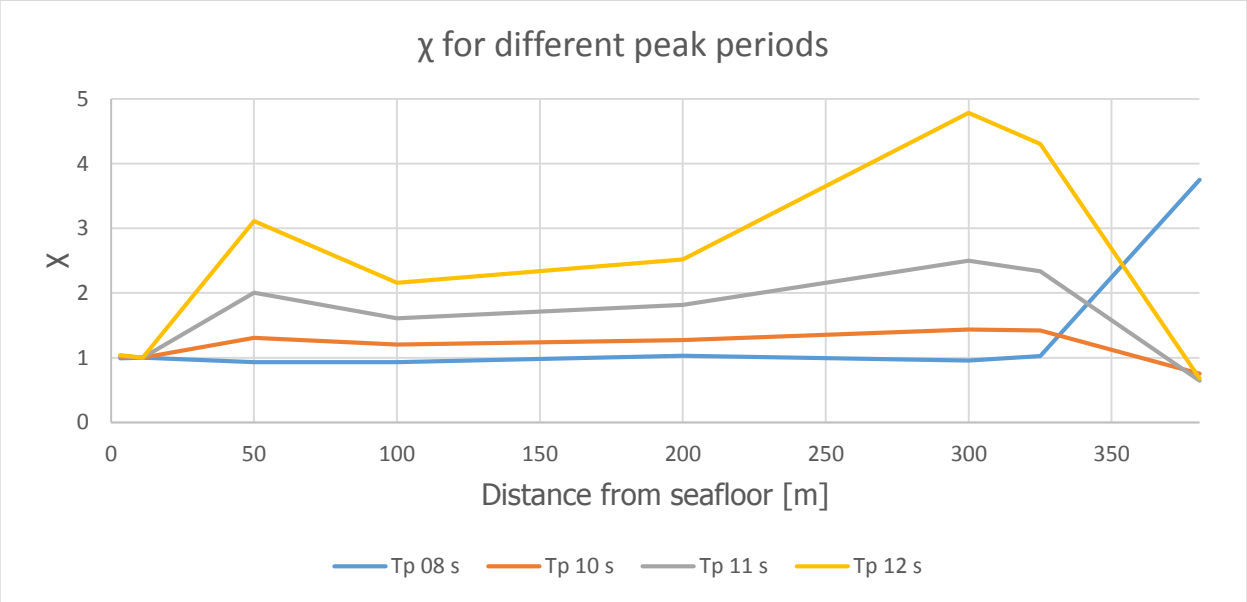

Figure 8.1: χ for different peak periods

8.2 Fatigue Extrapolation Validation

In order to evaluate the fatigue monitoring strategy, four additional analyses are run in Flexcom, where a combination of the sensitivities previously run are applied. This is done in order to evaluate the validity of equation (8.3), which assumes that the different environmental sensitivities do not influence each other. Each of the four validation analyses combine two previously run sensitivities.

Case 1. Peak period changed from 9 to 10 seconds. Current magnitude reduced to 50 % of its initial value.
Case 2. Peak period changed from 9 to 12 seconds. Vessel offset changed from 0 to 20 meters.
Case 3. Riser tension increased to 50 metric tons overpull. Current magnitude reduced to 75 % of its initial value.
Case 4. Current magnitude reduced to 10 % of its initial value. Current direction changed from 0 to 90 degrees along the entire water depth.

Based on the results from these analyses, fatigue lives calculated by two procedures. For control, the various components' fatigue lives are calculated by the same procedure as the previous sensitivities. In addition to this, the fatigue lives are estimated by extrapolation, according to equation (8.1). These two procedures for calculating fatigue life are compared, their differences seen in table 8.2. It is seen that the error introduced in cases one and two are low. This implies that parameters such as peak period, current magnitude and vessel offset does not influence each other's effect on fatigue life. Thus, equation (8.3) is valid for the combination of these parameters.

Table 8.2: Fatigue life extrapolation error

	WHD	***LSS***	***50***	***100***	***200***	***300***	***LV***	***LJ***
Case 1	0.3 %	0.0 %	3.0 %	2.1 %	4.7 %	2.2 %	1.0 %	2.9 %
Case 2	-1.3 %	0.0 %	4.1 %	2.1 %	3.2 %	1.8 %	0.8 %	1.7 %
Case 3	0.1 %	0.0 %	0.1 %	2.8 %	6.0 %	9.2 %	17.1 %	20.5 %
Case 4	1.0 %	0.0 %	16.1 %	23.3 %	138 %	204 %	408 %	418 %

At cases three and four however, large errors are introduced when the parameters are combined. In case three, this error is caused by the increased riser tension. As was seen in section 6.9, the riser tension is an important parameter. A change in riser tension alters the system's stiffness, which clearly affects the influence of other parameters. In case four, the error is extreme. This can, however, quite easily be explained. It was seen in sections 6.5 and 6.6 that both a reduction of current magnitude, and a 90-degree change in current direction, are severe with respect to the fatigue life at the LSS. The fatigue life at the upper end of the riser is however largely unaltered by these sensitivities. To account for this, the χ factors for the upper end of the riser are large for both these sensitivities, as can be seen in appendix C. When combining these factors according to equation (8.3) however, an error is introduced; a reduction

in current magnitude will necessarily reduce the importance of current direction. Thus, the combination of reduced current magnitude and current direction in case four will be less severe that its individual sensitivities imply. This is demonstrated by table 8.3 and figure 8.2, where the value calculated for χ according to equation (8.3) is compared to its ideal value. From this, it is seen that the estimated χ is too high. The ideal χ value is almost identical to the value obtained from current magnitude alone. This implies that for low current magnitudes, the current direction becomes insignificant.

Table 8.3: χ contributions for case four

	WHD	LSS	50	100	200	300	LV	LJ
10 % Current	1.013	1.000	0.998	1.030	2.361	3.389	8.643	17.139
Current dir 90	1.010	1.000	1.178	1.224	2.399	3.038	5.145	5.270
Calculated χ	1.024	1.000	1.175	1.261	5.664	10.294	44.472	90.315
Real χ	1.014	1.000	1.012	1.023	2.377	3.386	8.748	17.445

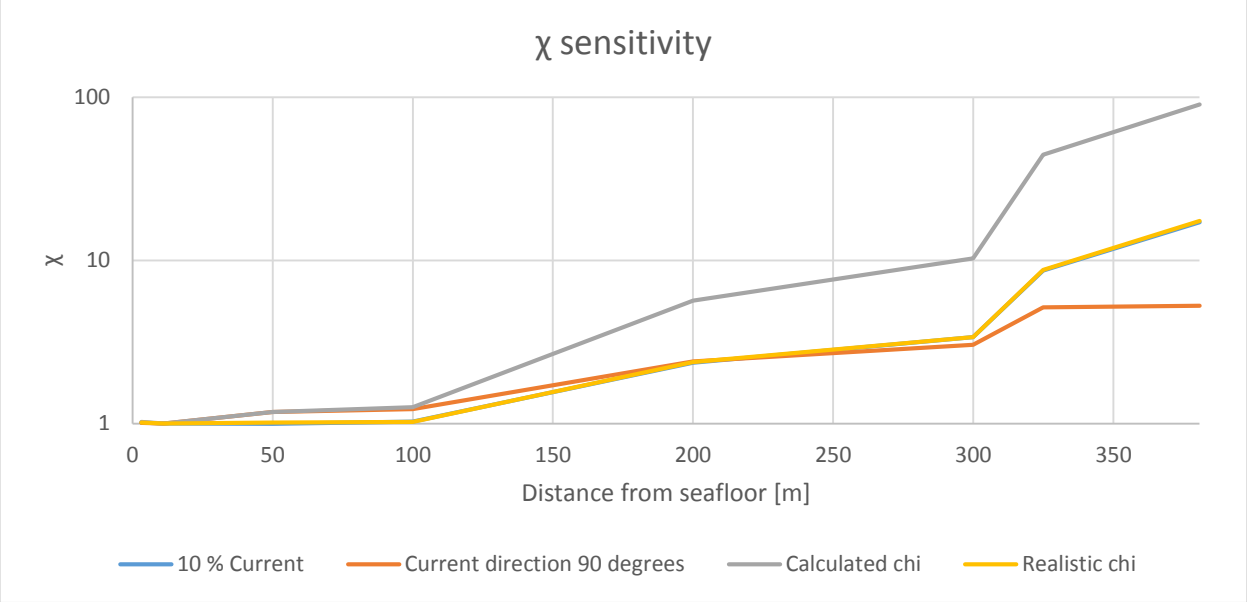

Figure 8.2: χ contributions for case four

8.2.1 Improvements of Fatigue Extrapolation

It has been seen that the procedure for extrapolation of fatigue damage proposed by equation (8.1) works well for most of the influential parameters. However, the effect of variations in riser tension cannot be described by this simple procedure. The effect of current direction will also require a more complex description, as its importance is dependent on current magnitude. Based on the available analysis results, there is insufficient data to draw a conclusion regarding the best way of accounting for riser tension and current direction. In order to map the influence of riser tension, it is proposed to run a full set of sensitivities combined with different levels of riser tension. Particular attention should be given to the effect of peak period, as a change in riser tension will alter its natural frequencies. Further analyses must also be run in order to investigate the effect of current direction, though this is believed to be a simpler problem. As

the importance of current direction is dependent on current magnitude, an additional scaling factor due to current magnitude can be introduced.

In this thesis, only extrapolation from the lower strain sensor is considered. This works well when all parameters are known, but it might not be as accurate during real operations, where additional effects are present, such as VIV. Unknown effects can reduce the accuracy of fatigue damage extrapolation. The components that are farthest from the strain sensor will have the highest level of uncertainty. It is thus suggested to include the upper strain sensor into the system. This sensor can be used as reference location for the surrounding components, such as landing joint and lubricator valve. It can further be theorized that the system's uncertainty can be reduced by comparing the lower and upper strain sensors. Their relative load level and load direction might potentially be useful for increasing the system's accuracy. This theory has not been investigated by the author of this thesis.

8.3 Evaluation of Monitoring System Accuracy

It has been seen in the previous sections that fatigue life can be extrapolated from the LSS with high accuracy, as long as the environmental conditions are known, and the influence of all parameters are properly investigated. However, acquiring the environmental data required for this will be challenging. For most parameters, such as peak period, vessel offset and riser tension, the knowledge is already present, and can easily be reported to the monitoring system.

8.3.1 Uncertainty Due to Current

The main source of uncertainty is due to current. It has been seen that current, both magnitude and direction, is an essential parameter to represent accurately in the monitoring system. However, understanding the effect of current is of little use for monitoring, as long as the current profile is unknown. Acquiring the continuous current profile as a function of depth is not realistic, as this would require several current sensors along the riser. Thus, a current measuring system featuring more than two sensors must be considered unrealistic. One of these two sensors will be located near the sea surface, and the other should be located near the seafloor. Further studies are required in order to determine how accurately the current can be described by these two measurements. Achieving an accurate model of how the riser's fatigue life changes, as a function of real current measurements is vital for the development of a riser monitoring system. Due to the extreme importance of current, as found in section 6.5, a riser monitoring system cannot be used for the upper parts of the riser unless it can account for current in an accurate manner. Fatigue can still be monitored at the stress joint and wellhead, but not components at higher elevations. Accurate representation of current, based on measured data, is thus a prerequisite for the development of a monitoring system considering the entire riser.

8.3.2 Uncertainty Within a Seastate

As mentioned in section 8.1.1, the extrapolation factor γ is found from the mean level of all seastate realizations for the base case analysis. Ideally, the four analyses should provide identical fatigue lives, and thus identical estimates of γ. However, as seen in table 8.1, the

extrapolation factors suggested by the different seastate realizations differ. The differences in fatigue life extrapolation are important to quantify, as the accuracy of the monitoring system cannot surpass the uncertainties in each seastate. In order to investigate this uncertainty, the four seastate realization analyses from table 8.1 are each divided into one-hour time series, creating a total of twelve samples. Fatigue life is then calculated for each of these samples, and their extrapolation values are compared to the γ value found in section 8.1.1. The results of this are seen in figure 8.3. It is seen that the highest level of uncertainty is found at the landing joint, where the highest offset of these twelve samples is almost as high as 7 %. Along the other riser segments, uncertainty in fatigue life is seen to be below 5 % for the twelve samples. Uncertainties in the range of 5-7 % are considered negligible for fatigue calculations, though all sources of uncertainty must be considered. It will likely be required for the monitoring system to estimate upper bound fatigue values.

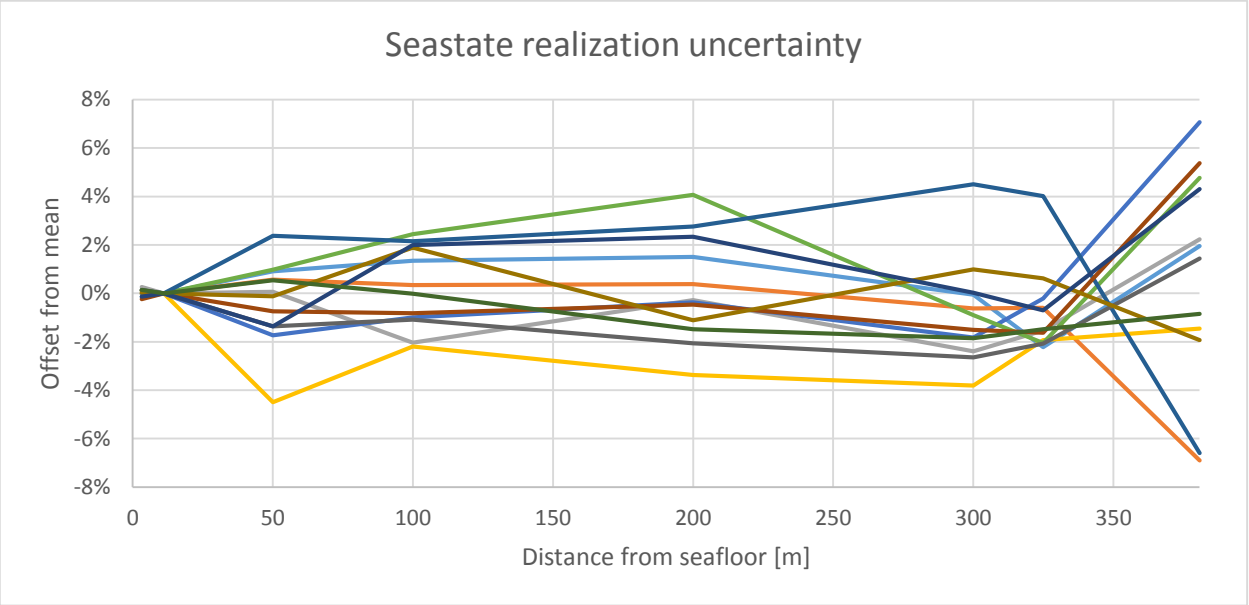

Figure 8.3: Fatigue life uncertainty in seastate realization. 1-hour samples

8.3.3 Known and Unknown Parameters

A vital part of the monitoring system is acquisition of important parameters. It has been seen that parameters like peak period, current and riser tension are important for extrapolation of fatigue life. Some important parameters are easily available, while others might prove difficult to estimate properly. The parameters studied in this thesis are listed in table 8.4, along with an evaluation of their importance and the difficulty of their acquisition.

Table 8.4: Importance and state of the various parameters

Parameter	Importance	Acquisition
Seastate	High	Known
Current	High	Must be measured. Discussed in section 8.3.1
Vessel offset	Low	Easily measured
Vessel tilt	Low	Easily measured
Wellhead tilt	Low	Assumed static and known
Riser tension	High	Easily measured
Hydrodynamic coefficients	Medium	Must be found in advance
Density of content	Medium	Known
TF orientation	Low	Known
Wireline model	Low	Known

As found previously, it is seen that seastate, current and riser tension are the most important parameters. Of these three parameters, systems are already in place for measuring two of them. The seastate is forecasted, as well as measured by radars. The riser tension can be measured from the applied tension at the vessel, or calculated from the mean strain of the strain sensors. Acquisition of correct current profile remains an issue, as previously discussed. Less important, though still highly significant are the hydrodynamic coefficients. These cannot easily be measured during operation, and should be known in advance. Two procedures are suggested. Either the values from table 5.2 are accepted, or the hydrodynamic coefficients can be altered by calibration of the monitoring system. All other parameters investigated in this thesis can be determined with ease.

8.4 Monitoring System Feasibility

Based on the studies done in this thesis, the feasibility of a riser monitoring system appears promising. The effect of riser tension must be studied further, and the combination of current magnitude and current direction must be mapped more thoroughly. Though many challenges remain, no aspect of the riser system considered so far has proven impossible. It is stressed that the majority of work in order to develop this system remain. Other effects, like VIV and vessel slow drift have yet to be considered. It must be kept in mind that a single influential effect, which the monitoring system fails to represent accurately, can make the system unfeasible for parts of the riser. Based on the parameters already studied, the degree of accuracy is high for all riser components. However, for the finished monitoring system it will likely prove that the highest accuracy is achieved near the strain sensors. Parameter that are too complex to be fully accounted for by the monitoring system, and parameters that cannot be measured accurately, are likely to reduce the accuracy of extrapolation. However, by using both the upper and lower strain sensor, most critical components are near a strain sensor.

Due to this, it appears feasible to develop a riser monitoring system that estimates fatigue damage for the various riser components, though a definite conclusion regarding feasibility cannot be drawn until all parameters are accounted for.

In this thesis, the economic aspect of a riser monitoring system has not been considered. The feasibility of such a system will however in part depend on economics – developing such a system is time consuming, and thus expensive. Whether the increased operational efficiency caused by implementing this system is worth the development, cannot be answered by the author of this thesis. There is also no guarantee of achieving a sufficient accuracy of the final monitoring system, regardless of the resources invested in the project.

9. Conclusion

The effect of several parameter variations on the fatigue life of a workover riser has been investigated. The riser is designed for operation at the Kristin field, which is operated by the semisub Scarabeo 5. These studies have been made in order to evaluate the feasibility of a monitoring system for the workover riser. In this thesis, the monitoring system considers fatigue life. Other parameters, like expected extreme response, have not been covered by this thesis.

9.1 Current Sensitivity

When performing the various parameter variations, it has been found that current is an essential parameter for the fatigue life of this workover riser. The expected outcome was for the current to provide a near static contribution, and thus be almost insignificant with respect to riser fatigue. However, the drag force's quadratic velocity-dependence causes the damping level to increase with current. Thus, a higher current magnitude is beneficial with respect to fatigue life. The damping effect of current is at its highest when the current direction is tangential to the riser's response oscillations. Current normal to the riser response gives a similar effect as a severely reduced tangential current. For fatigue monitoring, the combination of current magnitude and direction must clearly be considered.

9.2 Fatigue Monitoring

A fatigue monitoring system has been suggested, where each riser component's fatigue life is calculated based on the real-time accumulation of fatigue damage at the stress joint. The stress joint is selected as reference, as strain sensors are attached to it. Thus, accumulation of fatigue damage can be calculated real-time at this location. The proposed monitoring system extrapolates fatigue damage by two factors; one factor accounts for each component's position, while the other factor accounts for environmental conditions. The proposed system appears to work well for certain parametric variations, while other parameters require further studies in order to determine the appropriate value of the environmental extrapolation factor. The combination of peak period, current magnitude and vessel offset are examples of parameters that appear to work well. Examples of parameters that require further study are riser tension, as well as the combination of current magnitude and current direction.

Though the proposed fatigue monitoring system is far from finished, its feasibility appears promising. Several parameters are yet to be investigated, such as VIV and vessel slow drift. A single, influential parameter that the monitoring system fails to account for can severely reduce the system's accuracy for some riser segments. Thus, while the feasibility of such a monitoring system for the entire riser appears feasible, it cannot be assumed that there will not be unexpected issues during further development. Implementing fatigue monitoring near the strain sensors should however not cause large difficulties.

10. Recommendations for Further Work

In this thesis, the foundation of a riser monitoring system for fatigue life has been suggested. The ultimate target of this system is to provide a live estimate of each riser component's fatigue damage accumulation, as well as other parameters. Obviously, this system is far from complete. Only the basics of extrapolation methods are founded in this thesis. Further studies are suggested in these areas:

- Real monitoring data from the riser's strain sensors must be incorporated in the model. The riser's finite element model must be calibrated, so that its reported forces and moments corresponds to what is really reported by the strain sensor. Ideally, this calibration should take place with a wide range of environmental conditions. During this process, it is vital that the most important parameters, such as waves and current, are known.
- The effect of riser tension and current direction must be investigated more thoroughly in order to develop a reliable monitoring system.
- A six DOF RAO should be acquired for the platform. The effect of various wave directions can then be investigated, as well as the effect of wave spreading.
- The effect of other parameters must be mapped. In this thesis, higher order effects, such as vessel slow drift, have been neglected. Neither the effect of vortex-induced vibrations have been investigated. These parameters might prove to have an important contribution on the riser's fatigue life. All influential parameters must be mapped thoroughly if the monitoring system is ever to produce an accurate estimate of fatigue life.
- A riser monitoring system should not only estimate the components' fatigue lives. It is also desired to estimate the riser's expected extreme response at a given seastate. When the environmental conditions get rough, the operator must make a decision to stay connected, or to disconnect. Without an estimate of the riser's expected extreme response, a conservative decision must be made. A monitoring system that estimates extreme riser response will thus allow the operator to stay connected longer. This will increase operation efficiency. The estimation of extreme response can potentially be a completely separate system from fatigue life estimation.
- Shear stress has been neglected for fatigue calculations in this thesis. This assumption might be invalid near the lower end of the riser, as well as at the landing joint. A study should be conducted, where the influence of shear stress is accounted for.
- Fatigue extrapolation from the lower strain sensor will have a high accuracy near the sensor. At distant locations however, such as the landing joint, complex relations might ruin the system's accuracy. By including other input parameters, the system's accuracy can be increased. Suggested parameters that can be considered are the upper strain sensor, measured vessel motion, and possibly SFT acceleration.

References

. (2014). Retrieved 29.05, 2014, from http://www.akersolutions.com/Documents/Subsea/Datasheets/2014_02_19_riserLOCK_flyer_A4_screen.pdf

Al-Shawly, A. S., Al-Buali, M. H., Al-Omran, M. R., Dashash, A. A., & Gurani, W. (2010). Wireline Well Tractor Technology Experience in Extended Reach Horizontal Well.

Bai, Y., & Bai, Q. (2005). Chapter 25 - Steel Catenary Risers. In Y. Bai & Q. Bai (Eds.), *Subsea Pipelines and Risers* (pp. 437-451). Oxford: Elsevier Science Ltd.

DNV. (2005). Recommended practice DNV-RP-F204, riser fatigue. *Hovik, Norway*.

DNV. (2010). Fatigue design of offshore steel structures. *DNV Recommended Practice DNV-RP-C203*.

Drange, C. (2010). Bringing Wireline and Coiled Tubing to New Frontiers on a Light Well Intervention Unit.

Faltinsen, O. (1993). *Sea loads on ships and offshore structures* (Vol. 1): Cambridge university press.

Fleumer, B. (2007). Scarabeo 5 near Snorre. Retrieved 27.05, 2014, from http://www.panoramio.com/photo/1394691

. Flexcom - Introductory Manual. (2013): MCS Kenny.

. Flexcom - Technical Manual. (2013): MCS Kenny.

Grattan, K., & Sun, T. (2000). Fiber optic sensor technology: an overview. *Sensors and Actuators A: Physical, 82*(1), 40-61.

Halvorsen, T., & Araujo, L. (1993). *Standardization Of Subsea Production Systems: Practical Experience From Draugen, Statfjord Satellite, And Heidrun Projects.* Paper presented at the Offshore Technology Conference.

ISO. (2005). ISO 13628-7 Petroleum and natural gas industries - Design and operation of subsea production systems - Part 7: Completion/workover riser systems.

Kirkvik, R. H., & Berge, T. (2011). *Integrity Management System For Work-Over Risers (WORs).* Paper presented at the The Twenty-first International Offshore and Polar Engineering Conference.

Kruger, C., & Schwanitz, B. J. (2008). Optimize Well Performance with Electrical Wireline Interventions.

Kumar, A., & Hogan, M. E. (2002). *Performance Related Parameters of Flexible Connections Used in Offshore Pipelines.* Paper presented at the ASME 2002 21st International Conference on Offshore Mechanics and Arctic Engineering.

Leising, L., & Newman, K. (1993). Coiled-Tubing Drilling. *SPE drilling & completion, 8*(4), 227-232.

Maaskant, R., Alavie, T., Measures, R. M., Tadros, G., Rizkalla, S. H., & Guha-Thakurta, A. (1997). Fiber-optic Bragg grating sensors for bridge monitoring. *Cement and Concrete Composites, 19*(1), 21-33. doi: http://dx.doi.org/10.1016/S0958-9465(96)00040-6

The marine riser. Retrieved 29.05, 2014, from http://dc718.4shared.com/doc/pPyWIA1L/preview.html

McNamara, J., O'Brien, P., & Gilroy, S. G. (1988). Nonlinear analysis of flexible risers using hybrid finite elements. *Journal of offshore mechanics and arctic engineering, 110*, 197.

Mody, R. K., & O'Malley, E. (2011). Oilfield Automation *Pumps and Pipes* (pp. 9-20): Springer.

Mollestad, E. (1983). Techniques for Static and Dynamic Solution of Nonlinear Finite Element Problems. *Dr. Ing. Dissertation*, 84-81.

Morooka, C., Coelho, F., & Shiguemoto, D. (2006). DYNAMIC BEHAVIOR OF A TOP TENSIONED RISER IN FREQUENCY AND TIME DOMAIN.

Nieslony, A. (2010). Rainflow Counting Algorithm. Retrieved from http://www.mathworks.com/matlabcentral/fileexchange/3026-rainflow-counting-algorithm#comments

Pierson Jr, W. J., & Moskowitz, L. (1964). A proposed spectral form for fully developed wind seas based on the similarity theory of SA Kitaigorodskii. *Journal of geophysical research, 69*(24), 5181-5190.

Ramsnes, T. I. (2010). Subsea well intervention; Learning from the past - planning for the future. Retrieved 02.06, 2014, from http://www.slideshare.net/Statoil/subsea-well-intervention-learning-from-the-past-planning-for-the-future

Revå, C. (2014) *christian.reva@akersolutions.com*.

. RIFLEX Theory Manual. (2013). In Marintek (Ed.).

. RIFLEX User Manual. (2013). In Marintek (Ed.).

Robert F, A. (2001). Application of a Fiber Optic Distributed Strain Sensor System to Woven E-Glass Composite.

Russo, M., Holden, H., Reinås, L., & Sæther, M. (2012). *Fatigue assessment of subsea wells for future and historical operations based on measured riser loads.* Paper presented at the ASME 2012 31st International Conference on Ocean, Offshore and Arctic Engineering.

Sarpkaya, T. (1981). *A Critical Assessment of Morison's Equation.* Paper presented at the INTERNATIONAL SYMPOSIUM ON HYDRODYNAMICS IN OCEAN ENGINEERING. PREPRINTS, 1981.

Sirohi, J., & Chopra, I. (2000). Fundamental understanding of piezoelectric strain sensors. *Journal of Intelligent Material Systems and Structures, 11*(4), 246-257.

Söding, H., Blok, J., Chen, H., Hagiwara, K., Isaacson, M., Jankowski, J., . . . Richer, J. (1990). Environmental forces of offshore structures: a state-of-the-art review. *Marine structures, 3*(1), 59-81.

Tennyson, R., Mufti, A., Rizkalla, S., Tadros, G., & Benmokrane, B. (2001). Structural health monitoring of innovative bridges in Canada with fiber optic sensors. *Smart Materials and Structures, 10*(3), 560.

Turner, D. R., Harris, T. W. R., Slater, M., Yuratich, M. A., & Head, P. F. (1999). Electric Coiled Tubing Drilling: A Smarter CT Drilling System.

Tuttle, M. (1989). Fundamental strain-gage technology *Manual on Experimental Methods for Mechanical Testing of Composites* (pp. 17-26): Springer.

WAFO-group. (2000). WAFO - A Matlab Toolbox for Analysis of Random Waves and Loads - A Tutorial. Retrieved from http://www.maths.lth.se/matstat/wafo

Wolfram, J., & Naghipour, M. (1999). On the estimation of Morison force coefficients and their predictive accuracy for very rough circular cylinders. *Applied Ocean Research, 21*(6), 311-328. doi: http://dx.doi.org/10.1016/S0141-1187(99)00018-8

WordNet. ((2010). from Princeton University http://wordnet.princeton.edu

Yang, Y. S., Avakov, V. A., Smith, D. E., Martin, J. R., & Wu, J. (1998). Coiled Tubing Fatigue Damage on Floating Vessels.

Zhang, Q., Zhang, R., Huang, Y., & Yang, H. (2010). Design and Analysis of Taper Stress Joint for Top Tensioned Risers.

Zijderveld, G. H. T., Tiebout, H. J., Hendriks, S. M., & Poldervaart, L. (2012). Subsea Well Intervention Vessel and Systems.

Appendices

Appendix A: Riser Model and Environmental Data

The data in this appendix are extracted from the riser's design report, which is provided by Aker Solutions. This report has been provided to the author by Aker Solutions.

A.1 Riser Specifications

The riser models, both in Flexcom and RIFLEX, have been created based on the data in the following tables. Where the tables does not sufficiently describe the riser's geometry, the illustrations in figure 5.1 and figure 5.2 have been used.

Name	Mass [kg/m]	Eiyy [Nm^2]	Eizz [Nm^2]	GJ [Nm^2]	EA [N]	iD [m]	oD [m]
CB bails	6.06E+01	1.08E+06	1.08E+06	8.30E+05	1.68E+09	0	0.099
CB elevator	0.00E+00	5.00E+12	5.00E+12	3.83E+12	3.61E+12	0	0
TF vertical	2.12E+02	5.21E+07	1.77E+07	3.99E+07	3.08E+09	0	0.185
TF top	2.16E+03	1.16E+09	1.16E+09	8.87E+08	5.49E+10	0	0.591
TF bottom	2.16E+03	1.16E+09	1.16E+09	8.87E+08	5.49E+10	0	0.591
CT chains	0.00E+00	4.16E+01	4.16E+01	3.19E+01	1.04E+07	0	0
Gooseneck	3.01E+02	3.18E+07	3.18E+07	2.43E+07	5.26E+09	0.179	0.284
CT injector	2.35E+03	6.66E+08	6.66E+08	5.10E+08	3.67E+10	0.179	0.641
CT stripper	1.78E+03	2.04E+08	2.04E+08	1.56E+08	1.84E+10	0.179	0.566
CT dual stripper	2.33E+03	2.04E+08	2.04E+08	1.56E+08	1.84E+10	0.179	0.639
CT BOP	3.91E+03	6.66E+08	6.66E+08	5.10E+08	3.67E+10	0.179	0.815
CT spool	1.51E+02	3.16E+07	3.16E+07	2.42E+07	5.22E+09	0.18	0.238
TF bails	6.88E+01	1.08E+06	1.08E+06	8.30E+05	1.68E+09	0	0.105
ST elevator	0.00E+00	5.00E+12	5.00E+12	3.83E+12	3.61E+12	0	0
Riserlock adp	4.13E+02	6.66E+08	6.66E+08	5.10E+08	3.67E+10	0.179	0.314
SFT	5.86E+03	3.53E+08	3.53E+08	2.71E+08	2.56E+10	0.179	0.989
SFT adp	3.02E+03	3.98E+07	3.98E+07	3.05E+07	5.88E+09	0.19	0.723
Landing joint	2.85E+02	3.98E+07	3.98E+07	3.05E+07	5.88E+09	0.19	0.286
Upper pup jts	4.52E+02	3.98E+07	3.98E+07	3.05E+07	5.88E+09	0.19	0.33
Tension joint	2.20E+02	3.98E+07	3.98E+07	3.05E+07	5.88E+09	0.19	0.267
Upper riser jts	2.55E+02	2.70E+07	2.70E+07	2.07E+07	5.07E+09	0.164	0.261
Upper lubricator adp	2.00E+02	2.70E+07	2.70E+07	2.07E+07	5.07E+09	0.164	0.243
Lubricator valve	8.00E+02	2.70E+07	2.70E+07	2.07E+07	5.07E+09	0.164	0.395
Lower lubricator adp	2.00E+02	2.70E+07	2.70E+07	2.07E+07	5.07E+09	0.164	0.243
Lower pup jts	4.26E+02	3.98E+07	3.98E+07	3.05E+07	5.88E+09	0.19	0.324
Middle riser jts	2.55E+02	2.70E+07	2.70E+07	2.07E+07	5.07E+09	0.164	0.261
Safety joint	6.33E+02	2.70E+07	2.70E+07	2.07E+07	5.07E+09	0.164	0.359
Lower riser jts	2.55E+02	2.70E+07	2.70E+07	2.07E+07	5.07E+09	0.164	0.261
Stress joint pipe	1.80E+02	3.98E+07	3.98E+07	3.05E+07	5.88E+09	0.19	0.255
Stress joint 6	2.40E+02	4.33E+07	4.33E+07	3.32E+07	6.45E+09	0.184	0.27
Stress joint 5	2.62E+02	5.20E+07	5.20E+07	3.99E+07	7.36E+09	0.184	0.276
Stress joint 4	3.00E+02	6.36E+07	6.36E+07	4.87E+07	8.48E+09	0.184	0.287
Stress joint 3	3.39E+02	7.39E+07	7.39E+07	5.66E+07	9.41E+09	0.184	0.298
Stress joint 2	3.67E+02	8.04E+07	8.04E+07	6.16E+07	9.96E+09	0.184	0.305
Stress joint 1	6.46E+02	3.27E+08	3.27E+08	2.50E+08	2.42E+10	0.184	0.372
EDP	1.22E+04	2.99E+09	2.99E+09	2.29E+09	8.31E+10	0.179	1.415
WCP	1.12E+04	2.99E+09	2.99E+09	2.29E+09	8.31E+10	0.179	1.356
Subsea tree	1.69E+04	2.99E+09	2.99E+09	2.29E+09	8.31E+10	0.179	1.664
Wellhead	2.19E+03	8.29E+08	8.29E+08	6.35E+08	1.22E+10	0.711	0.927

Name	L [m]	Ca [-]	Cd [-]
CB bails	3.3	1	0
CB elevator	1	1	0
TF vertical	14.15	1	0
TF top	2.08	1	0
TF bottom	2.08	1	0
CT chains	1	1	0
Gooseneck	2.66	1	0
CT injector	2.43	1	0
CT stripper	0.762	1	0
CT dual stripper	1.245	1	0
CT BOP	1.403	1	0
CT spool	0.995	1	0
TF bails	1.453	1	0
ST elevator	1	1	0
Riserlock adp	0.865	1	0
SFT	1.702	1	0
SFT adp	0.199	1	0
Landing joint	14.02	1	0.8445
Upper pup jts	9.76	1	0.7323
Tension joint	12.8	1	1.1679
Upper riser jts	25.6	1	1.1008
Upper lubricator adp	1	1	1.1807
Lubricator valve	2	1	0.5492
Lower lubricator adp	1	1	0.8915
Lower pup jts	11	1	0.8915
Middle riser jts	256	1	0.8312
Safety joint	3.048	1	0.6037
Lower riser jts	38.4	1	0.8312
Stress joint pipe	1.11	1	0.9484
Stress joint 6	0.949	1	0.9058
Stress joint 5	3.658	1	0.9178
Stress joint 4	2.743	1	0.9201
Stress joint 3	1.829	1	0.9159
Stress joint 2	0.914	1	0.9098
Stress joint 1	0.26	1	1.0341
EDP	2.05	1	3.6262
WCP	3.13	1	3.7842
Subsea tree	2.36	1	3.0828
Wellhead	3.2	1	0.74

A.2 Wave Statistics

Hs		Peak period									
		0	3	4	5	6	7	8	9	10	11
		3	4	5	6	7	8	9	10	11	12
0	1	83	734	2300	3836	4332	3816	2857	1917	1194	707
1	2	9	319	2435	7725	13998	17408	16665	13251	9215	5813
2	3	0	5	161	1399	5181	10734	14711	14911	12083	8279
3	4	0	0	2	61	620	2660	6162	9023	9330	7386
4	5	0	0	0	1	26	301	1465	3679	5552	5624
5	6	0	0	0	0	0	13	174	910	2343	3451
6	7	0	0	0	0	0	0	8	113	589	1457
7	8	0	0	0	0	0	0	0	7	82	392
8	9	0	0	0	0	0	0	0	0	6	65
9	10	0	0	0	0	0	0	0	0	0	7
10	11	0	0	0	0	0	0	0	0	0	0
11	12	0	0	0	0	0	0	0	0	0	0
12	13	0	0	0	0	0	0	0	0	0	0
13	14	0	0	0	0	0	0	0	0	0	0
14	15	0	0	0	0	0	0	0	0	0	0
15	16	0	0	0	0	0	0	0	0	0	0
Sum		92	1058	4898	13022	24157	34932	42042	43811	40394	33181

Hs		Peak Period									Sum
		12	13	14	15	16	17	18	19	20	
		13	14	15	16	17	18	19	20		
0	1	404	225	124	67	36	20	11	6	7	22676
1	2	3413	1901	1019	531	271	137	68	34	33	94245
2	3	4996	2738	1394	672	310	139	61	26	19	77819
3	4	4756	2609	1263	555	226	87	32	11	6	44789
4	5	4162	2402	1138	461	165	53	16	5	2	25052
5	6	3251	2137	1051	409	132	37	9	2	1	13920
6	7	1973	1638	911	366	112	28	6	1	0	7202
7	8	862	1009	702	318	101	24	4	1	0	3502
8	9	256	466	447	252	91	22	4	1	0	1610
9	10	51	155	222	168	75	21	4	1	0	704
10	11	7	37	83	90	53	19	4	1	0	294
11	12	1	7	23	37	31	14	4	1	0	118
12	13	0	1	5	12	14	9	3	1	0	45
13	14	0	0	1	3	5	4	2	1	0	16
14	15	0	0	0	1	2	2	1	0	0	6
15	16	0	0	0	0	0	1	1	0	0	2
Sum		24132	15325	8383	3942	1624	617	230	92	68	292000

Appendix B: Matlab Scripts

Matlab has been used for calculating fatigue lives based on the time series reported from Flexcom and RIFLEX, as well as the current sensitivity validation found in section 7.4. Here follows the Matlab scripts created, along with a short description of each script. User created functions, which are required for the main scripts to run, are included below each main script.

B.1 Import Time Series from Flexcom

Time series are extracted from the Flexcom databases, using a batch script provided by Aker Solutions. This batch script creates text files, which Matlab read using the following script. The time series data are stored in 3D matrices of dimensions 54001x4x8. The matrix dimensions are utilized like this:

1. Time series. Each of the 54001 lines corresponds to a time step.
2. The first column contains the time, ranging from 100 to 10900 with steps of 0.2. The following three columns contain M_y, M_z and M_{tot}.
3. The final dimension contains measurements at different locations. These locations are listed in table 6.1.

```
clear

clc

parentfolder='C:\Users\Arne\Documents\Batching\Results\';
studies=cell(29,1);
studies{1}='Base_Case';
studies{2}='current010';
studies{3}='current050';
studies{4}='current075';
studies{5}='currentdir_45';
studies{6}='currentdir_90';
studies{7}='currentdir_135';
studies{8}='currentdir_180';
studies{9}='Drag08';
studies{10}='Drag12';
studies{11}='Inertia18';
studies{12}='Inertia22';
studies{13}='Light_Content';
studies{14}='offset10';
studies{15}='offset20';
studies{16}='offset40';
studies{17}='RigTilt';
studies{18}='Seed1';
studies{19}='Seed2';
studies{20}='Seed3';
```

```
28. studies{21}='tension_35';
29. studies{22}='tension_50';
```

```
30. studies{23}='TFdir';
31. studies{24}='Tp08';
32. studies{25}='Tp10';
33. studies{26}='Tp11';
34. studies{27}='Tp12';
35. studies{28}='WHDTilt';
36. studies{29}='Wireline';
37. if exist('new_timeseries','var')
38.     delete('new_timeseries')
39. end
40. for i=1:29
41.     clc
42.     %disp(studies{i})
43.     fullpath=[parentfolder, studies{i}];
44.     variable=flexcom_filereader(fullpath);
45.     eval([studies{i},'=variable;'])
46.     if i==1
47.         eval(['save(''new_timeseries'',''',studies{i},''');'])
48.     else
49.         eval(['save(''new_timeseries'',''',studies{i},''',''-append'');'])
50.     end
51. end
```

52.

Published with MATLAB® R2013a

```
function timeseries=flexcom_filereader(filepath)
LOI=cell(8,1);
LOI{1}='\WHD.txt';
LOI{2}='\LSS.txt';
LOI{3}='\50.txt';
LOI{4}='\100.txt';
LOI{5}='\200.txt';
LOI{6}='\300.txt';
LOI{7}='\LV.txt';
LOI{8}='\LJ.txt';
timeseries=zeros(54001,4,8);
for i=1:8
    fid=fopen([filepath, LOI{i}],'r');
    for k=1:54001
        str=fgetl(fid);
        num=str2num(str); %#ok<*ST2NM>
        timeseries(k,:,i)=num(1:4);
    end
end
```

Published with MATLAB® R2013a

B.2 Import Time Series from RIFLEX

RIFLEX directly produces time series in the form of text files. The data in these files are read by the following script, and stored as Matlab matrices with the exact same dimensions as the Flexcom time series.

```
clear

clc

fid=fopen('C:\Users\Arne\WO_Riser\WO_riser_simple1\Initial\3565-
20140506083401\sima_elmfor.asc','r');
data_temp=zeros(54500,81);

for i=1:54500
    str=fgetl(fid);
    num=str2num(str); %#ok<*ST2NM>
    data_temp(i,:)=num;
end
fclose(fid);

i=1;
while data_temp(i,1)<100
    i=i+1;
end

data=zeros(54500-(i-1),4,8);
data(:,1,1)=data_temp(i:end,1);

for j=1:8
    data(:,1,j)=data_temp(i:end,1);

    data(:,2,j)=-data_temp(i:end,10*(j-1)+4).*1000;
    data(:,3,j)=-data_temp(i:end,10*(j-1)+6).*1000;

    data(:,4,j)=sqrt((data(:,2,j)).^2+(data(:,3,j)).^2);
end

Base_Case_RIFLEX=data;

save('RIFLEX_timeseries.mat','Base_Case_RIFLEX','-append');
```

Published with MATLAB® R2013a

B.3 Fatigue Calculation

Based on the time series created from Flexcom and RIFLEX, this script calculates fatigue life (or rather fatigue damage). The script converts bending moments to bending stresses, and uses a rainflow counting algorithm created by Nieslony (2010). The accumulated damage from the three-hour time series are then found. These values are used as input for the excel spreadsheet, where the monitoring extrapolation has been evaluated.

```
function [n_cycles, x_bins, D_hour]=fatigue(loadcase)


% Creates bending stress time series at n points at each cross section.
%  The bending stress will have units N/m2

[stressjoint, riserjoint, wellhead]=csecs;
SCF=zeros(8,1);
SCF(1)=1.5;
SCF(2)=1.5;
SCF(3)=1.5;
SCF(4)=1.5;
SCF(5)=1.5;
SCF(6)=1.5;
SCF(7)=1.5;
SCF(8)=1.5;

n_points=40;
angles=(2*pi./n_points).*(0:(n_points-1));

sigma_M=zeros(54001,n_points,8);

for i=1:54001
    for j=1:n_points

sigma_M(i,j,1)=(loadcase(i,2,1)*sin(angles(j))+loadcase(i,3,1)*cos(angles(j)))*...
            ((wellhead.od-wellhead.tfat)/(2*wellhead.I))*SCF(1);

sigma_M(i,j,2)=(loadcase(i,2,2)*sin(angles(j))+loadcase(i,3,2)*cos(angles(j)))*...
            ((stressjoint.od-stressjoint.tfat)/(2*stressjoint.I))*SCF(2);
        for k=3:8

sigma_M(i,j,k)=(loadcase(i,2,k)*sin(angles(j))+loadcase(i,3,k)*cos(angles(j)))*...
                ((riserjoint.od-riserjoint.tfat)/(2*riserjoint.I))*SCF(k);
        end
    end
end

% Converting time series to rainflow counting
extrema=cell(n_points,8);
rf=extrema;
```

```
n_cycles=extrema;
x_bins=extrema;

bins=4000;

for i=1:n_points
    for j=1:8
        extrema_nr=findextrema(sigma_M(:,i,j));
        extrema{i,j}=sigma_M(extrema_nr,i,j);
        rf{i,j}=rainflow(extrema{i,j});
        [n_cycles{i,j}, x_bins{i,j}]=rfhist(rf{i,j},bins,'ampl');
    end
end


% S-N curve
%  A conservative selection of free corrosion has been made. The curve B1
%  is selected based on the mosley report

m=3;
loga=12.436;

a=10^loga;

% Fatigue estimation

D=zeros(n_points,8);
for i=1:n_points
    for j=1:8
        D(i,j)=0;
        for k=1:bins
            D(i,j)=D(i,j)+(1/a)*n_cycles{i,j}(k)*(x_bins{i,j}(k)*1e-6)^m;
        end
    end
end

D=max(D);
D_hour=D/3;
```

Published with MATLAB® R2013a

```
function [stressjoint, riserjoint, wellhead]=csecs

inch2mm=25.4;

t_corr=3/1000;
d_rj_in=9.492;
t_rj_in=1.518;
```

```
d_sj=interp1([11 11.914],[0.3085 0.3029],11.1);
id_sj=0.1842;
tfat_sj=((d_sj-id_sj)/2)-0.5*t_corr;

d_whd=0.762;
id_whd=0.711;
tfat_whd=((d_whd-id_whd)/2)-0.5*t_corr;


d_rj=d_rj_in*inch2mm/1000;
t_rj=t_rj_in*inch2mm/1000;

tfat_rj=t_rj-0.5*t_corr;

stressjoint.od=d_sj;
stressjoint.id=id_sj;
stressjoint.tfat=tfat_sj;
stressjoint.I=(pi/64)*((stressjoint.od)^4-(stressjoint.id)^4);

riserjoint.od=d_rj;
riserjoint.id=(d_rj-t_rj)/2;
riserjoint.tfat=tfat_rj;
riserjoint.I=(pi/64)*((riserjoint.od)^4-(riserjoint.id)^4);

wellhead.od=d_whd;
wellhead.id=id_whd;
wellhead.tfat=tfat_whd;
wellhead.I=(pi/64)*((wellhead.od)^4-(wellhead.id)^4);
```

Published with MATLAB® R2013a

B.4 Current Sensitivity Analysis

As described in section 7.4, this Matlab script uses shear forces from RIFLEX analyses as input, and estimates response amplitude discretely along the riser. This is done by several scripts, with the following hierarchy:

1. Mother-script. This script is in charge of the overall process. It initiates the Morison solver at each discrete location along the riser.
   1.1. Shear force import. This script reads a RIFLEX output file, obtaining the shear force time series for each location along the riser.
   1.2. Time domain solver. This function is invoked by the mother-script. It is given vertical position, shear force time series and current profile as input. The harmonic functions of particle velocity and acceleration are created, and it invokes the iterative solver.

1.2.1. Iterative time domain solver. Step-by-step, it solves the system in the time domain. Each step is iterated, until the excitation force correspond to the relative velocity and acceleration. At each iteration, it invokes the simple, time integration function.

1.2.1.1. This simple function utilizes Euler-Gauss time integration in order to find the riser motion at the next time step, based on current motion and excitation force.

```
clear

clc



import_sheardata_from_dynamic_model



currentprofile=[0 0.67 0.067;

    -20 0.67 0.067;

    -50 0.61 0.061

    -100 0.58 0.058

    -200 0.52 0.052

    -300 0.51 0.051

    -356 0.43 0.043];



lengths=diff(z);

% netshear_current=diff(shearamps_current);
% netshear_lowcurrent=diff(shearamps_lowcurrent);
pos=z(1:end-1)+lengths./2;

n=1;
while pos(n)<0
    n=n+1;
end
n=n-1;

responseamplitudes=zeros(n,3);
responseamplitudes(:,1)=pos(1:n);
time.dt=timedata(2)-timedata(1);
```

```
time.t_total=timedata(end);
time.n=length(timedata)+1;

netshear_current=diff(shear_current,1,2);
netshear_lowcurrent=diff(shear_lowcurrent,1,2);

for i=1:n
    disp(i)
    current=interp1(currentprofile(:,1),currentprofile(:,2),pos(i));
    lowcurrent=interp1(currentprofile(:,1),currentprofile(:,3),pos(i));


responseamplitudes(i,2)=morison_timedomain_solver(pos(i),lengths(i),netshear_current(:,
i),current,time);

responseamplitudes(i,3)=morison_timedomain_solver(pos(i),lengths(i),netshear_lowcurrent
(:,i),lowcurrent,time);
end

% hold all
% plot(responseamplitudes(:,1)+356,responseamplitudes(:,2),'linewidth',2)
% plot(responseamplitudes(:,1)+356,responseamplitudes(:,3),'linewidth',2)
% leg=legend('Base Case','10 % Current',2);
% xlab=xlabel('Distance from seafloor [m]');
% ylab=ylabel('Response amplitude [m]');
% tit=title('Response amplitude along the riser calculated with a simplified model');
% ylim([0 1])
% set(gca,'yscale','log')
```

Published with MATLAB® R2013a

```
clear

clc



fidcurrent=fopen('C:\Users\Arne\WO_Riser\WO_riser_simple1\Regularwave_basecase\3402-
20140423130334\sima_elmfor.asc','r');
fidlowcurrent=fopen('C:\Users\Arne\WO_Riser\WO_riser_simple1\Regularwave_current010\340
2-20140423130329\sima_elmfor.asc','r');
shear_current=zeros(400,203);
shear_lowcurrent=shear_current;

for i=1:400
    strc=fgetl(fidcurrent);
    strlc=fgetl(fidlowcurrent);
    if strc==-1
```

```
        break
    end
    strc2=strsplit(strc,' ');
    strlc2=strsplit(strlc,' ');

    for j=1:203
        shear_current(i,j)=str2double(strc2{10*j+1});
        shear_lowcurrent(i,j)=str2double(strlc2{10*j+1});
    end
end

fclose(fidcurrent);
fclose(fidlowcurrent);

fidcurrent=fopen('C:\Users\Arne\WO_Riser\WO_riser_simple1\Regularwave_basecase\3402-
20140423130334\sima_noddis.asc','r');

str=fgetl(fidcurrent);
str2=strsplit(str,' ');
z=zeros(1,203);
timedata=zeros(400,1);
timedata(1)=str2double(str2{2});
for i=2:400
    str=fgetl(fidcurrent);
    str2=strsplit(str,' ');
    timedata(i)=str2double(str2{2});
end

for i=1:203
    z(i)=str2double(str2{3*i+2});
end
fclose(fidcurrent);

shearamps_current=(max(shear_current)-min(shear_current)).*1000./2;
shearamps_lowcurrent=(max(shear_lowcurrent)-min(shear_lowcurrent)).*1000./2;
```

Published with MATLAB® R2013a

```
function amplitude=morison_timedomain_solver(z,L,sheardata,current,time)
% Wave parameters
H=4;
T=9;
%z=-356+50;

% Current
uc=current;

% Damping
struct.ksi=0.0;
```

```
Kdamp=0;
Mdamp=0;
dampingtype='relative';


load=sheardata;
% Coefficients
Cd=0.9;
Cm=2;

% Environment
rho=1025;

% Time
%t_end=200;
%dt=0.1;


% Structure
M=255.156*L;
K=(max(load)-min(load))./150;
D=0.261;
%L=1;

% External load
%amp=1;
%amp=abs(S_amp);
%phase=pi/2;


coeff.Cd=Cd;
coeff.Cm=Cm;
env.rho=rho;
%time.dt=dt;
%time.t_total=t_end;
%time.n=time.t_total/time.dt+1;
env.a=@(t)((2*pi/T)^2)*(H/2)*exp((((2*pi/T)^2)/9.81)*z)*cos((2*pi/T)*t);
struct.M=M;
struct.k=K;
%load=@(t)amp*sin((2*pi/T)*t+phase);

struct.D=D;
struct.L=L;
switch dampingtype
    case 'relative'
        struct.c=struct.ksi*2*sqrt(struct.M*struct.k);
    case 'Rayleigh'
        struct.c=Kdamp*struct.k+Mdamp*struct.M;
end
```

```
% hold all
% xlim([0 150])
env.uc=uc;
env.u=@(t)(2*pi/T)*(H/2)*exp((((2*pi/T)^2)/9.81)*z)*sin((2*pi/T)*t)+uc;

temp=morison_response_iteration(env,struct,coeff,time,load);
Response=temp(:,[1 2]);
Response(:,2)=Response(:,2)-mean(Response(300:end,2));

   %plot(Response(:,1,i),Response(:,2,i),'linewidth',2)


% str1=sprintf('Current %.4f m/s',uc(1));
% str2=sprintf('Current %.4f m/s',uc(2));
% legend(str1,str2)
% xlim([200 250])

amplitude=max(Response(:,2))-min(Response(:,2));
end
```

Published with MATLAB® R2013a

```
function Response=morison_response_iteration(env,struct,coeff,time,ext_load)

Cdstar=0.5*env.rho*coeff.Cd*struct.L;
Cmstar=env.rho*coeff.Cm*0.25*pi*struct.D.^2*struct.L;
Response=zeros(time.n,4);
Response(:,1)=0:time.dt:time.t_total;

accepted_error=1E-5;
Response(1,2)=((Cdstar*(env.uc).^2)+ext_load(1))./struct.k;

for i=1:time.n-1
    r_ass=Response(i,2);
    rd_ass=Response(i,3);
    rdd_ass=Response(i,4);
    tt=Response(i+1,1);
    n=0;
    while 1
        n=n+1;
        if n==1000
            error('Failed at timestep %.0f',i)
        end
        urel=env.u(tt)-rd_ass;
        arel=env.a(tt)-rdd_ass;
        load=ext_load(i);
        Fd=Cdstar*urel*abs(urel);
        Fm=Cmstar*arel;
```

```
        Pi_plus=Fd+Fm+load;
        response_step=morison_timedomain_step(struct,time,Response(i,2:4),Pi_plus);
        r_calc=response_step(1);
        rd_calc=response_step(2);
        rdd_calc=response_step(3);
        errorval=(r_calc-r_ass)^2+(rd_calc-rd_ass)^2+(rdd_calc-rdd_ass)^2;
        if errorval<accepted_error
            break
        else
            r_ass=r_calc;
            rd_ass=rd_calc;
            rdd_ass=rdd_calc;
        end
    end
    Response(i+1,2:4)=[r_calc, rd_calc, rdd_calc];
end
% h=figure;
% hold all
% plot(Response(:,1),Response(:,2))
% %plot([0 time.t_total],[env.xstat env.xstat])
% xlabel('Time [s]')
% ylabel('Response [m]')
% legend('Dynamic response','Static response (current only)')
% title('Time domain. Response velocity included')
% saveas(h,'Td_response_velocity.jpg')
% clf
% end
```

Published with MATLAB® R2013a

```
function response_next=morison_timedomain_step(struct,time,response,Pi_plus)

ri=response(1);
ridot=response(2);
riddot=response(3);

ri_plus=(Pi_plus+struct.M*riddot+(4/time.dt*struct.M+struct.c)*ridot+...
    (4/(time.dt^2)*struct.M+2/time.dt*struct.c)*ri)/(4/(time.dt^2)*struct.M+...
    2/time.dt*struct.c+struct.k);
riddot_plus=4*(ri_plus-ri-ridot*time.dt)/(time.dt^2)-riddot;
ridot_plus=ridot+0.5*(riddot+riddot_plus)*time.dt;
response_next=[ri_plus,ridot_plus,riddot_plus];
end
```

Published with MATLAB® R2013a

Appendix C: Fatigue Life Extrapolation

In this appendix, the extrapolation factors for all investigated sensitivities are listed.

C.1 Gamma

As described in section 8.1.1, gamma accounts for the relative fatigue life at a reference condition, between the lower strain sensor and the riser component in question. It is found as each individual riser component's mean lifetime, at the reference environmental condition. The reference environmental condition are defined as the following:

- JONSWAP wave distribution, with significant wave height 4 meters, and peak period 9 seconds. Head sea.
- Current applied in the same direction as the waves, current profile selected as one-year current according to table 5.4.
- No static vessel offset
- No static vessel and wellhead angle
- 25 metric tons overpull
- Drag coefficient 0.9, inertia coefficient 2.0
- Model set up for coiled tubing operation
- Content density 2070 kg/m^3
- No further effects, like VIV or slow drift

Four three-hour time series are created for this condition. One of these are referred to as the "base case" analysis, while the three others are used to investigate the effect of changing seastate realization. The following gamma values for found for the four different analyses:

	WHD	LSS	50	100	200	300	LV	LJ
Base Case	6.784	1.00	165.81	240.64	726.99	422.43	43.32	0.0694
Seed 1	6.781	1.00	162.14	240.36	723.42	417.59	43.33	0.0725
Seed 2	6.779	1.00	165.03	241.03	723.02	426.84	43.95	0.0701
Seed 3	6.780	1.00	164.45	244.31	722.64	425.84	43.74	0.0705

	WHD	LSS	50	100	200	300	LV	LJ
Gamma mean	6.781	1.00	164.36	241.59	724.02	423.18	43.59	0.0706
Gamma std	2.23E-03	0.00E+00	1.58E+00	1.84E+00	2.01E+00	4.18E+00	3.12E-01	1.33E-03

C.2 Chi

The description and evaluation of chi is found in section 0. As mentioned, this factor accounts for changes in fatigue life due to conditions that deviate from the reference condition. Each

environmental parameter that deviates from the reference condition will have a contribution to chi, and the final value of chi is the product of all these contributions, as described in equation (8.3). The analyzed sensitivities result in the following chi contributions:

Peak period

	WHD	LSS	50	100	200	300	LV	LJ
Tp 08 s	0.99	1.00	0.93	0.93	1.03	0.95	1.03	3.75
Tp 10 s	1.01	1.00	1.31	1.20	1.27	1.43	1.42	0.76
Tp 11 s	1.03	1.00	2.01	1.61	1.82	2.50	2.33	0.65
Tp 12 s	1.04	1.00	3.11	2.16	2.52	4.78	4.30	0.68

Current

	WHD	LSS	50	100	200	300	LV	LJ
10 % Current	1.01	1.00	1.00	1.03	2.36	3.39	8.64	17.14
50 % Current	1.00	1.00	0.96	1.24	2.27	3.09	5.39	6.69
75 % Current	1.00	1.00	0.99	1.13	1.61	1.89	2.40	2.43

Current direction

	WHD	LSS	50	100	200	300	LV	LJ
Current dir 45	1.01	1.00	1.09	1.19	1.98	2.21	2.86	2.85
Current dir 90	1.01	1.00	1.18	1.22	2.40	3.04	5.15	5.27
Current dir 135	1.01	1.00	1.12	1.20	2.07	2.29	2.95	2.93
Current dir 180	1.00	1.00	1.04	1.00	1.05	1.05	1.01	1.00

Vessel offset

	WHD	LSS	50	100	200	300	LV	LJ
10 m offset	1.00	1.00	1.01	0.99	1.00	1.00	1.00	0.99
20 m offset	1.00	1.00	1.02	0.99	1.00	1.01	1.03	0.98
40 m offset	1.00	1.00	1.07	0.99	1.04	1.03	1.12	0.96

Vessel and wellhead tilt

	WHD	LSS	50	100	200	300	LV	LJ
Vessel tilt	1.00	1.00	1.01	1.00	1.00	0.99	0.99	0.97
Wellhead tilt	1.00	1.00	1.01	0.99	1.00	1.00	0.99	0.98

Riser tension

	WHD	LSS	50	100	200	300	LV	LJ
35 mt overpull	0.91	1.00	1.63	1.36	1.56	1.31	1.20	1.03
50 mt overpull	0.80	1.00	3.16	2.11	2.67	2.05	1.60	1.02

Drag coefficient

	WHD	LSS	50	100	200	300	LV	LJ
Drag coeff 80 %	1.00	1.00	1.04	1.12	1.53	1.71	2.04	1.95
Drag coeff 120 %	1.00	1.00	0.98	1.01	1.22	1.33	1.24	1.47

Inertia coefficient

	WHD	LSS	50	100	200	300	LV	LJ
Inertia coeff 90 %	1.00	1.00	1.06	1.02	1.03	0.98	0.95	0.87
Inertia coeff 110 %	1.00	1.00	0.97	0.97	0.97	1.02	1.04	1.11

TF orientation, wireline model and content density

	WHD	LSS	50	100	200	300	LV	LJ
TF orientation	1.00	1.00	1.01	0.99	1.00	0.99	0.99	1.07
Wireline	1.00	1.00	1.00	1.00	1.00	1.00	1.00	1.05
Light Content	1.01	1.00	1.08	0.93	0.87	0.76	0.72	0.77

Appendix D: Riser Tension

The following spreadsheet is used for calculating riser tension. The data validates the Flexcom model, as the values reported from Flexcom corresponds to the calculated values.

Component	# of Components	Dry Mass [kg]	Content Mass [kg]	Buoyancy [kg]	Tension (top of component) [kN]	Tension in Flexcom [kN]	Error
CB Bails	2	400.0	-	-	508.9	508.6	0.05 %
Tension Frame Top	1	4500.0	-	-	504.9	504.6	0.07 %
Tension Frame Vertical	2	6011.5	-	-	460.8	460.4	0.08 %
Tension Frame Bottom	1	4500.0	-	-	401.8	401.6	0.05 %
TF Bails	2	200.0	-	-	357.7	357.4	0.08 %
Gooseneck	1	800.0	138.6	-	0.0	0.0	-
CT Injector	1	5700.0	126.6	-	-9.2	-9.2	0.00 %
CT Stripper	1	1360.0	39.7	-	-66.4	-66.4	0.01 %
CT Dual Stripper	1	2903.0	64.9	-	-80.1	-80.1	0.00 %
CT BOP	1	5485.0	73.1	-	-109.2	-109.2	0.01 %
CT Spool	1	150.0	52.4	-	-163.7	-163.7	0.02 %
Riserlock Adapter	1	357.0	45.1	-	-165.7	-165.7	0.01 %
SFT above TF Elevator	1	2621.1	23.3	-	-169.7	-169.7	0.02 %
SFT below TF Elevator	1	7358.9	65.4	-	160.1	159.8	0.19 %
SFT Adapter	1	600.0	11.6	-	87.3	87.0	0.32 %
Landing Joint	1	3993.0	819.4	-	81.3	81.3	0.07 %
Upper Pup Joints	1	4133.6	534.2	-	34.1	34.1	0.06 %
Tension Joint above Tension Ring	1	932.7	118.1	-	-11.7	-11.7	0.00 %
Tension Joint below Tension Ring	1	1879.3	237.9	-	1351.3	1350.0	0.10 %
Upper Riser Joints	1	6532.0	1120.8	1170.8	1330.5	1330.0	0.04 %
Upper LV Adapter	1	200.0	43.8	47.5	1267.0	1266.0	0.08 %

Lubricator Valve	1	1600.0	87.6	251.2	1265.0	1264.0	0.08 %
Lower LV Adapter	1	200.0	43.8	44.1	1250.9	1250.0	0.07 %
Lower Pup Joints	1	4686.0	642.9	929.6	1249.0	1248.0	0.08 %
Middle Riser Joints	1	65319.9	11207.7	14039.0	1205.8	1205.0	0.07 %
Safety Joint	1	1930.0	133.4	316.2	592.8	592.0	0.14 %
Lower Riser Joints	1	9798.0	1681.2	2105.8	575.7	574.9	0.13 %
Stress Joint Pipe section	1	199.5	64.9	58.1	483.7	483.0	0.15 %
Stress Joint Section 6	1	227.6	52.3	55.7	481.7	480.9	0.16 %
Stress Joint Section 5	1	956.6	201.8	224.3	479.5	478.7	0.17 %
Stress Joint Section 4	1	822.6	151.3	181.9	470.3	469.6	0.15 %
Stress Joint Section 3	1	619.4	100.9	130.8	462.6	461.7	0.19 %
Stress Joint Section 2	1	335.2	50.4	68.4	456.8	455.9	0.19 %
Stress Joint Section 1	1	168.0	14.3	29.0	453.7	452.8	0.19 %
EDP	1	25000.0	106.8	3304.3	452.2	451.3	0.19 %
WCP	1	35000.0	163.0	4633.2	238.3	237.5	0.33 %
Subsea Tree	1	40000.0	122.9	5260.6	-61.2	-62.0	1.34 %
Wellhead	1	7000.0	2630.0	2213.7	-403.2	-404.0	0.19 %

Appendix E: Calculated Fatigue Lives

The following values are calculated fatigue lives in years, constant operation at the given environmental condition. The fatigue lives are calculated at eight locations along the riser, as listen in table 6.1. Fatigue lives are calculated by the procedure described in section 2.6, with the parameters seen in section 6.2.1. It is once again stressed that fatigue lives are calculated for comparison of relative values. The calculated lifetimes are not representative of the riser's actual lifetime.

E.1 Flexcom Data

	WHD	LSS	50	100	200	300	LV	LJ
Base Case	4388.6	646.9	107257.1	155665.1	470276.9	273260.6	28021.0	44.9
10 % Current	271.6	39.5	6479.0	9832.3	67558.7	56669.9	14887.3	47.8
50 % Current	741.2	109.1	17147.2	32680.7	179087.8	142757.0	25637.8	51.5
75 % Current	1923.1	284.1	46247.9	77628.3	330982.8	226681.0	29686.1	48.7
Current dir 45	1640.5	240.6	42979.1	69366.2	344376.8	225003.5	29964.3	48.4
Current dir 90	956.3	139.6	27032.3	41295.2	242489.8	179489.4	31311.7	52.0
Current dir 135	1657.5	242.9	44766.9	70588.0	363590.0	235556.9	31216.4	50.2
Current dir 180	4548.0	668.9	114508.0	161386.6	510383.9	295885.3	29514.4	47.2
Drag coeff 80 %	2416.1	354.7	60879.2	95830.7	391839.4	256638.5	31601.4	48.9
Drag coeff 120 %	2721.7	401.8	64659.5	98267.2	354676.9	226676.7	21710.6	41.8
Inertia coeff 90 %	4938.5	726.4	126107.9	179173.5	543994.4	302052.3	30077.9	44.4
Inertia coeff 110 %	3912.0	577.7	92025.8	135816.2	406429.0	249343.7	26196.2	45.3
Light Content	5708.3	837.0	148250.3	187558.4	528533.2	270247.1	26115.1	45.4
10 m offset	4445.1	654.2	108499.5	156410.2	473613.2	276525.1	28622.6	45.5
20 m offset	4509.8	664.6	111270.8	158272.3	483496.0	282835.1	29810.5	46.1
40 m offset	4703.9	693.3	122137.0	165774.4	522307.6	300892.7	33876.4	46.9
Vessel tilt	4393.6	647.6	106991.7	155751.1	468365.3	271653.4	27846.3	44.5
Seed 1	4444.8	655.5	106279.0	157546.2	474183.4	273716.3	28403.5	47.5
Seed 2	4393.3	648.0	106945.0	156198.5	468541.1	276608.1	28480.0	45.4
Seed 3	4360.6	643.2	105769.8	157140.0	464795.8	273898.8	28135.4	45.3
35 mt overpull	3858.1	627.7	168073.8	206263.4	710682.7	347422.2	32862.6	45.7
50 mt overpull	3461.3	641.4	332743.8	327136.3	1238273.0	556025.0	44853.2	46.0
TF orientation	4366.7	643.8	106739.4	154302.4	467287.7	270882.7	27829.6	48.6
Tp 08 s	2576.8	383.1	58766.6	86002.8	285405.8	154806.1	17163.0	101.5
Tp 10 s	4187.0	609.7	130777.8	176918.8	561111.8	369867.1	37749.4	32.5
Tp 11 s	3776.0	541.8	178729.2	210707.9	712947.0	573113.5	55124.2	24.8
Tp 12 s	2985.5	423.8	216827.2	221011.5	773223.7	858084.1	79493.4	20.3
Wellhead tilt	4400.7	648.3	107275.8	155692.8	470219.4	273488.1	28040.1	44.9
Wireline	4252.8	626.6	102664.3	151119.6	451858.6	264578.8	27384.1	46.4

Validation Case 1	729.4	106.3	21169.2	37454.8	211854.5	195040.1	35141.7	36.9
Validation Case 2	3224.2	451.6	226180.2	227310.7	802551.0	903337.3	86486.3	20.9
Validation Case 3	1801.1	334.5	171796.5	187847.3	981050.5	500927.5	47923.8	48.4
Validation Case 4	266.2	38.7	6441.7	9567.6	66641.3	55494.0	14766.3	47.7

E.2 RIFLEX Data

	WHD	LSS	50	100	200	300	LV	LJ
Base Case RIFLEX	2605.9	61.59	13658.5	24267.1	124778.5	51812.4	6790.2	0.150
75 % Current RIFLEX	1443.8	34.12	7580.9	13559.8	93983.3	46022.0	6896.9	0.146
50 % Current RIFLEX	767.8	18.15	4564.4	6740.8	54015.4	35343.0	5986.9	0.150
10 % Current RIFLEX	653.7	15.45	3633.2	5165.5	39011.5	30979.2	5665.9	0.146
Base Case no current above 25 m	2609.3	61.67	13723.0	24320.0	124901.1	51611.2	6914.6	0.153
Base Case no current above 50 m	2652.8	62.70	16600.7	24650.8	117943.3	45543.7	7252.5	0.150
Base Case no current above 100 m	2162.7	51.11	12389.3	17670.7	75931.6	40887.3	6926.6	0.147
Base Case no current above 150 m	1532.8	36.22	8918.0	11227.3	51151.3	39141.4	6811.6	0.147
Base Case no current above 200 m	1119.3	26.44	6494.6	7954.7	40623.1	38975.4	6676.7	0.150
Base Case no current below 25 m	659.8	15.59	3901.6	5768.1	43036.3	33792.2	6169.1	0.151
Base Case no current below 50 m	702.3	16.60	4508.0	6661.7	51830.0	38064.8	5331.1	0.147
Base Case no current below 100 m	874.3	20.66	6337.9	8771.3	78092.5	42705.7	6024.3	0.145
Base Case no current below 150 m	1124.5	26.58	7967.8	11616.8	108531.8	44017.7	6099.1	0.144
Base Case no current below 200 m	1481.2	35.01	10927.6	15684.4	136568.8	46951.9	6411.7	0.144
10 % Current no current above 50 m	643.0	15.20	3592.3	5109.3	38186.2	30608.5	5653.5	0.149

10 % Current no current above 100 m	651.9	15.40	3626.3	5139.3	38515.6	30766.9	5649.6	0.152
10 % Current no current above 150 m	648.4	15.32	3627.0	5119.4	38335.5	30732.8	5651.9	0.152
10 % Current no current above 200 m	647.5	15.31	3609.4	5099.7	38092.2	30650.1	5625.6	0.152
10 % Current no current below 50 m	643.0	15.20	3592.3	5109.3	38186.2	30608.5	5653.5	0.149
10 % Current no current below 100 m	644.6	15.24	3605.4	5128.1	38424.6	30686.1	5644.0	0.151
10 % Current no current below 150 m	648.6	15.33	3612.5	5154.6	38681.4	30770.4	5650.7	0.147
10 % Current no current below 200 m	649.9	15.36	3621.6	5173.3	38813.9	30755.9	5679.1	0.149

Appendix F: Overview of Digital Appendices

A selection of the files used for the analyses in this thesis are included.

Flexcom Input Files

The files in this folder contains the files Flexcom requires to run the base case analysis. This analysis is run in four stages; the first file contains the information required for the static model, and the subsequent three files applies vessel offset, current and wave loading. Also included is the static model for wireline operation.

RIFLEX Input Files

From RIFLEX, the inpmod file for the basic analysis is included.

Post Processing

The post-processing folder contains time series files for Matlab, stored as matrices with dimensions 54001x4x8. The first dimension contain the time series. The second time series contain time in the first column, followed by M_y, M_z and M_{tot}. The third dimension contain data for the various locations along the riser, as listed in table 6.1. Separate file are given in order to separate between Flexcom and RIFLEX results. These files are large, and have to be excluded from the main submission of this thesis. They are submitted by an alternative upload protocol.

Also included is the spreadsheet "fatigue.xlsx". Here, all results from fatigue calculations in Matlab are found. The proposed extrapolation factors are based on this spreadsheet.